INVESTIGATING THE REGENERATION BEHAVIORS OF NEUROGLIAL CELLS ON ARTIFICIALLY MADE ELECTROSPUN PCL SCAFFOLDS EMBEDDED WITH CONDUCTIVE NANOMATERIALS

A Dissertation by

Madhulika Srikanth

Master of Science, Wichita State University, May 2012

Bachelor of Technology, Malaviya National Institute of Technology Jaipur, April 2010

Submitted to the Department of Mechanical Engineering
and the faculty of the Graduate School of
Wichita State University
in partial fulfilment of
the requirements for the degree of
Doctor of Philosophy

July 2015

INVESTIGATING THE REGENERATION BEHAVIORS OF NEUROGLIAL CELLS ON ARTIFICIALLY MADE ELECTROSPUN PCL SCAFFOLDS EMBEDDED WITH CONDUCTIVE NANOMATERIALS

The following faculty members have examined the final copy of this dissertation for form and content, and recommend that it be accepted in partial fulfilment of the requirement for the degree of Doctor of Philosophy with a major in Mechanical Engineering.

_____
Ramazan Asmatulu, Advisor, Committee Chair

_____
Li Yao, Committee Co-Chair

_____
T. S. Ravigururajan, Committee Member

_____
Kim Cluff, Committee Member

_____
Hamid Lankarani, Committee Member

Accepted for the College of Engineering

_____
Royce Boyden, Dean

Accepted for the Graduate School

_____
Kerry Wilks, Interim Dean

DEDICATION

To my parents

ACKNOWLEDGEMENTS

This dissertation has been a big part of my life—rather an exciting journey filled with ups and downs. I have learned much, research wise. But this experience taught me more—most importantly, the spirit and consequence of perseverance. Many people have played a big role in this part of my journey, and I consider myself very fortunate to be associated with them. I would like to express my regards to them from the bottom of my heart.

Dr. Ramazan Asmatulu continually and convincingly conveyed a sense of curiosity and adventure in regard to research. Without his guidance and persistent encouragement this dissertation would not have been possible. Dr. Li Yao believed in my work, taught me different characterization studies, and helped me analyze the data with his invaluable input. Dr. Ravigururajan offered infinite insight into different subject matters and molded me into a better researcher. He helped me push my boundaries and improve my analyzing ability by several fold. Dr. Kim Cluff is an amazing teacher, who brought much enthusiasm and optimism to this work. I will always cherish his calmness and systematic approach to problems. Dr. Hamid Lankarani was always being there for me, offering moral support and providing valuable tips and advice. Dr. Andrew Swindle offered resources from the Department of Geology for the x-ray analysis. Friends and colleagues provided considerable support and added a "fun" element. Notably, Leyla Saeednia, Ryan Becker, Max Hinman, and Amir Jabbarnia offered their assistance with various characterizations. Vishal Nageshkar, my husband, proof read many parts of this report and offered me constant encouragement. Mom and Dad have given me their infinite love and a value system that has made me who I am today.

ABSTRACT

Nerve tissue damage produces a significant decrease in the quality of life and represents a considerable public health burden in the United States and in the world. Current treatment methods are mostly preventative and suggestive, and even with existing technologies, progress is limited due to the complexity of the nervous system. Nerve tissue engineering is one of the most promising methods to restore a nervous system back to good health. Astrocytes (nerve glial cells) play a pivotal role in the health of the nervous system and are fundamental for controlling several activities, from synaptic transmission to homeostasis. Astrocytes are involved in all types of brain pathologies from acute lesions to chronic neurodegenerative processes and psychiatric diseases. Effective scaffold design with polymer blending plays a crucial role in nerve tissue engineering.

In this dissertation, four types of electrospun fibers were created: polycaprolactone (PCL), PCL-graphene, PCL-fullerene, and PCL-carbon nanotube (CNT) at 0.05%, 0.1%, and 0.2% by weight. From these fibers, scaffolds having nano-sized diameters were successfully fabricated. Microscopic, goniometric, thermal, x-ray, spectral, and electrical characterizations were performed to study the structural characteristics, surface free energy, crystallinity, chemical/molecular composition, and dielectric properties of these scaffolds. Toxicity levels of all scaffolds were very low. Astrocytes harvested from neonatal rats were successfully cultured on these scaffolds. An immunostaining process using rhodamine phalloidin confirmed the presence of F-actin filaments, and the anti-glial fibrillary acidic protein (GFAP) antibody test confirmed the presence of GFAP, which is a characteristic of only astrocytes. Scanning electron microscopy (SEM) analysis further confirmed the healthy morphology and successful attachment of astrocytes to the scaffolds. Apart from PCL fibers, the PCL-CNT fibers seemed to have the highest cell adhesion and proliferation.

TABLE OF CONTENTS

TABLE OF CONTENTS (continued)

LIST OF TABLES

LIST OF FIGURES

LIST OF FIGURES (continued)

LIST OF FIGURES (continued)

LIST OF FIGURES (continued)

Figure Page

LIST OF ABBREVIATIONS

ADP	Adenosine Diphosphate
ALS	Amyotrophic Lateral Sclerosis
ATP	Adenosine Triphosphate
BBB	Blood-Brain Barrier
BSB	Blood-Spinal Barrier
CA	Cellulose Acetate
CHI	Chitosan
CNS	Central Nervous System
CNT	Carbon Nanotube
CNTF	Ciliary Neurotrophic Factor
CS	Chondroitin Sulfate
CVDE	Crystal Violet Dye Elution
DMEM	Dulbecco's Modified Eagle Medium
DNA	Deoxyribonucleic Acid
DSC	Differential Scanning Calorimetry
EAAT	Excitatory Amino Acid Transporters
ECM	Extracellular Matrix
EDS	Energy Dispersive Spectroscopy
FDA	Food And Drug Administration
FTIR	Fourier Transform Infrared Spectroscopy
GDA	GRP-Derived Astrocyte

GF	Graphene Foam
GFAP	Glial Fibrillary Acidic Protein
GLAST	Glutamate-Aspartate Transporter
GLT	Glutamate Transporter
GLU	Glucose
GO	Graphene Oxide
GRP	Glial-Restricted Precursor
HIV	Human Immunodeficiency Virus
HIV-P	HIV Protease
LDH	Lactate Dehydrogenase
LDHe	Extracellular Lactate Dehydrogenase
MEM	Minimum Essential Medium
MMP-2	Matrix Metalloproteinase-2
MTT	(Di)-Methyl-Thiazol (Diphenyl)-Tetrazolium
MWCNT	Multi-Walled Carbon Nanotube
NFMP	Nanofiber Micropore
NIH	National Institutes of Health
NSC	Neural Stem Cell
PAC	Phosphatase Acid
PBS	Phosphate-Buffered Saline
PC	Phaeochromocytoma

PCL	Polycaprolactone
PG	Proteoglycan
PGA	Polygllycolide
PHB	Polyhydroxybutyrate
PH-BV	Polyhydroxybutyrate Hydroxyvalerate
PLLA	Poly-L-Lactic Acid
PNS	Peripheral Nervous System
ROS	Reactive Oxygen Species
RPM	Revolutions per Minute
SCI	Spinal Cord Injury
SEM	Scanning Electron Microscopy
SRB	Sulforhodamine B
SWCNT	Single-Walled Carbon Nanotube
TBI	Traumatic Brain Injury
TNF	Tumor Necrosis Factor
Tuj	Beta-Tubulin II
UV	Ultraviolet
UVA	Ultraviolet A
WAXD	Wide-Angle X-Ray Diffraction
XRD	X-Ray Diffraction
XTT	Bis-(methoxy-nitro-sulfophenyl) Tetrazolium Carboxanilide

CHAPTER 1

INTRODUCTION

The central nervous system (CNS) consists of two main components—the brain and the spinal cord. It controls the physiological and psychological aspects of a living system and governs the biology within. It is very complex and has been studied for decades, and yet it is not completely understood. Nevertheless, scientific knowledge in the last couple of decades has grown exponentially, owing to the numerous advances in this field. Traumatic brain injury (TBI) and spinal cord injury (SCI) are one of the leading causes of lifelong disability, both physical and mental. The Centers for Disease Control and Prevention has reported that there has been an increase in the total number of TBI cases from 2001 to 2010. About 2.54 million people suffered from TBI in 2010, and 54,000 of them died. According to reports by the National Spinal Cord Injury Statistical Center, the number of people who are alive with SCI is roughly 276,000, with an average age of 42. The leading cause of both types of injuries is vehicular accident. The average lifetime cost to people suffering from SCI/TBI is about two million dollars [1-5].

Other factors leading to nerve damage are congenital defects, neurodegenerative diseases, drug side-effects, nutritional deficiencies, infectious diseases, and cancer. Because of the complexity of the brain and the spinal cord, very little spontaneous regeneration, repair, or healing occurs. The neuroscience community of the world has recognized several injury mechanisms that lead to primary and secondary loss of tissue. These injury mechanisms are complex, thus making it difficult to find a treatment. However, despite the hurdles, the mortality rate of individuals with SCI in the last 50 years has significantly been reduced from 50% to less than 5%. Several methods have been proposed, trials have been conducted, and progress has been made to maximize recovery. But we are still very far away from our goal where every patient with a spinal cord or a

head injury recovers completely from an accident. Hence, it is the responsibility of the scientific community to bridge that gap. Considerable work has been done in studying the endogenous repair system, which uses growth factors to regenerate and stimulate the already-existing neural stem cells in the brain and spinal cord without any promising results. Most of these fail to give functional recovery, and there is an added risk of tumors. According to Dr. Charles Tator, a leading neuroscientist, an exogenous repair system involving tissue/cell transplantation is more viable [5].

This study deviates from the popular neurocentric research and focusses on neuro glial tissues. Astrocytes are star-shaped glial cells that comprise the brain environment by building up the micro-architecture of the central nervous system. They have been recently recognized as one of the most important cells in the body because they perform a number of vital functions. They maintain brain homeostasis, control the metabolism of neural cells, control synaptic activity, and maintain the blood-brain barrier (BBB)/blood-spinal cord barrier (BSB), among other functions. The death or survival of astrocytes affects the ultimate clinical outcome and rehabilitation through the effects on neuron genesis and reorganization [6].

Tissue transplantation has been in use since the early 1900's. Unfortunately, the scientific knowledge and surgical techniques required for successful transplantation came much later [7]. One of the major problems with tissue transplantation is the tendency of the body's immune system to become activated against a foreign entity, which increases the chances of rejection. Tissue engineering opens a whole new field of medical therapy as an alternative to conventional transplantation methods. Here, the chances of rejection are reduced because the engineered tissue is customized to suit the specific needs of an individual. It can be made up of polymeric biomaterials, which may or may not contain precursor cells. It is non-toxic and degrades to carbon and water, which is easily absorbed by the body. It can be very easily tailored to mimic the

morphology of surrounding tissues and organs. The polymeric scaffolds promote cell adhesion, maintain differentiated cell function without hindering proliferation, act as a template to organize and direct the growth of cells, and help in the function of the extracellular matrix [8].

The work in this dissertation involved the fabrication of three-dimensional (3D) polymeric scaffolds by electrospinning. This process involves using an electric field to convert a viscous polymer solution into a fibrous mesh. By altering the processing parameters and the composition, different characteristics, such as morphology, surface, mechanical, and biological characteristics, can be manipulated [9]. This process is capable of fabricating scaffolds that closely resemble the extracellular matrix (ECM). Polycaprolactone (PCL), a semi-crystalline linear aliphatic polyester was used as the base scaffold material. Its in-vitro and in-vivo biocompatibility and efficacy studies have already been established and approved by the U.S. Food and Drug Administration (FDA) for a number of medical and drug-delivery devices.

This research aims to contribute to this process by introducing nanomaterials into the scaffolds. Three types of nanomaterials—graphene, carbon nanotubes, and fullerene—were incorporated into a PCL scaffold. Nanoparticles exhibit some exclusive properties that enhance the functionality of the PCL scaffold. Fullerene is known to act as a radical sponge by reducing the degenerative effect of oxygen in the surrounding area. Graphene is known to promote the differentiation of nerve cells (oligodendrocytes), and carbon nanotubes are known to provide structural reinforcement and ionic conductivity [10].

This work is an effort to improve the existing tissue engineering methods by bringing together both nanotechnology and micro-fabrication and then using it to grow neuroglial cells with the future possibility for use in spinal cord transplantation.

1.1 Objectives

This study has the following objectives:

- Fabrication of PCL scaffolds by electrospinning process to closely resemble the extra cellular matrix of the body.
- Infusion of nanomaterials to the scaffolds and study of the effect on scaffold morphology.
- Goniometric and surface characterization to study the work of adhesion.
- Spectral analysis to confirm the presence of nanomaterials by studying the molecular structure.
- Thermal and x-ray characterizations to study the effect of crystallinity on cell growth.
- Dielectric studies to compare the dielectric values of nerve cells.
- Cytotoxicity tests to check the viability of the scaffolds.
- Induction of astrocyte cell growth on the scaffolds and proliferation characterization.

1.2 Purpose

The ultimate aim of this study is to successfully grow astrocytes on artificially fabricated PCL scaffolds infused with conductive nanomaterials and perform characterization studies to extend the future scope of this process.

CHAPTER 2

LITERATURE REVIEW

This chapter provides a thorough review of nanomaterials that were used during this study, their characteristics and applications, the electrospinning process, types and properties of different electrospun fibers, their bio-compatibility, the function of scaffolds, their applications in the nervous system, properties of astrocytes, existing knowledge on the significance of astrocytes, different characterization techniques, and their importance.

Carbon is one of the most common elements in our ecosystem, and depending on its morphology, carbon is capable of exhibiting a variety of characteristics. The next few sections will discuss the morphology and characteristics of carbon, its impact in the biomedical field, and its applications.

2.1 Nanomaterials

Nanomaterials have unique benefits that can be applied to solve multifaceted challenges based on neuro-protective and regenerative therapies. They can be used in the following applications [11]:

- Carriers that provide particular advantages for neuro-protection.
- Targeted drug delivery.
- Potential material to cross barriers like the blood spinal cord barrier and cell membrane walls.
- Potential material for attaching targeting moieties.
- Reactive oxygen species (ROS) scavengers.
- An aid for regeneration by providing a growth-permissive environment, blocking inhibitory factors, and promoting neurotrophic factors.

- Scaffolds to mimic the natural cell environment and influence cellular growth, differentiation, and proliferation.

2.1.1 Fullerene

In 1985, Smalley and his research group at Rice University developed a very stable cluster consisting of 60 carbon atoms by vaporizing graphite using a laser irradiation method. They developed geometric cage-like structures of carbon atoms that were composed of hexagonal and pentagonal faces. The first, closed, convex structure thus formed was the C_{60} molecule, also known as fullerene, named after the architect known for designing geodesic domes, R. Buckminster Fuller. Commonly referred to as a bucky balls, fullerenes are condensed ring aromatic compounds with extended pi systems and unique cage structures. As shown in Figure 2.1, they are very small in diameter—about 1 nm. Some have tried to image fullerenes and only a few have succeeded. One such image by Delago et al. is shown in Figure 2.2, where the fullerene is budding out of a carbon nanotube backbone [12-14].

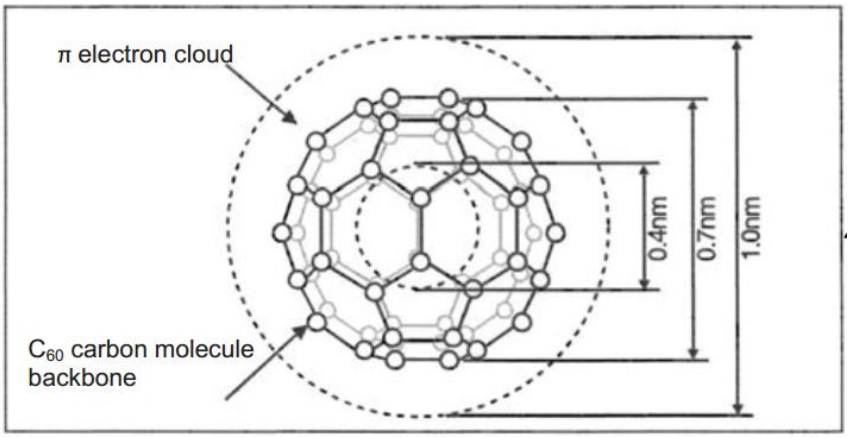

Figure 2.1: Schematic diagram showing the size of a fullerene (original data copyrights belong to Otsuka Co., Ltd.).

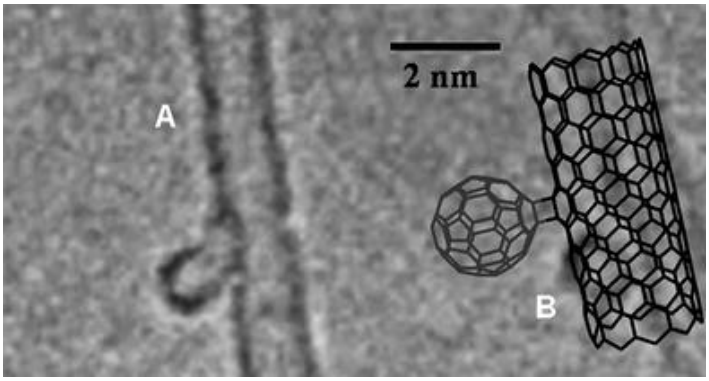

Figure 2.2: Fullerene budding out of carbon nanotube backbone [15].

2.1.1.1 Physical Characteristics of Fullerene

Ever since the discovery of fullerene, there has been a wave of research to study its properties. The physical properties of the fullerene C_{60} are provided below [16, 17]:

Density: 1.65 g /cm^{-3}

Standard Heat of Formation: 9.08 kcal/mol

Index of Refraction: 2.2 (600 nm)

Boiling Point: Sublimes at 800 K

Resistivity: 1,014 ohms m

Crystal Form: hexagonal cubic

Vapor Pressure: 5 x 10^{-6} torr at room temperature and 8 x 10^{-4} torr at 800 K

Organoleptic Properties:

Appearance: Soot/very finely divided black powder fullerite/brown-black powder

Odor: odorless

2.1.1.2 Biological Characteristics of Fullerene

The C_{60} molecule and others in the fullerene family have exquisite photo-, electro-, chemical, and physical properties, which make them appealing in different biological fields. One of the most extensively researched characteristics of fullerene is its radical scavenging properties.

Apart from the fact that it has been used as a carrier for gene and drug delivery systems, serum protein profiling, anti-viral functions, etc., fullerene has the capacity to fit inside the hydrophobic cavity of human immunodeficiency virus (HIV) proteinase (HIV-P) and hence can inhibit the access of substrates to the catalytic site of the enzyme. According to researchers, including Mashino et al., some fullerene derivatives can inhibit HIV-reverse transcriptase and hepatitis C virus replication. They can either be cationic, anionic, or amino acid type fullerene derivatives. Of these, the amino acid type derivatives are most active. It is interesting to note that the anionic fullerene derivatives show antioxidant properties, whereas cationic fullerene derivatives have antibacterial and anti-proliferative activities [18-20].

Some fullerene compounds can exhibit antiviral activity and have a number of applications in the field of medicine and pharmaceuticals. These antiviral compounds can be used to suppress replication of the HIV. C_{60} fullerenes and their derivatives may be used for the treatment of HIV infection. The unique molecular architecture of fullerenes contributes to their antioxidant activity. They can inhibit by forming a complex with HIV-P. Molecular structures of fullerene derivatives are shown in Figures 2.3(a). Cationic and anionic derivatives of fullerene [20] are shown in Figure 2.3(b).

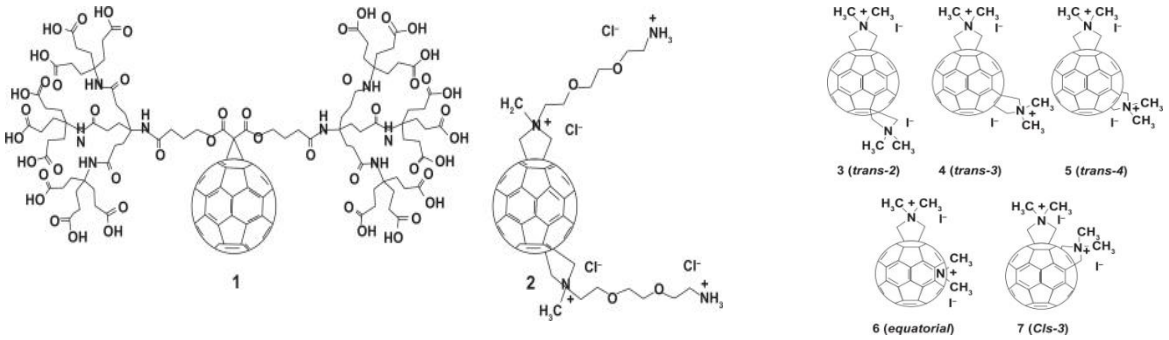

(a) (b)

Figure 2.3: (a) Molecular structures of fullerene derivatives that inhibit and make a complex with HIV-P; (b) structures of fulleropyrrolidines [13, 21]

Fullerenes have gained considerable attention due to their anti-oxidant and radical scavenging properties. Reactive oxygen species are basically oxygen-based molecules formed as a by-product of aerobic cell metabolism in an organism and contribute to the process of ageing. ROS can lead to oxidative damage of deoxyribonucleic acid (DNA), lipids, and proteins. The free-radical theory plays a large role in modern biological concepts of aging [22, 23]. According to D. Harman in 2006, among others, the free-radical theory states that organisms age because they accumulate free radicals (an atom/molecule with an unpaired electron in the outer shell), which damage healthy cells over a period of time. Antioxidants can retard senility [24-27]. Fresh vegetables, fruits, red wines, and spices do the same thing to stimulate longevity. This process is largely determined by the existence of compounds such as deprotonated xanthones [28], carotenoids [28], anthocyanins and pyranoanthocyanins [29], and flavonoids and terpenoids [30].

According to research by Krusic et al. in 1991, fullerenes have one of the world‘s most efficient radical scavenging properties [31] They have a large number of conjugated double bonds and the lowest unoccupied molecular orbital, which can easily take up an electron, thus making the possibility of an attack of radical species highly favorable. Up to 34 methyl radicals can be added onto a single C_{60} molecule. Fullerenes can react with many superoxides (O_2^-) without being consumed in the catalytic process. They are considered to be the most-efficient radical scavengers in the world, localizing within the cell mitochondria and other cell compartment sites where the production of free radicals takes place [20]. Lipids, which are the major constituent of cell walls, degrade by the oxidation process, known as lipid peroxidation. Free radicals (atom/molecule having unpaired electrons $HO^{\bullet}$ $OOH^{\bullet}$) bond with lipids in the cell membrane and results in cell damage. Research conducted by Wang et al. showed that C_{60} showed higher protection from lipid peroxidation than Vitamin E [32].

According to research by Yadav and Kumar, fullerene's geroprotective activity is higher than those of the most powerful ROS scavengers [33]. According to Chistyakov et al. [34], C_{60} has the ability to acquire a positive charge by being absorbed inside several protons, and this complex can infiltrate into mitochondria. There is a mild uncoupling of respiration and phosphorylation (addition of a phosphate group to a protein thereby altering its property), which leads to a decrease in ROS production.

In in-vivo treatments, the antioxidant behavior of fullerenes has extended the lifespan of geriatric mice as well as improved their advanced-age cognition. Certain water-soluble fullerenes are capable of catalytically removing potentially harmful oxidant species, acting as a synthetic analogy to naturally occurring superoxide dismutase. As a result, water-soluble fullerenes (such as C_{60} pyrrolidine tris-acid) are explored for applications in therapies against a variety of degenerative conditions involving an excess of ROS [35].

According to some researchers, $C_{60}(OH)_{24}$ pre-treatment maintains redox homeostasis directly (due to its action as a free-radical scavenger) or stimulates an increase in antioxidant enzyme activity. Gharbi et al. [36] reported protection against CCl_4 free-radical-mediated liver damage by C_{60}. The protective effect of $C_{60}(OH)_{24}$ against doxorubicin toxicity is better than that exhibited by vitamin C, as reported by Injac et al. [20, 37]. Another budding medical application of C_{60} in photodynamic therapy is related to the photoexcitation of fullerenes, which can be excited from the ground state to a higher state ($^1C_{60}$) by radiating with photons. The state $^1C_{60}$ is then converted to $^3C_{60}$ via an intersystem crossing and has a longer life (Figure 2.4).

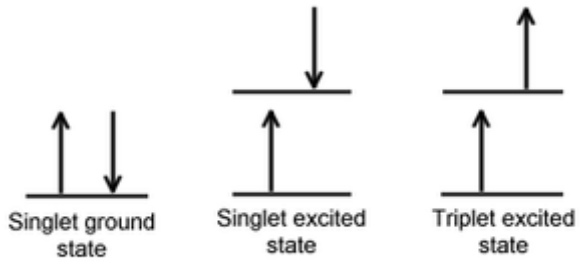

Figure 2.4: Fullerene photoexcitation via intersystem crossing

Fullerene can decay from its triplet state to its ground state in the presence of molecular oxygen, there by transferring its energy to O_2 and generating singlet oxygen $^1O_2$, which is known to be highly toxic. The $^1C_{60}$ and $^3C_{60}$ states are excellent acceptors and, in the presence of a donor, can undergo a different process. Fullerene also conjugates with different functional groups, possessing biological affinity to nucleic acids or proteins, which is being investigated for anticancer activity and genetic engineering, including DNA cleaving [38].

Fullerene has been widely studied for potential drug delivery applications. The direct delivery of drugs and biomolecules through cell membranes into cells can be a challenge. The passage of any compound into the nucleus of a cell is a major task because its passage is limited by at least three membrane barriers (cell membranes). It is vital to fully understand the mechanism through which carriers can enter cells. There are four major groups of drug and gene carriers: organic cationic compounds, viral carriers, recombinant proteins, and inorganic nanoparticles. Fullerene derivatives have the capacity to cross cell membranes and bind to the mitochondria, as discussed previously [39, 40]. Modified fullerenes have the potential to provide a slow-release system (lipophilic), which can be significant for anticancer research. A lipophilic (ability to dissolve in lipids), slow-release, drug delivery system enhances therapeutic efficacy in tissue culturing [41]. According to research by Rasmussen et al., the ability of fullerenes to penetrate through intact skin is broadening their research in cellular drug and gene delivery [42].

2.1.1.3 Fullerene and the Nervous System

The effect of fullerene on the central nervous system has been studied by researchers and neuro scientists. According to Yamada et al. [43], fullerenes have potential uses as materials in novel medical devices targeting the brain. They concluded that fullerene did not cross the blood-brain barrier, and the intracerebral injection of C_{60} affected neurotransmission in the brains of mice, thus improving their locomotion. Tykhomyrov et al. [44] studied the protective effect of fullerenes against oxidant-mediated damage within the brain. Here hydrated C_{60} was used to protect a rat brain against alcohol impact. They showed that administration of aqueous solutions of hydrated C_{60} fullerenes (C_{60}HyFn) with a C_{60} concentration of 30 nM as drinking water during chronic alcoholization of rats did the following: (a) protected tissues of the central nervous system from damage caused by oxidative stress with high efficacy; (b) prevented the pathological loss of both astrocytes (main cells of the CNS) and the astrocytic marker (GFAP); and (c) due to their adaptogenic effects, significantly improved the behavioral response and eliminated emotional deficits induced by chronic alcohol uptake. The wide range of beneficial biological effects, zero-toxicity, and efficacy, even in super-small doses, provide a rationale for the possible application of C_{60}HyFn for the treatment of alcohol-induced encephalopathy as well as alcoholism prophylaxis.

Dugan et al. [45] showed that carboxyfullerenes show vigorous neuroprotection against excitotoxic, apoptotic, and metabolic insults in cortical cell cultures. According to their research, systemic administration of the carboxyfullerene isomer can delay motor deterioration and death in a mouse model with familial amyotrophic lateral sclerosis (ALS). Current studies in other animal models of CNS disease show that these novel antioxidants are potential neuroprotective agents for other neurodegenerative disorders, including Parkinson's disease. Carboxyfullerenes, C_{60}, have

demonstrated potent free-radical scavenging properties and neuroprotective effects against two forms of apoptosis through reduction of hydroxyl radical and superoxide radical concentrations [46]. Several studies with implications of spinal cord injury have been performed to better characterize the neuroprotective potential of fullerenes. According to Jin et al., C_{60} derivative fullerenols were shown to be effective neuroprotectors by blocking glutamate pathways and reducing intracellular Ca^{2+} [47]. Another study using ebselen, which is another potent scavenger of hydroperoxides, demonstrated that covalently bonded C_{60}-ebselen derivatives were more effective than C_{60} alone, ebselen alone, or a combination of the two agents in preventing cell injury in an H_2O_2 challenge model of cell injury [48].

2.1.1.4 Toxicity of Fullerene

According to previous research involving cancerous cells pristine fullerenes have shown very-low toxicity levels and no reported risks to biological systems. But as is the case, most available studies only mention the short-term risks. There is very little or no data that talks about the long-term risks of fullerene [43, 45, 49]. The present effect of fullerene on biological systems cannot be extrapolated to predict long-term risks. Contrary to what is discussed in the previous section relative to biological characteristics, fullerene can be extremely cytotoxic. A number of investigators have demonstrated that fullerenes are capable of causing toxicity that is determined by the stimulation of an inflammatory response and an oxidative stress. According to another study, the pulmonary exposure, intraperitoneal exposure, dermal exposure, oral administration, and intravenous injection were assessed. The cytotoxicity of fullerols (polyhydroxy fullerene) was observed to be enhanced with ultraviolet A (UVA) and visible light exposure during treatment, illustrating that there is a photosensitive aspect to fullerol toxicity. The potential for fullerene internalization, enhanced ROS production, and interactions with cellular components was

highlighted within this study. Nielsen et al. [50] acknowledged that fullerenes are able to absorb ultraviolet or visible light to stimulate the generation of ROS and to ultimately increase their toxic potency through the promotion of oxidative-mediated damage. The contribution of photocatalytic reactions to fullerene toxicity has been a focus of a number of previously discussed studies [51, 52]. This phenomenon has been exploited within the destruction of tumors in mice, but more work is required to determine the specificity of the response and how this may be exploited within the treatment of humans. In addition, the uptake of fullerenes by cells will be addressed, because this has the ability to promote not only their cell-clearance but also their toxicity. Nonetheless, out of the available knowledge, it is possible to make an educated estimation of the concentration of fullerene used so that no cytotoxic harm is posed.

2.1.1.5 Other Applications of Fullerene

The production of fullerenes and their use in consumer products is expected to increase in future. Apart from biological applications, fullerenes have many other applications: In materials science, the rich electronic and electrochemical behavior of C_{60} has generated great expectations. C_{60} is insoluble or only sparingly soluble in most solvents and aggregates very easily. The major areas of applications (but still too expensive) of inorganic electronics and bioscience include the following [13, 14]:

- Electrical conductivity of alkali-doped C_{60}: K_2C_{60} is an insulator, but K_3C_{60} becomes a superconductor at 18K, and Rb_3C_{60} becomes a superconductor at 30K.
- Catalysts for hydrocarbon upgrading: This includes the conversion of heavy oils and methane into higher hydrocarbons.
- Pharmaceuticals: Derivatives of C_{60} are highly hydrophobic and antioxidants (ability to soak cell-damaging free radicals) and hence can be used as protease inhibitors.

- Battery anodes.
- Proton transport membranes.
- Bucky films.
- A sharper scanning microscope.
- Sporting goods, such as badminton racquets that have fullerenes incorporated into the polymer matrix composite.
- Cosmetics, such as the Vitamin C_{60} skin creams.

2.1.2 Carbon Nanotubes

The discovery of carbon nanotubes (CNTs) has been controversial. According to popular knowledge and as cited in numerous journals, carbon nanotubes were discovered independently in Japan by Ijima and Ichihashi [53] and in California by Bethune et al.[54] and published in the journal *Nature* in 1993. A controversial image of a carbon nanotube was published in a paper in 1976 by Oberlin et al.[55] and by Russian researchers in 1952 The transmission electron microscopy imaging technique was not very advanced to support data at that time. The popularity of the papers in 1993 was due to the pre-existing popularity of fullerenes, the ability of the scientists and researchers to comprehend the term "nano," and the advanced imaging techniques to provide concrete scientific data. Carbon nanotubes are tube-shaped materials composed of sp^2 bonded carbon with a diameter in the nanometer scale ranging from <1 nm up to 50 nm [11]. Their lengths are typically several microns, but recent advancements have created nanotubes that are much longer and measured in centimeters [56]. A nanotube is basically a rolled-up graphite layer with a continuous, unbroken, hexagonal mesh with carbon molecules at the apexes of the hexagons (Figure 2.5) [53-55].

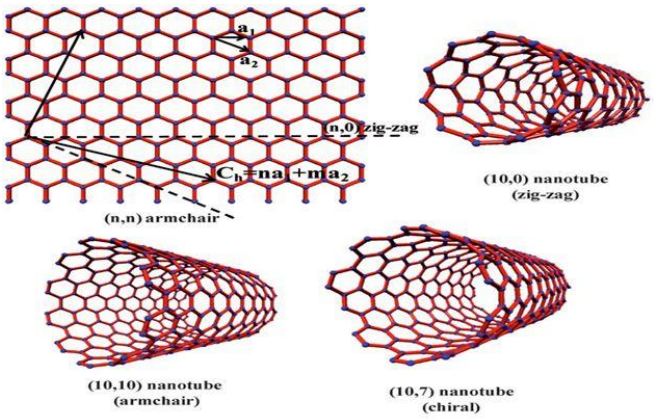

Figure 2.5: Computerized images of different configurations of multi-walled carbon nanotubes [57].

2.1.2.1 Physical Characteristics of Carbon Nanotubes

Carbon nanotubes have multiple structures, differing in length, thickness, type of helix, and number of layers. Although they are essentially formed from the same graphite sheet, their characteristics differ depending on these variations, especially electrical properties [58].

The physical and mechanical properties of carbon nanotubes depend on the number of walls and their different orientations (arm-chair, zigzag, chiral):

- Young's Modulus—single-walled carbon nanotube (SWCNT): 0.9–1 TPa; multi-walled carbon nanotube (MWCNT): 0.2–0.9 TPa [59, 60].
- Tensile Strength—SWCNT: 13–126 GPa; MWCNT: 11–150 GPa [59, 60].
- Electrical Properties—These depend on the orientation, which in turn depends on whether they have metallic or semiconductor properties. Theoretically, metallic nanotubes can carry an electric current density of 4×10^9A/cm^2, which is more than 1,000 times greater than those of metals, such as copper. For copper interconnects, current densities are limited by electromigration [61-63]. Ballistic conduction is applicable to both electrons (holes and phonons) and can affect both electrical and thermal conductivity, which is the unimpeded flow of charge, or energy-carrying particles, over relatively long distances in a

material. This means that the mean free path is longer than the dimensions of the material. Conduction speeds can attain relativistic speeds [61, 63-65].

- Thermal Stability—2,800ºC (vacuum); 750ºC (air).

2.1.2.2 Biological Characteristics of Carbon Nanotubes

From a biological point of view, the properties of carbon nanotubes do not depend on their orientations. An important property of nanotubes is that they can easily penetrate membranes such as cell walls. Their long and narrow shape makes them look like miniature needles, which enables them to function like a needle at the cellular level. Medical researchers are using this needle-like property by attaching molecules that are attracted to cancer cells to nanotubes to deliver drugs directly to diseased cells [4]. Also, electrical resistance of the nanotube changes significantly when other molecules attach themselves to the carbon atoms. Researchers are using this property to develop highly sensitive sensors that can detect chemical vapors such as carbon monoxide or biological molecules at the nano level [66]. Nanotubes bound to an antibody produced by chickens have been shown to be useful in laboratory tests to destroy breast cancer tumors. The antibody that carries those nanotubes is attracted to proteins produced by one type of breast cancer cell. The nanotubes are then used to absorb light from an infrared laser, which incinerates the nanotubes and subsequently the tumor cells [67].

An inexpensive nanotube-based sensor can be used to detect bacteria in drinking water. Antibodies sensitive to that particular bacteria bind to the nanotubes, which are then deposited onto a paper strip [68]. According to studies conducted by Pantarotto et al., functionalized CNTs are able to cross cell membranes and accumulate in the cytoplasm, even reaching the nucleus, without being cytotoxic (in concentrations up to 10 mM) [69].

Because of their size and morphology, CNTs are excellent for transporting and translocating therapeutic molecules. They can be functionalized with bioactive peptides, proteins,

nucleic acids, and drugs, and used to effectively deliver these chemicals to different organs; hence, they can be used to develop new and efficient drug delivery systems. Many functionalized CNTs exhibit low toxicity and are not immunogenic (body does not produce any immunity when it comes in contact with these chemicals); therefore, such systems hold great potential in the field of nanobiotechnology and nanomedicine [70, 71].

According to research by Dai et al. [72], functionalization of CNTs without affecting the conjugate bonds is an important aspect of preserving its basic structure. They developed a simple and general approach to non-covalently functionalize and subsequently immobilize various biological molecules onto nanotubes. The mechanism of protein immobilization on nanotubes involves the nucleophilic substitution of N-hydroxysuccinimide by an amine group on the protein, resulting in the formation of an amide bond. This unique physical property of molecular-scale or nanoscale solids (dots or wires), when utilized in conjunction with the remarkable biomolecular recognition capabilities, could lead to miniature biological electronic devices, including probes and sensors. Research conducted by Zanello et al. [73] shows the possibility of using CNTs to develop bone graft materials and techniques. Here they have shown a promising biocompatibility with osteoblast cells, appearing to modulate the cell phenotype Abarrategi et al. [74] studied the use of MWCNT/chitosan (CHI) scaffolds composed of a major fraction of MWCNT (up to 89 wt%) and a minor fraction of CHI to form a well-defined micro-channel porous structure. They performed in vitro assays of cell adhesion, viability, and proliferation onto the external surface of MWCNT/CHI scaffolds with myoblastic mouse cells, which is a multipotent cell line able to differentiate towards different phenotypes under the action of some chemical or biological factors. It has also been reported that CNTs could be very efficient as free-radical scavengers [72]. Watts et al. [75] reported that MWCNTs and boron-doped CNTs could act as antioxidants. He explained

that the acceptor-like electronic properties of CNTs were mainly responsible for the radical termination. Fenoglio et al. also demonstrated that MWCNTs exhibit a remarkable scavenging capacity against an external source of hydroxyl or superoxide radicals [76, 77].

2.1.2.3 Carbon Nanotubes and the Nervous System

The electrical properties of nanotubes can provide a mechanism to monitor or stimulate neurons through artificial scaffolds. The ease with which carbon nanotubes can be patterned makes them attractive for studying the organization of neural networks and has the potential for developing new devices for neural prosthesis and spinal cord implants.

In the work of Lovat et al., the possibility of using CNTs as potential devices to improve neural transfers while supporting dendrite elongation and cell adhesion was tested [78]. CNTs used for neuronal growth were first functionalized, allowing uniform solvation, and then deposited onto a glass substrate. Following evaporation of the solvent, CNTs were defunctionalized by thermal treatment—generating glass coverslips covered by a film (i.e., a nano meshwork) of native/non-functionalized CNTs. This strategy allowed a long-term and stable retention of CNT films on glass and, moreover, long-term neuronal cell survival in culture. They reported that neuronal circuits on CNT grids significantly increased network activity (Figure 2.6). The authors speculated that CNTs might provide a bidirectional electrotonic current transfer, causing a redistribution of charge along the surface of the membrane, ultimately increasing neuronal excitability. It is interesting to note that several electrophysiological membrane properties measured on the cultured hippocampal neurons did not indicate the occurrence in these cells of changes in ionic conductance brought about by the CNT layers directly [79].

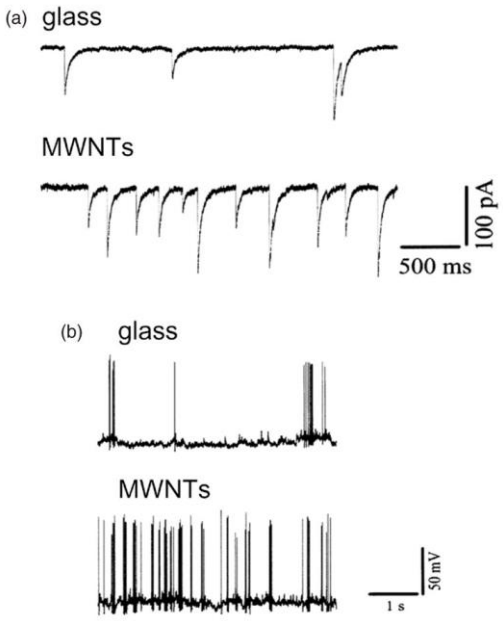

Figure 2.6: CNT substrate affecting synaptic activity and neuronal excitability. Compared to neurons grown on glass coverslips, neurons grown on MWCNT-based substrate display increase in frequency of (a) spontaneous post-synaptic currents, and (b) "firing rate" [78].

A prerequisite for exploiting CNTs in such biomedical devices is to understand their actions on neurons, especially with respect to neuronal excitability, changes in ionic conductance, effect on glial cells, and intercellular signaling via synaptic transmission. Park [80] was the first to show that SWNTs can block ion fluxes through potassium ion channels expressed in a cell line. The exact mechanism is unknown but the author speculated that the CNTs blocked the channel pore and interrupted ion permeability. According to Ni et al.[81], SWNTs caused a significant impairment in cytoplasmic Ca^{2+} elevation when neurons were depolarized, which might be due to CNTs interfering with the functioning of Ca^{2+} channels [81]. Benabid et al. developed CNS implantation to control motor disorders [82]. Among others, Nuttin et al. [83] and Mayberg et al. [84] tried to control the drug resistant psychiatric conditions and to translate willful brain processes into specific actions through the control of external devices [83-86]. Thus, these results caution that CNTs used as a structural component in biological applications could inadvertently affect the

activity of cells with which they come into contact. In another research by Gottipati et al. [87], SWCNT films were used to modulate the morpho-functional and proliferative characteristics of astrocytes. They were able to grow astrocytes with decreased immune-reactivity of glial fibrillary acidic protein, thereby reducing astrogliosis. Mattson and his research group [88] developed embryonic rat-brain neurons on MWCNs. On unmodified nanotubes, neurons extended only one or two neurites, with very few branches. In contrast, neurons grown on nanotubes coated with the bioactive molecule 4-hydroxynonenal exhibited multiple neurites, with extensive branching. These findings establish the feasibility of using nanotubes as substrates for nerve cell growth and as probes for neuronal function at the nanometer scale.

2.1.2.4 Toxicity of Carbon Nanotubes

As discussed earlier, a CNT is a hollow cylinder formed by rolling graphite sheets. The bonding type is basically sp2. The circular curvature causes quantum confinement and $\sigma - \pi$ rehybridization in which three σ bonds are slightly out of plane and for compensating for the fact that the π orbital is slightly out of plane too. This makes nanotubes mechanically stronger, electrically and thermally more conductive, and chemically and biologically more active than graphite [89]. The cell toxicity of CNTs can be attributed to a variety of issues, namely metal impurities, surface area, dispersion, length and size distribution and aggregation status, coating or functionalization, immobilization, cellular uptake or internalization, and the cell type [90].

Several investigations in the past have demonstrated that single-wall carbon nanotubes present a noticeable cytotoxicity to human and animal cells, while multiwall carbon nanotubes not only show a more moderate toxicity than SWCNTs but sometimes act as suitable sites for the proliferation of bacteria. Several sources of contaminants cause toxicity in SWCNTs and MWCNTs. Carbonaceous contaminants in SWNTs contain amorphous carbon and graphitic

nanoparticles, and metallic contaminants typically contain metal catalysts. During the process of producing CNT nickel is done in combination with yttrium, which is used as a catalyst for the arc-discharge and induces toxicity in the nanopowder. Other SWNT purification methods based on oxidation may introduce functional groups. Currently, less-rigorous purification techniques are applied, for example, filtration, centrifugation, and chromatography.

In several studies, CNTs were suspended in a cell culture medium. Research has been done on a variety of cells, namely human fibroblast cells, the mesothelioma cell line, lung tumor cell lines, human skin fibroblast cell lines, human embryonic lung fibroblast cells, stem cells, and mouse fibroblast cells. It was shown that there was cytotoxic effect of CNTs on all these cells [91-95].

On the other hand, some studies where the CNT was immobilized by putting it in a substrate or by chemically modifying it or woven into a scaffold showed no cytotoxic effect. Research was done on MWCNTs and hydroxyapatite, CNTs and collagen, and CNTs with polystyrene and tested on human and mouse fibroblast cells, osteoblast mesenchymal cells, neurons, and smooth muscle tissues [73, 96-102]. Research conducted by Correa-Duarte et al. [103] shows a very interesting novel technique. They developed 3D scaffolds entirely of MWCNTs, prepared by inducing capillary forces upon the nanotubes chemically. The MWCNTs underwent a drastic transformation from being vertically aligned to an interlocking resistive network, to form a 3D sieve architecture. Despite several studies showing the toxicity of MWCNTs, this morphology favored the extensive growth and proliferation of the mouse fibroblast cells L929. MWCNT-based 3D networks possess structural integrity and stability to retain shape in vivo, along with strong mechanical strength to support developing tissue and withstand in vivo

forces. They could serve as matrices to restore, maintain, or reinforce damaged or weakened tissues or act as drug delivery devices.

Mechanisms of CNT-Induced Toxicity

If CNT's enter the body via inhalation, or dermal or oral routes, toxicity is induced by different methods, such as malignant transformation, oxidative stress or inflammatory responses, DNA [104] damage and mutation, formation of granuloma, and interstitial fibrosis (Figure 2.7).

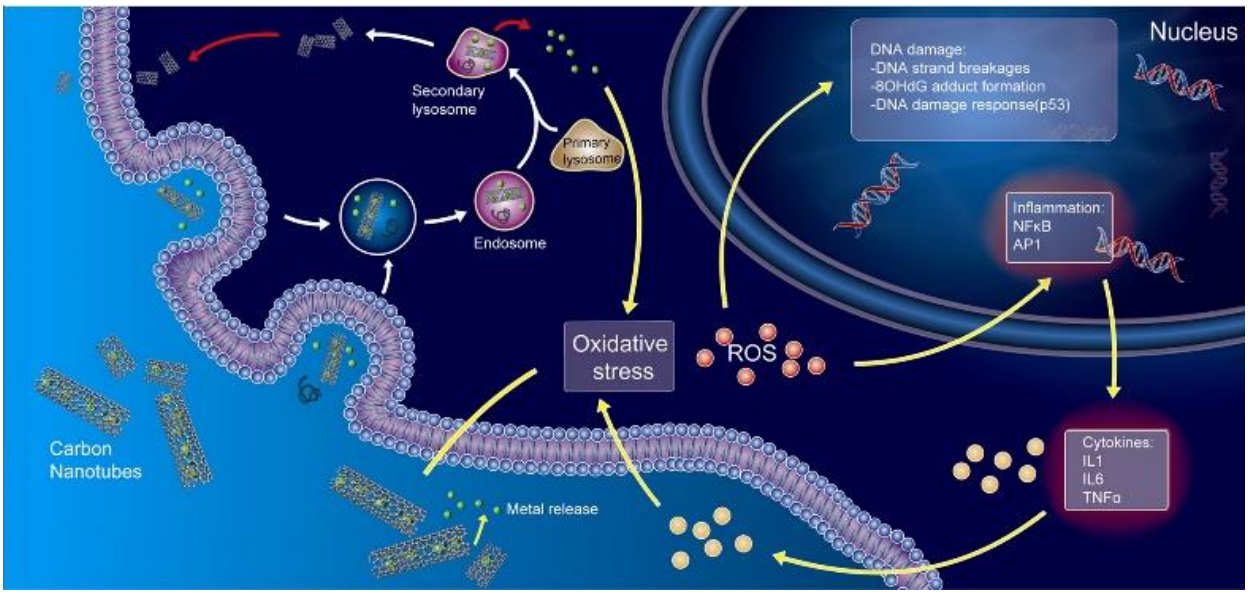

Figure 2.7: Mechanisms though which CNTs induce cell damage [105].

Oxidative Stress: This has been regarded as the most acceptable mechanism of CNT-induced toxicity. Increased intracellular ROS reacts with cellular macromolecules such as DNA, proteins, and lipids and disturbs the homeostasis of the intracellular atmosphere. As discussed in the previous section, CNTs are contaminated by the presence of transition metals that are used as catalysts during the production process. Therefore, metals released from CNTs have the capacity to cause the conversion of cellular oxygen metabolic products such as H_2O_2 and superoxide anions to hydroxyl radicals.

Surface Area: In many cases it has been reported that the availability of a high surface area induces the generation of ROS [106].

Intraperitoneal Injection: When MWCNTs were injected intraperitoneally into mice, inflammation was observed In vitro MWCNTs were able to activate the signaling pathway to increase the secretion of cytokines and chemokines that promote inflammation. Basically, CNTs develop a robust pulmonary inflammatory response culminating in the development of multifocal granulomatous pneumonia and interstitial fibrosis. Exposure of lung fibroblasts to SWCNTs resulted in an increase in cell proliferation and collagen production without producing cell damage [107, 108]. The mechanisms by which CNTs induce cell damage and inflammation are depicted in Figure 2.7.

Genotoxicity: This deadliest cause of cytotoxicity occurs when CNTs can enter the cytoplasm and localize within the cell nucleus and cause cell mortality by activating the tumor-suppressor protein. High-purity SWCNTs induced DNA strand breakage [75, 109, 110].

2.1.2.5 Other Applications of Carbon Nanotubes

The integration of biomaterials with CNT's encourages the use of hybrid systems as active field-effect transistors or biosensor devices. They have several applications, most of which are still under research. Double Walled Carbon Nanotubes of high fibers have been developed. (Figure 2.8). Researchers at NASA are developing a CN-based composite that bends when a voltage is applied to it. Only electrical voltage will be required to change the shape (morphing) of aircraft wings and other structures [66, 111].

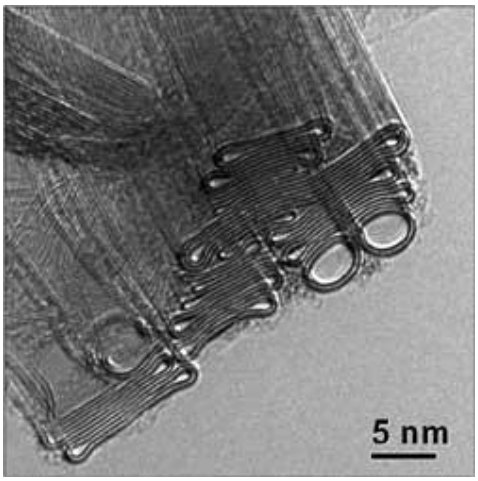

Figure 2.8: Auto-collapsed DWCNTs of high-performance fiber [112].

Researchers have found that carbon nanotubes can also be used to fill voids that occur in conventional concrete. Voids allow water to penetrate into concrete, resulting in the formation of cracks. Nanotubes can be used to stop cracks from forming, thus substantially increasing the life of the concrete [111]. Lightweight windmill blades can be made with an epoxy containing carbon nanotubes. The increase in the strength and reduction in the weight provided by the use of this nanotube-filled epoxy, allows longer windmill blades to be used, in turn increasing the amount of electricity generated by each windmill [111]. By using carbon nanotubes as pores in reverse osmosis membranes, the power needed to run reverse osmosis desalination plants can be decreased. This is because water molecules pass through carbon nanotubes more easily than through other types of nanopores since their inner walls are much smoother that other types of nanopores [67]. Other applications of CNs include the following [58, 113]:

- Electronics (wires, transistors, switches, interconnects, memory storage devices)
- Opto-electronics (light-emitting diodes, lasers)
- Sensors
- Field emission devices (displays, scanning electron probes, microscopes)

- Batteries/fuel cells
- Fibers/reinforced composites
- Medicine/biology (fluorescent markers for cancer treatment, biological labels, drug delivery carriers)
- Catalysis
- Gas storage

2.1.3 Graphene

Graphene was first discovered by Andre Geim and Konstantin Novoselov at the University of Manchester in 2004[114]. Graphene is a single-atom-thick sheet of sp^2-bonded carbon atoms in a closely packed honeycomb two-dimensional (2D) lattice with a very thin atomic thickness (0.345 nm) as shown in the schematic in Figure 2.9 and the scanning electron microscopy (SEM) image in Figure 2.10. It has three sigma bonds in one plane attached to neighboring carbon atoms and one pi bond oriented out of plane. This unique form of carbon in which the atoms are arranged in a hexagon is the thinnest and strongest material in the world. It is one of the most fascinating nanostructures, having unique physical, chemical, electrical, and mechanical properties, which qualify it as a promising nanomaterial in areas such as high-energy physics, material science, and a wide range of technological applications, such as bioelectronics and biosensing [114].

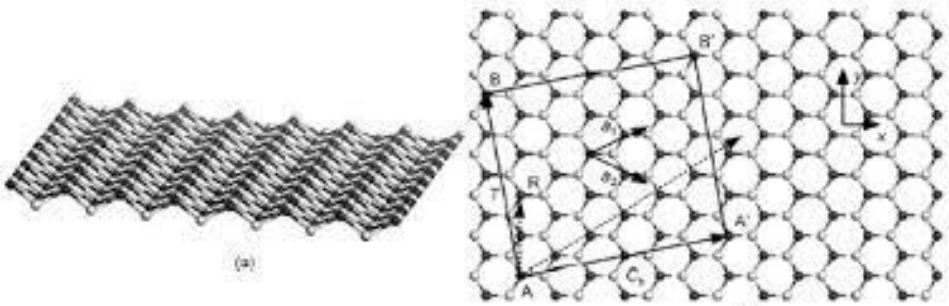

Figure 2.9: Graphene linkage [115]

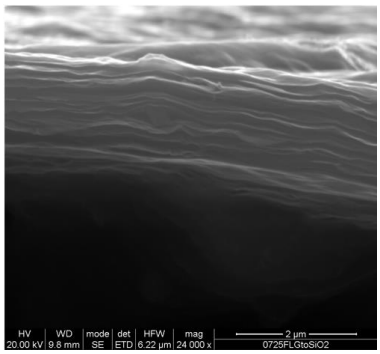

Figure 2.10: SEM image of cross section of graphene sheets.

2.1.3.1 Physical Characteristics of Graphene

Graphene can conduct electricity better than copper, and it is able to transfer heat better than any other material. In addition, it is transparent. Some of its properties are similar to those of carbon nanotubes [116]. Graphene is a zero-overlap semi-metal that has both holes and electrons as charge carriers, thereby giving it very high electrical conductivity. Highly mobile electrons in the p_z orbital, which are located out of plane, make it highly conductive. The electronic properties of graphene are dictated by the bonding and anti-bonding (valance and conduction bands) of the pi orbitals.

Graphene is a zero-band-gap semiconductor. In graphene, the Dirac point, electrons, and holes have zero effective mass because the energy-movement relation is linear for low energies near the six individual corners of the Brillouin zone, known as the Dirac fermions. Due to the zero density state at Dirac points, electronic conductivity is low. However, the Fermi level can be changed by doping to create a material that has better conductivity.

The electronic mobility of graphene is very high. Some previously reported results have indicated this to be 15,000 $cm^2V^{-1}s^{-1}$ and theoretically potential limits of 200,000 $cm^2V^{-1}s^{-1}$ (limited by the scattering of graphene's acoustic photons). Graphene electrons act like photons due to their lack of mass. These charge carriers are able to travel submicrometer distances without

scattering due to ballistic transport [114, 117, 118]. In the absence of any impurities or imperfections, the strength of graphene is solely dictated by the strength of its carbon bonds, which are 0.142 nm long. This makes graphene the strongest material ever discovered, with an ultimate tensile strength of 130 GPa. It has a very high specific strength due to its weight, which can be as low as 0.77 mg/m^2. This is important because graphene also contains elastic properties, being able to retain its initial size after strain. Atomic force microscopic tests on graphene sheets (with thicknesses between 2 and 8 Nm) have shown them having spring constants around 1–5 N/m and a Young's modulus of 0.5 TPa [119-121]. Despite the very stable structure, carbon atoms in graphene are all chemically accessible because of sp^2 hybridization. Covalent chemistry provides a powerful pathway to tailor the physical properties of pristine graphene, making graphene stronger and more attractive than other materials [122].

Graphene has very good aqueous processibility, amphiphilicity, surface functionalizability, surface-enhanced Raman scattering, and fluorescence quenching ability. Graphene oxide is also considered a promising material for biological applications. The graphene field effect transistor has been comprehensively studied to develop sensitive chemical sensors and biosensors. Detection of important biomolecules such as nucleic acids, proteins, and growth factors have been successfully demonstrated by using appropriately functionalized graphene derivatives [123-126].

2.1.3.2 Biological Characteristics of Graphene

In single-layered graphene sheets, two sides are exposed to the surface and hence provide more surface area than other previously discussed nanomaterials. According to research by Yang et al. [127], an extremely high tumor passive targeting effect for PEGylated nanographene was likely due to the tumor-enhanced permeability and retention effect, which is attractive for cancer therapy applications. Liu et al. [128] concluded that the passive tumor targeting effect of 2D

nanographene was more efficient than that of one-dimensional SWNTs. This could be important for biosensing devices because, compared to SWCNTs, graphene has higher reproducibility. SWCNTs can have a variety of chiralities within a given sample. According to current estimations, graphene will be widely used in biological applications by around 2030. There are still several questions about its biocompatibility, and it must undergo numerous safety, clinical, and regulatory trials. Nevertheless, it has the potential to revolutionize this area in a number of ways [127-129].

Graphene oxide (GO), produced by vigorous oxidation of graphite using the Hummers method, is an ideal nanocarrier for efficient drug and gene delivery. According to the research of Hu et al. [130], macroscopic freestanding GO and reduced GO paper was prepared from their suspension by a vacuum filtration technique. They concluded that those papers exhibited a strong antibacterial effect.

Liao et al. [131] studied the behavior of NIH-3T3 fibroblasts as a model of mammalian cells growing on a supported film of GO. According to their work, the GO film induced no significantly harmful effects on the mammalian cells with respect to adhesion, and it exhibited remarkably high gene transfection efficiency, which indicated the potential application of GO as a surface coating material for implants. A graphene/chitosan film produced by the solution casting method has also been investigated by Hu et al. as scaffold materials in tissue engineering. Their work indicates that the graphene-based film does not hamper the proliferation of human mesenchymal stem cells but rather accelerates their specific differentiation into bone cells in a controlled manner through the use of growth factors and osteogenic inducers. This suggests the potential use of graphene film for proliferation and transplantation of stem cells and their specific differentiation into muscles, bones, and cartilage for bone regeneration therapy [130, 132].

2.1.3.3 Graphene and the Nervous System

In a study conducted by Li et al. [133], graphene substrates exhibited excellent biocompatibility and promoted the growth of neutrite sprouting and outgrowth in the mouse model of hippocampus. Another area that has become promising is electric field stimulation for a variety of neurological diseases. Heo et al. [134] used non-contact electric field stimulation with a specific strength-to-control cell-to-cell interaction in vitro. Graphene and polyethylene terephthalate (PET) was used to create a non-cytotoxic in vitro graphene/PET film stimulator. A transient non-contact electric field was produced by charge-balanced biphasic stimuli through graphene/PET film electrodes and applied to cultured neural cells. Weak electric field stimulation as low as 4.5 mV/mm at 10 sec duration for 32 min was particularly effective in shaping cell-to-cell interaction. A significant increase in the number of cells forming new cell-to-cell couplings and in the number of cells strengthening existing cell-to-cell couplings was observed. The mechanism was not studied, but it was surmised that altered regulation of the endogenous cytoskeletal proteins fibronectin, actin, and vinculin was responsible for the increase in nutrite growth [129, 133, 134].

Neural stem cell (NSC)-based therapy is widely practiced and provides a promising approach for neural regeneration. A 3D scaffold plays an important role in the clinical application of NSC cell growth and appropriate synergistic cell guidance cues. Again, Li et al. [133] utilized a 3D graphene foam as a novel scaffold for NSCs in vitro. It was found that, in comparison to 2D graphene films, three-dimensional graphene foam (3D-GF) not only supports NSC growth but also keeps cells at an active proliferation state with the up-regulation of Ki67 expression. Phenotypic analysis indicated that 3D-GF can enhance the NSC differentiation towards astrocytes and neurons [129, 135]. Nucleotide bases in single-stranded DNA bind strongly to the graphene surface, which can be greatly weakened after DNA hybridization to form double-stranded DNA. Several different

groups have utilized this phenomenon, as well as the effective fluorescence quenching ability of graphene, to develop novel graphene-based DNA detection platforms to be used in biosensors [136-138]. In another instance Mohanty and Berry [123] for the first time successfully fabricated graphene electronic devices for detection of bacterium, DNA, and proteins Unlike SWCNTs, graphene does not have optical properties, and its application in imaging may need external labels. At the same weight concentration, the optical density of GO in the near-infrared region, which is useful for photo thermal therapy and potentially for photo acoustic imaging, is a few times lower than that of SWNTs (Figure 2.11)[127, 129].

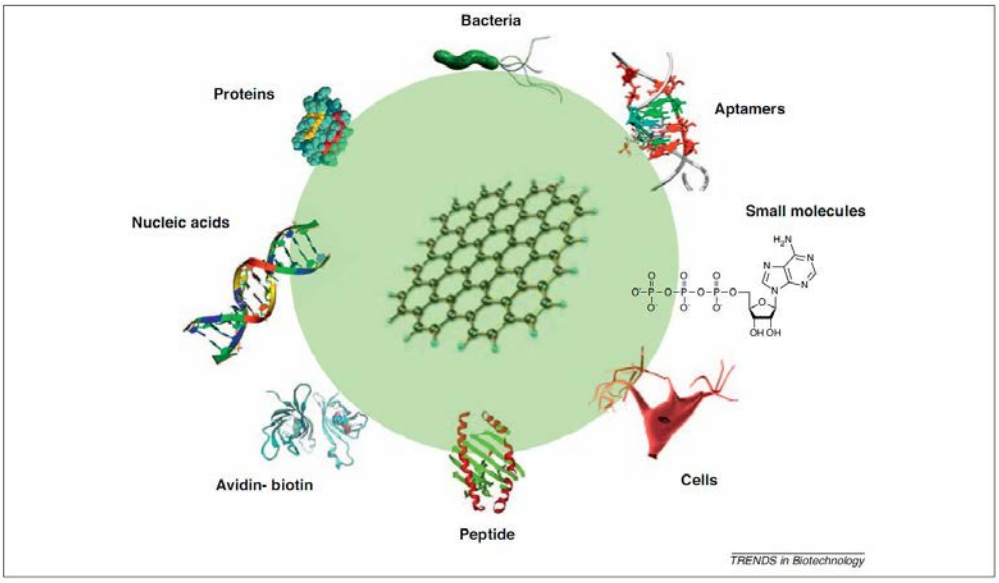

Figure 2.11: Graphene and its derivatives functionalized with avidin-biotin, peptides, nucleic acids, proteins, aptamers, small molecules, bacteria, and cells through physical adsorption or chemical conjugation [129].

2.1.3.4 Toxicity of Graphene

Cytotoxicity, the cellular uptake mechanism, and the intracellular metabolic pathway of graphene and its derivatives remain almost unknown, which are highly important research areas. According to research by Zheng et al. [139] graphene induced an oxidative stress which leads to apoptosis of neural phaeochromocytoma (PC)-derived cells (PC12 cells). In research conducted

by Liao et al. [131], graphene sheets were more damaging to mammalian fibroblasts than were less densely packed graphene oxide. They also found that the cytotoxicity depended on the exposure environment (presence/absence of aggregation) and the mode of interaction (suspension vs adherent cell types). According to Hu et al. [130], the cytotoxicity of graphene oxide arises from the interaction between the cell membrane and the nanosheets [130, 131, 139].

2.1.3.5 Other Applications of Graphene

Due to its recent discovery, graphene is still being analyzed for commercial applications. Scientists believe that it could be used for many different purposes such as the following [14]:

- Transistors
- Transparent conductors
- Surfactants
- Polymer reinforcement
- Biodevices

Recently, similar to that for CNTs, biological applications of graphene sheets and graphene oxide have attracted attention in the scientific community based on their great potential for the following [123]:

- Bacterial inhibition
- Drug delivery
- Photo-thermal therapy

2.2 Cytotoxicity

According to the medical dictionary by Farlex, cytotoxicity means the degree to which an agent possesses a specific destructive action on certain cells. Any substance or materials capable of killing or destroying live healthy cells, which may include snake venom or animal lymphocytes,

are considered cytotoxic [19]. Treating cells with a cytotoxic compound can result in a variety of cell deaths as provided below:

- Necrosis: During this process, cells lose their membrane integrity and die rapidly as a result of cell lysis. Cells undergoing necrosis typically exhibit rapid swelling, lose membrane integrity, shut down metabolism, and release their contents into the environment, as shown in Figure 2.12. Cells that undergo rapid necrosis in vitro do not have sufficient time or energy to activate apoptotic machinery and do not express apoptotic markers [19].

Figure 2.12: Cell undergoing necrosis [140]

- Apoptosis: During apoptosis, first a change in the refractive index of a cell takes place. This is followed by cytoplasmic shrinkage and nuclear condensation. The cell membrane starts showing blebs or spikes, which are protrusions of the cell membrane. Depending on the type of cell, these blebs separate from the dying cell and form apoptotic bodies. They also cease to maintain phospholipid asymmetry in the cell membrane. The mitochondrial outer membrane also undergoes changes that include loss of its electrochemical gradient. Then adjacent cells or macrophages employ phagocytosis to remove apoptotic bodies and the dead cell. There is no inflammatory response as in the previous case. This process is depicted in Figure 2.13 [140].

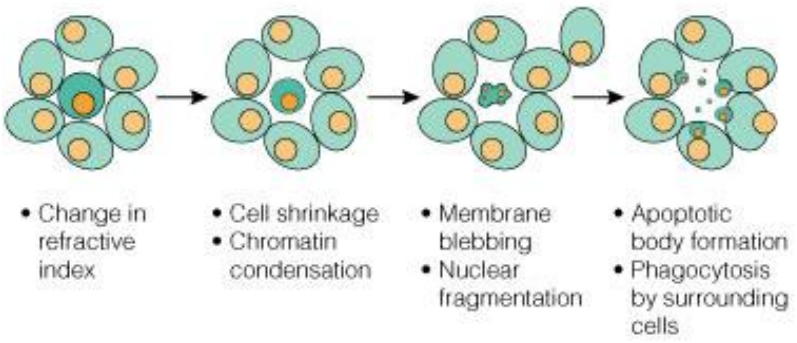

Figure 2.13: Cells undergoing apoptosis [140]

In summary, morphology changes during apoptosis begin with the cell membrane beginning to show blebs or spikes, depending on the type of cell. Eventually these separate from the dying cell and form apoptotic bodies that are phagocytosed by neighboring cells. Figure 2.14 shows the regions within a cell where a particular cytotoxicity test would cause trouble. The tests and their affected areas are as follows:

- Membrane integrity (extracellular lactate dehydrogenase [LDHe])
- Metabolic activity (glucose [GLU])
- Respiratory chain activity (bis-methoxy-nitro-sulfophenyl Tetrazolium Carboxanilide [XTT]/(dimethyl-thiazol-diphenyl-tetrazolium [MTT])
- Total protein synthesis
- DNA content (crystal violet dye elution [CVDE])
- Lysosomal activity (phosphatase acid [PAC]

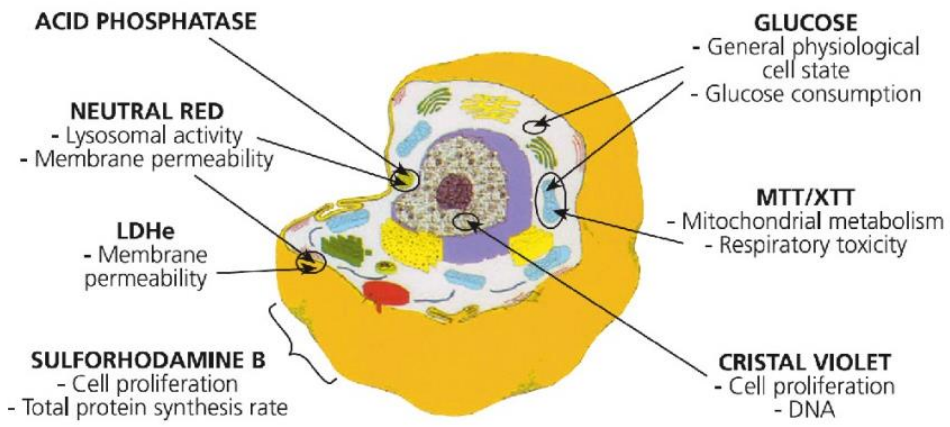

Figure 2.14: Cytotoxicity test systems.

almarBlue®

This test is used to determine in vitro cell proliferation and cytotoxicity. It is a simple, reliable, sensitive, rapid, efficient, safe, and cost-effective method to measure cell viability. One must ensure that there is no interference with the compound to be tested. This system combines an oxidation-reduction indicator that both fluoresces and changes color in response to chemical reduction of the growth medium resulting from cell growth. Higher sensitivity is achieved by using the fluorescent property. As few as 80 cells give a reproducible and sensitive signal, which is in the range of radioactive methods. The alamarBlue® test is nontoxic to cells and does not necessitate killing them to obtain measurements (as opposed to MTT); hence, there are no waste disposal issues. This allows cells to be reused for further investigations, thereby saving time and money. Automation can be easily set up in microplates and analyzed using microplate readers. Double wavelength fluorescent readers allow correlation.

The oxidized, blue, non-fluorescent alamarBlue® is reduced to a pink fluorescent dye in the medium by cell activity, hypothesized as being reduced by mitochondrial enzymes (alamarBlue® Assay U.S. Patent No. 5,501,959). It is still unknown whether this occurs intra-cellularly, at the plasma membrane surface, or just in the medium as a chemical reaction.

The predecessor of the alamarBlue® test is the resazurin reduction test, which works similarly. It has been used since the 1950s to assess bacterial or yeast contamination in biological fluids and milk. It has been assessed several times on different types of cell for its cytotoxicity reliability, i.e., fibroblasts, and immortalized and cancer cell lines, and for its cell proliferation reliability on mouse and human lymphocytes and primary neuronal cell cultures [20, 141].

Optical Density

A transmissive material absorbs some light falling on it, reflects some, and passes on the remainder. The fraction of light that is passed is called transmittance. When the intensity of light incident on a translucent material is denoted as I_0, and the intensity of that which passes through is denoted by I, the transmittance T is defined by

$$T = I/I_0$$

Transmittance takes on values between 0 and 1. Nearly all transmittance values are less than 1 and, in many instances, provide decimals that are difficult to correlate with visual impressions. For example, the transmittance of 0.0001 has very little correlation with a visual interpretation of what that means, since the eye tends to react to radians more in a logarithmic manner. Because of this, the negative logarithm of transmittance is used. This is known as optical density, or D :

$$D = -log_{10}(T)$$

Density reflects the values of incident light that fails to pass through a material. Density takes on values from zero to infinity. Spectroscopy is a method used to study the absorption and emission of light, and spectrophotometry is the quantitative measurement of the reflection or transmission properties of a material as a function of wavelength. Figure 2.15 shows a spectrophotometer, which is usually used for almarBlue® assay cytotoxicity testing [141, 142].

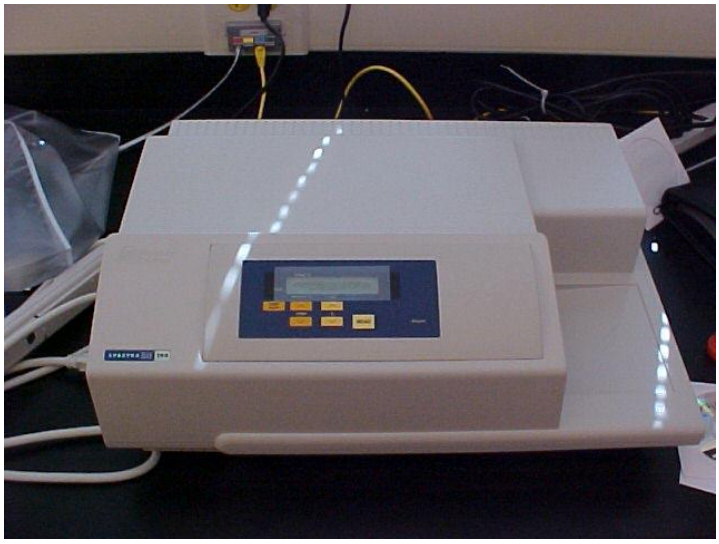

Figure 2.15: Spectrophotometer used for colorimetric assay during almarBlue® assay.

2.3 Neural Cytotoxicity

Diseases associated with nanoparticles are bronchitis, lung cancer, asthma, neurodegenerative diseases (such as Parkinson`s and Alzheimer`s diseases), Crohn`s disease, colon cancer, etc. Arteriosclerosis, blood clots, arrhythmia, heart diseases, and ultimately cardiac death may result from nanoparticles that enter the circulatory system. [143, 144].

One investigation conducted by Zhang et al. [139] included a study of the effect of graphene and SWCNTs in neural PC12 cells, suggesting that both graphene and SWCNTs induce cytotoxic effects that are dependent on concentration and shape. Graphene induced a stronger metabolic activity than SWCNTs at low concentrations, and a weaker metabolic activity than SWCNTs at higher concentrations. Belyanskaya et al.[145] researched the influences of SWCNTs on primary cultures derived from chicken embryonic spinal cord or dorsal root ganglia. A Hoechst assay showed that mixed neuro-glial cultures with up to 30 μg/mL SWCNTs significantly decreased the overall DNA content. Using a cell-based enzyme-linked immunosorbent assay, they found that SWCNTs reduce the amount of glial cells in both the peripheral and central nervous

systems. SWCNT suspensions used in this study induced acute toxic effects in primary cultures. Some of the reasons for cytotoxicity, according to previous research work, are as follows:

- They have better absorbability due to their size; hence, they have more toxicity than larger-sized particles.
- Their fiber-like shape induced asbestos-like behavior due to their needle-like shape.
- They are basically graphitic and hence non-biodegradable.
- The toxicity of functionalized CNTs-oxidized nanotubes can be more than their unmodified counterparts.
- Certain types of CNTs functionalized with lipids are highly water soluble, which facilitates their movement through the human body, possibly blocking vital body organ pathways [67, 131].

2.4 Mode of Transport of Nanomaterial within Human body

Because of their very small size, nanoparticles are capable of entering the human body by ingestion, skin penetration, inhalation injections, etc., and they have the potential to interact with intracellular structures and macromolecules for long periods of time. Spread of the deposited particles in the respiratory tract takes place by physical translocation of particles by different mechanisms or chemical clearance processes:

- Oberdorster et al. [146, 147] found significant amounts of labeled carbon particles (22–30 nm in diameter) in the livers of rats as soon as six hours after inhalation exposure.
- Colvin et al. [148] found that inhaled CNTs reached the olfactory bulb and also the cerebrum and cerebellum, suggesting translocation to the brain through the nasal mucosa along with the olfactory nerve.

- Fluorescent magnetic nanoparticles (50 nm) can penetrate the blood-brain barrier without causing significant toxicity.

Figure 2.16 is a schematic representation of the spread of nanomaterials through the human body. According to this flowchart, nanoparticles can enter the human body through inhalation. After passing through the respiratory tract they may enter either the neural system, circulatory system, or lymphatic system, eventually affecting the spleen, heart, kidneys, bone marrow, or liver. Distribution in the respiratory system is called primary distribution; that in the nervous, circulatory, and lymphatic systems is called secondary distribution; and the remaining is called tertiary distribution.

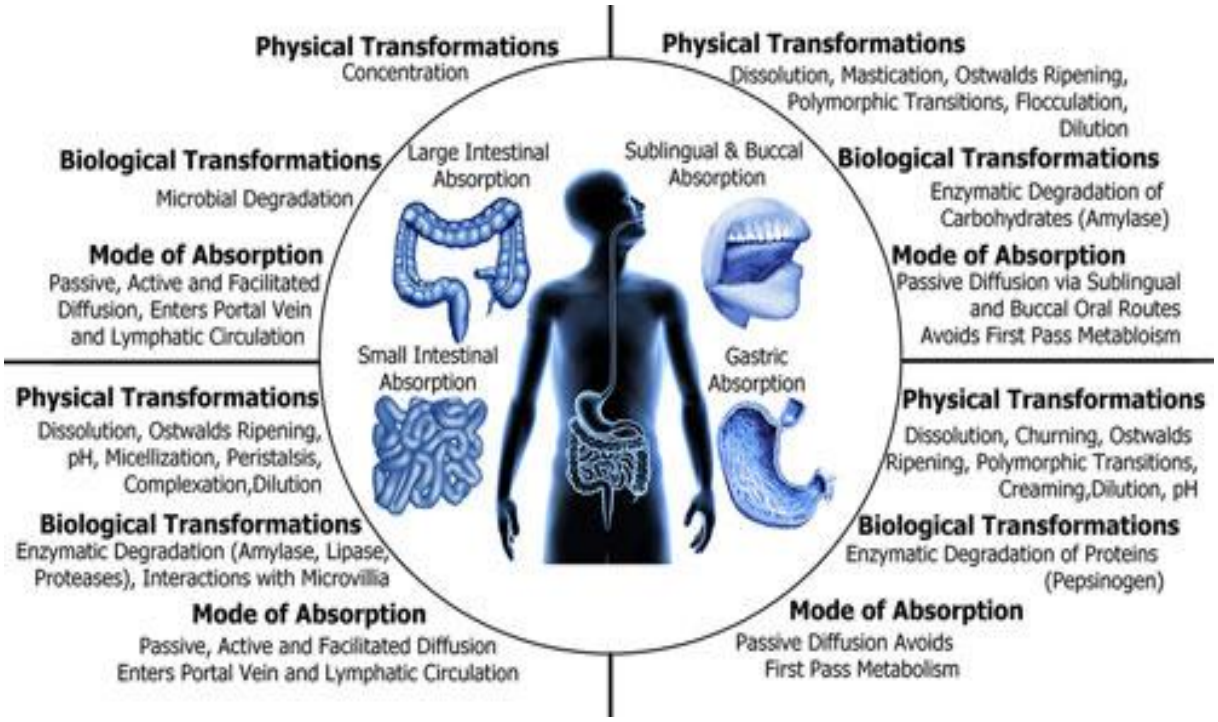

Figure 2.16: Endogenous modifications to nanomaterials within alimentary tract during transport from time of consumption to excretion (reprinted with permission by American Chemical Society).

2.5 Electrospinning

Electrospinning is the process of spinning non-woven fibers with very small diameters by using an electric field. Here the electric field is used to create a charged jet of a polymer solution, which is basically held by its surface tension. The polymer solution is ejected out of a syringe and travels towards an oppositely charged metal screen. As the jet travels in air, the solvent evaporates, leaving behind a charged fiber. Fibers with a variety of cross-sectional shapes and sizes can be produced from different polymers.

The polymer solution exiting the syringe is originally a hemisphere. As the intensity of the electric field is increased, the hemispherical surface of the solution at the tip of the capillary tube elongates to form a conical shape known as the Taylor cone. According to several research works, electrospun nanofibers exhibit many exceptional characteristics, such as high surface-to-mass ratio, high interconnected porosity, high flexibility with reasonable strength, flexibility in selection of polymer materials, and ability to incorporate other materials such as chemicals, polymers, biomaterials, and nanoparticles into the nanofibers through electrospinning [149]. Parameters affecting the process can be divided into two main categories: solution properties and operating parameters (Figure 2.17).

2.5.1 Solution Properties

Solution Properties depends on several factors such as, polymer structure, molecular weight, solubility), solvent (e.g. boiling point, dielectric properties) and solution properties (e.g., viscosity, concentration, conductivity, surface tension.)

Chemical Composition

The chemical composition of the solution and its inbuilt properties affects the quality of the fibers.

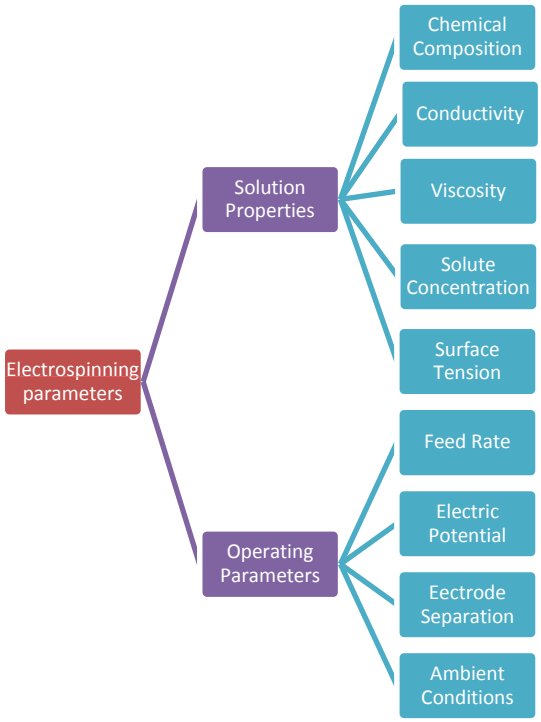

Figure 2.17: Flowchart showing electrospinning parameters.

Presence of Salt

According to research by Beachley and Wen [150], the addition of salts to a polymer solution increases its conductivity and the surface charge density of the solution jet. Previously, the addition of salts to polymer solutions reduced bead defects and decreased the fiber diameter when a rotating drum was used as the collecting device. However, some decrease in fiber diameter was observed by increasing the salt (NaCl) concentration, and fibers with beads were observed only when NaCl was not present in the polymer solution.

Solute Concentration

A solute concentration below a certain threshold value will result in drops instead of fibers. High solute concentrations result in solutions with high viscosities, which could lead to processing problems, wherein the polymer solution flow to the needle tip becomes difficult to control, and the cohesive nature of the viscoelastic solution resists jet elongation. This could also lead to

discontinuous fibers and larger fiber diameters. A power law relationship governs the resulting fiber diameter and the solution concentration, which would correlate to a larger fiber diameter produced. In statistics, a power law is a functional relationship between two quantities, where one quantity varies as a power of the other quantity. The value of the exponent is dependent on the polymer/solvent system used in the process. According to research conducted by Stanger et al. [151] on the power law relationship for polyvinyl alcohol, the mass deposition rate and the electric current were linearly related in all combinations of electric voltages and electrode separation there by exhibiting a constant charge density of 96.1C/kg. Beachley and Wen [150] experimented using PCL fibers and determined that the maximum fiber length and fiber diameter increased with increasing polymer concentration at significant levels, while keeping all other parameters constant. They used Holm's test to identify the variation between different concentrations. Uniformity was observed to slightly (insignificantly) decrease with increasing polymer concentration. They also observed that the fiber formation was occasionally impeded by the high viscosity of the solution at a very high polymer concentration (20%). In research conducted by Cheng and Kisaalita, who measured the effect of solute concentration on the mechanical strength, it was shown that as the solute concentration increased, the mechanical strength of the scaffold also increased [152].

Viscosity

It was found that a solution film in the thickness range of 0.5 mm ~ 2 mm was likely to form Taylor cones and could reduce the critical voltage. Different polymer solutions have different requirements. For example, for electrospinning of aqueous polyethylene oxide dissolved in ethanol and water solutions, viscosities in the range of 1–20 poises and surface tension between 35 and 55 dynes/cm were suitable for fiber formation. It was found that at viscosities above 20 poises, electrospinning was prohibited because of the instability of flow caused by the high cohesiveness

of the solution. Droplets were formed when the viscosity was too low (<1 poise). Similarly, according to Liu et al.[153], for electrospinning cellulose acetate (CA) in 2:1 acetone/dimethylacetamide, viscosities between 1.2 and 10.2 poises were applicable. Outside that range, the CA solutions could not be electrospun into fibers at room temperature—either only a few fibers could be obtained from an even higher viscosity solution, or the fluid jet broke up to droplets due to too low viscosity (<1.2 poise). These two examples clearly demonstrate that the viscosity ranges for different polymer solutions are different [153-157].

Surface Tension

Beads are mainly caused by lower surface tension. With a higher surface tension, the size and number of beads in electrospun products are smaller and fewer. Both theoretical analysis and experimental results have shown that the formation of beads strongly depend upon the solvent, solute concentration, and secondary additives. Either a suitable solute concentration or a suitable salt additive can completely prevent the occurrence of beads in the electrospinning process; solvents can affect the number of beads and the morphology of electrospun fibers [158].

Conductivity is an important requirement for electrospinning. A nonconductive solution can be made conductive with the addition of secondary particles. Salt is a common additive to improve conductivity. Nanoparticles can also be added to improve conductivity.

2.5.2. Operating Parameters

Feed Rate

Feed rate was not found to have a significant effect on maximum fiber length, diameter, or uniformity over all parameter variations. Once the feed rate is sufficient for forming fibers, a higher feed rate only provides more polymer solution than needed. This rate must be adjusted so that a stable Taylor cone is formed. A low flow rate can form a vacuum in the needle, causing the Taylor

cone to disappear and temporarily stop the electrospinning process. High flow rates could cause a build-up of solution at the needle tip. As the flow rate increases, the surface charge density decreases; therefore, the rate of charge withdrawal into the solution is dependent upon the residence time of ions in contact with the needle. At higher flow rates, the solution spends less time in contact with the needle[150].

Electric Potential

Fiber length and diameter decreased with increasing voltage. Uniformity of the fibers increased with increasing voltage at significant levels. Subsequent analysis of individual groups using Holm's test resulted in significant differences among the 10 kV, 15 kV, and 20 kV groups for both fiber diameter and fiber uniformity. It can be concluded that the surface charge density is the driving force behind electrospinning, which is directly affected by flow rate [150].

In needle electrospinning, the critical applied voltage for electrospinning is given by

$$V_c^2 = 4ln\left(\frac{2h}{R}\right)(1.3\pi R\gamma)(0.09) \tag{2.1}$$

where h is the distance from the needle tip to the collector, R denotes the needle outer radius, and γ is the surface tension. The factor 0.09 was inserted into this equation to predict the voltage. Lukas et al. [159] explained the self-organization of jets occurring on a free liquid surface in needleless electrospinning process. The critical electric field intensity for electrospinning nanofibers is

$$E_c = \sqrt[4]{4\gamma\rho g/\varepsilon^2} \tag{2.2}$$

where ρ is the liquid mass density, g is the gravity acceleration, γ is the surface tension, and ε is the permittivity. In both models, electric force plays a crucial role in the jet initiation. In a static electric field, it is well known that the relationship between voltage and electric field intensity can be expressed as [154]

$$E = -\nabla V \tag{2.3}$$

Temperature

A useful attempt was recently made by Demir et al. [149] to electrospin polyurethane nanofiber. They recognized that the fiber diameters obtained from the polymer solution at a high temperature (70°C) were much more uniform than those at room temperature. The viscosity of the polyurethane solution with the same concentration at some higher temperature was significantly lower than that at room temperature. Temperature and viscosity are closely linked. Also, at higher temperatures it is possible to have a higher solute concentrations [157, 160].

Increasing the collecting distance between electrodes reduces the electric field strength in the electrospinning zone. Reducing the fiber collecting distance has a similar effect as increasing the applied voltage. For effective collection of solid nanofibers, the collecting distance must be large enough to ensure sufficient solvent evaporation from the jet before deposition. The minimal collecting distance is dependent on the solution property and the geometry of fiber generator [154].

Ambient Environment

Ambient parameters, including temperature, humidity, and air velocity in the electrospinning chamber, affect the quality of electrospinning. If the ambient temperature is too cold, the fibers may get prematurely cooled [161].

2.5.3 Applications of Electrospun Fibers

As discussed previously, electrospun fibers have a very large surface area-to-volume ratio (this ratio for a nanofiber can be as large as 1,000 times that of a microfiber), flexibility in surface functionalities, and excellent mechanical performance (e.g., stiffness and tensile strength), compared to any other known form of the material. These outstanding properties make polymer nanofibers optimal candidates for many important applications. Electrospun nanofibers find their

applications in release control, catalyst and enzyme carriers, sensors filtrations, affinity membranes, recovery of metal ions, energy storage, and tissue engineering scaffolds [157].

An examination of all biological structures will show that almost all of human tissues and organs are deposited onto nanofibrous forms or structures, for example, bone, dentin, collagen, cartilage, and skin (Figures 2.18 to 2.22). All of them are characterized by well-organized hierarchical fibrous structures realigning on a nanometer scale.

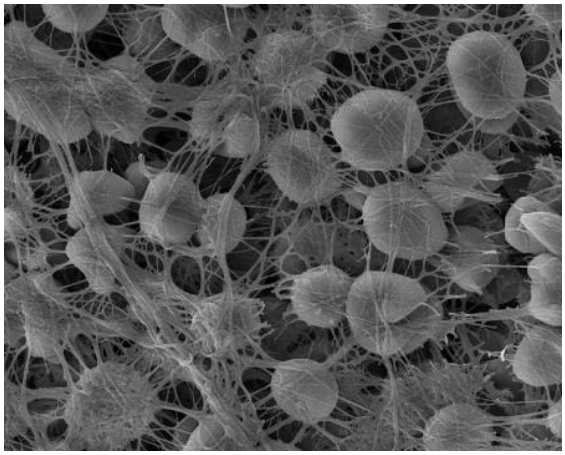

Figure 2.18: Electrospun structure
(acquired by Zophie Lim from Victor Nurcombe and Simon Cool's Laboratory and Adrian Boey from the IMB-IMCB Joint Electron Microscopy Suite)

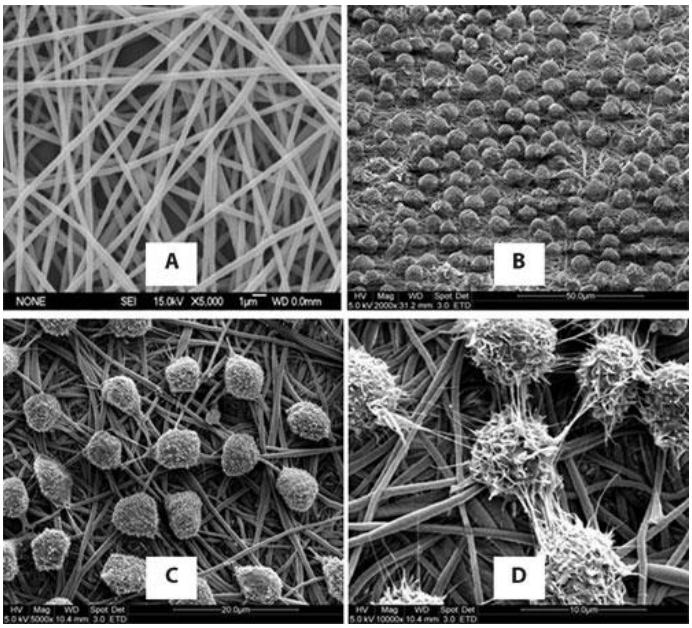

Figure 2.19: Nanex, developed by Hai-Quan Mao at Johns Hopkins University.

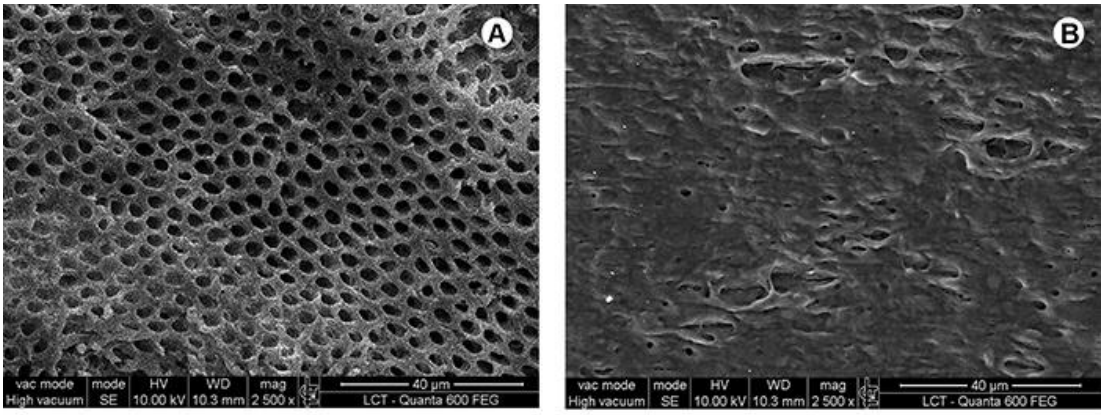

Figure 2.20: SEM micrographs of open dentinal tubules: (A) control group showing dentinal surface free of smear layer with open dentinal tubules; (B) experimental group showing dentin fusion and resolidification after laser irradiation with no smear layer or debris [162] .

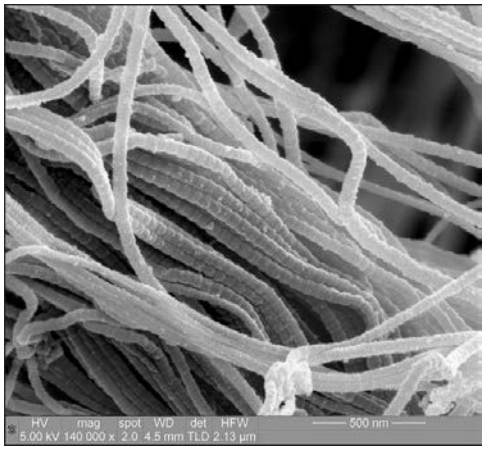

Figure 2.21: SEM image of collagen fibrils from knee joint capsule (Paul Gunning and Nephew, Nova NanoSEM).

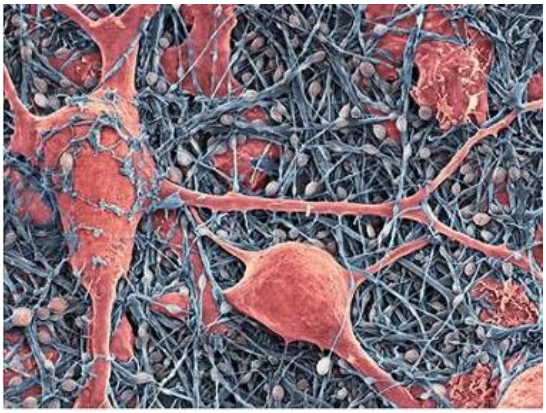

Figure 2.22: Colored SEM image of nerve and glial cells.

Medical prostheses

Polymer-based nanofibers fabricated via electrospinning have been extensively researched for soft tissue prosthesis applications. They have been used for blood vessels, muscle growth, breast implants, etc. In addition, they act like an interface between the prosthetic implant and the tissue to reduce the stiffness mismatch. The morphology of nanofibers has been shown to effectively induce cell adhesion and cell culture, thereby reducing the possibility of rejection from the body. In such cases, the nanofibers are electrospun onto the prosthetic device before implantation [163-167].

Wound Dressing

Polymer nanofibers have also been extensively researched for wound dressing for bruises, burns, cuts, etc. A biodegradable polymer is sprayed onto the wound and forms a fibrous mat. It lets the wound heal by inducing growth on skin cells. This type of wound dressing has pores of the size 500 nm to 1 μm, which prevents the penetration of bacteria. It also eliminates the formation of scar tissue, which would normally occur in traditional treatment [168, 169].

Drug Delivery and Pharmaceutical Composition

The electrospinning method has also been extensively used in the delivery of drug/pharmaceuticals to patients in the most physiologically suitable method. Typically, the smaller the dimensions of the drug and the coating material required to encapsulate the drug, the easier it is for the human body to absorb the drug. Since electrospun fibrous mesh offers a high surface area-to-volume ratio, the dissolution rate of the drug increases. The drug can be intermixed in different ways; for example, the drug particles can be suspended in capsules in the polymer mesh, they can form a mesh and be a part of the scaffold, or the carrier material can be electrospun around the drug into a tubular or spherical form [170].

Cosmetics

Electrospun materials have also been used for skin care for skin healing, cleansing, and treatments. Their high surface area is used to deliver therapeutic additives to the pores of the skin, thereby enhancing the overall effect. A cosmetic skin mask is painlessly sprayed onto the skin that allows deposition of the fibers to the deepest pores of the skin [171]

Other Functional Applications

Apart from biomedical applications, the electrospinning method has also been used to manufacture protective military clothing, as well as for applications in the fields of electronics and optics. They are also being investigated for use in sensors [172-175].

Tissue Culture

It is possible to treat various degenerative diseases by implanting an artificial scaffold to induce a cell culture. One of the major challenges in the field of tissue engineering is the design of an ideal scaffold that can imitate the existing structure and the biological functions. Human cells have shown to attach and grow very well around fibers that have diameters smaller than those of the cell themselves. Since most of the cells in the human body are on the microscale, nanoscale scaffolds provide an optimal template for cells to seed onto and grow. As discussed in the previous sections, it has been shown that scaffolds with nanofibers and microsize pores provide the best morphology for cell growth. Synthetic biopolymers have exhibited properties that are conducive to cell growth and proliferation. This topic will be discussed in more detail in the following sections [157, 176].

2.6 Scaffolds

The field of tissue engineering has now become interdisciplinary. Researchers in this field are now applying the principles of cell biology, material science, and biomedical engineering to

create biological substitutes that restore and maintain normal function of diseased and injured tissues/organs. As discussed previously, artificially engineered tissues must be precise and perform three basic functions: (a) facilitate the localization and delivery of tissue-specific cells to the appropriate location, (b) maintain a 3D architecture that is conducive to the formation of new tissues, and (c) guide the development of new tissues with appropriate function.

Ideally, synthesized scaffolding must possess a structure similar to the natural extracellular matrix [177]. Cells in the body live in a microenvironment consisting of both nanoscale and microscale structures. It has been reported in some studies that the nanofibrous architecture and its high surface area could improve cell adhesion, migration, proliferation, differentiation, and other cellular activities [178, 179]. At microscale, it has been suggested that pore topography, size, and interconnectivity are important for cell penetration, mass transport, and 3D tissue formation [180]. Considerable research has been done in the field of cell viability [181], attachment [182], proliferation, differentiation [183], and cellular functionalities. It has been shown that the presence of nanofibers in a conventional microscale scaffold to be very efficient. Cheng and Kisaalita [152] investigated three types of scaffolds: nano, micro, nanoscaffoldand nanofiber/micropore (NFMP).

According to research conducted by Pham et al. who created a nano/microfiber-combined scaffold by using electrospun PCL on top of microscale scaffolds to study cell infiltration, the presence of nanofibers enhanced cell spreading, and increasing the thickness of the nanofiber layer reduced the infiltration of cells into scaffolds under both static and flow-perfusion cultures [184]. To manufacture 3D scaffolds, the pore size of a scaffold should be at least the size of a cell —a value of 10 μm. The reduced cellular infiltration into the depths of the scaffold has been attributed to pore diameters being smaller than that of a cell. In a study by Cheng and Kisaalita [152], a

systematic comparison of single- and dual-scale scaffolds was carried out by investigating human neural stem and fibroblast cellular responses on three scaffold groups: micro only, nano only, and microsize/nanosize combination. A nanofibrous poly-l-lactic acid (PLLA) scaffold consisting of interconnected microscale pores was created by combining the techniques of phase separation and particulate leaching. Their study indicated that the microscaffold promoted 3D cell growth and cell-cell interactions, while the nanoscaffold promoted neural differentiation and induced 3D matrix adhesion. Interestingly, NFMP combination scaffold possessed the advantages found in both micro- and nanoscaffolds.

2.6.1 Scaffold Characterization

Porosity

Cheng and Kisaalita [152] measured the porosities of scaffolds by a modified liquid displacement method. A new method called constant pressure liquid displacement method was developed and tested by Lee et al. [185]. to measure the pore size distribution of porous membranes. Permeability, defined as the ratio of the flow rate to the pressure applied, was previously assumed to be constant, either for a conventional liquid displacement method or for a bubble point method, leading to the erroneous interpretation of pore-size distribution. In that study, 70% ethanol was used as the displacement liquid. Pham et al. used mercury porosimetry to measure the porosity [184].

Mechanical Strength

The mechanical strength of scaffolds was evaluated by Cheng and Kisaalita [152] by determining the ability of the scaffold to absorb fluid-mechanical energy without damage. Briefly, a syringe pump (Orion, Boston, MA) connected to a standard 200 μL pipette tip was used to perpendicularly eject water onto the surface of polymer scaffolds for five seconds. The flow rate

inducing scaffold rupturing for all three scaffolds is shown in Figure 2.23. The force, *F*, against the scaffolds was calculated as

$$F = \beta . A . v^2 \tag{2.4}$$

where β is the density of the deionized water, *A* is the area of the opening of the pipette tip, and *v* is the fluid flow rate just before impact (which depends on the rate of the syringe piston movement and the diameter of the nozzle tip.). According to Cheng and Kisaalita [152], the rupture force required to rupture a nanoscaffold is seven times that of NFMP combination structure.

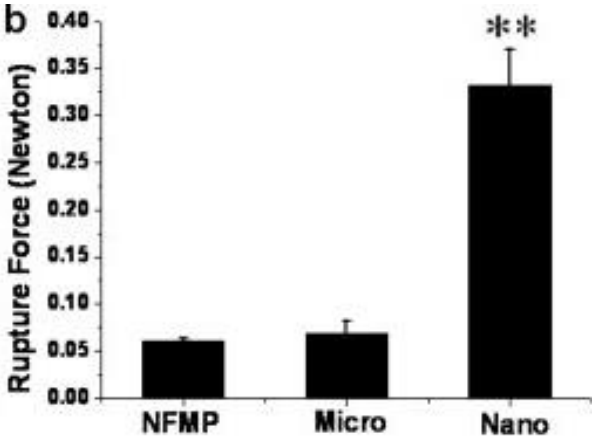

Figure 2.23: Comparison of rupture force in NFMP scaffold, microscaffold, and nanoscaffold.

SEM Analysis

SEM analysis has proven to be very useful in studying nanostructures. Figure 2.24 shows several SEM images. Several researchers have used SEM to analyze the fiber morphology of scaffolds. According to Cheng and Kisaalita [142], the dual-scale scaffold successfully combined the advantages of both single-scale structures. The microporous structure facilitated cell infiltration and multi-cellular organizations in the pores; the nanofibrous structures promoted cell differentiation and a more in-vivo-like cell-matrix adhesion. Dual-scale scaffold structures may provide a better choice for tissue engineering and 3D cell culture applications [152].

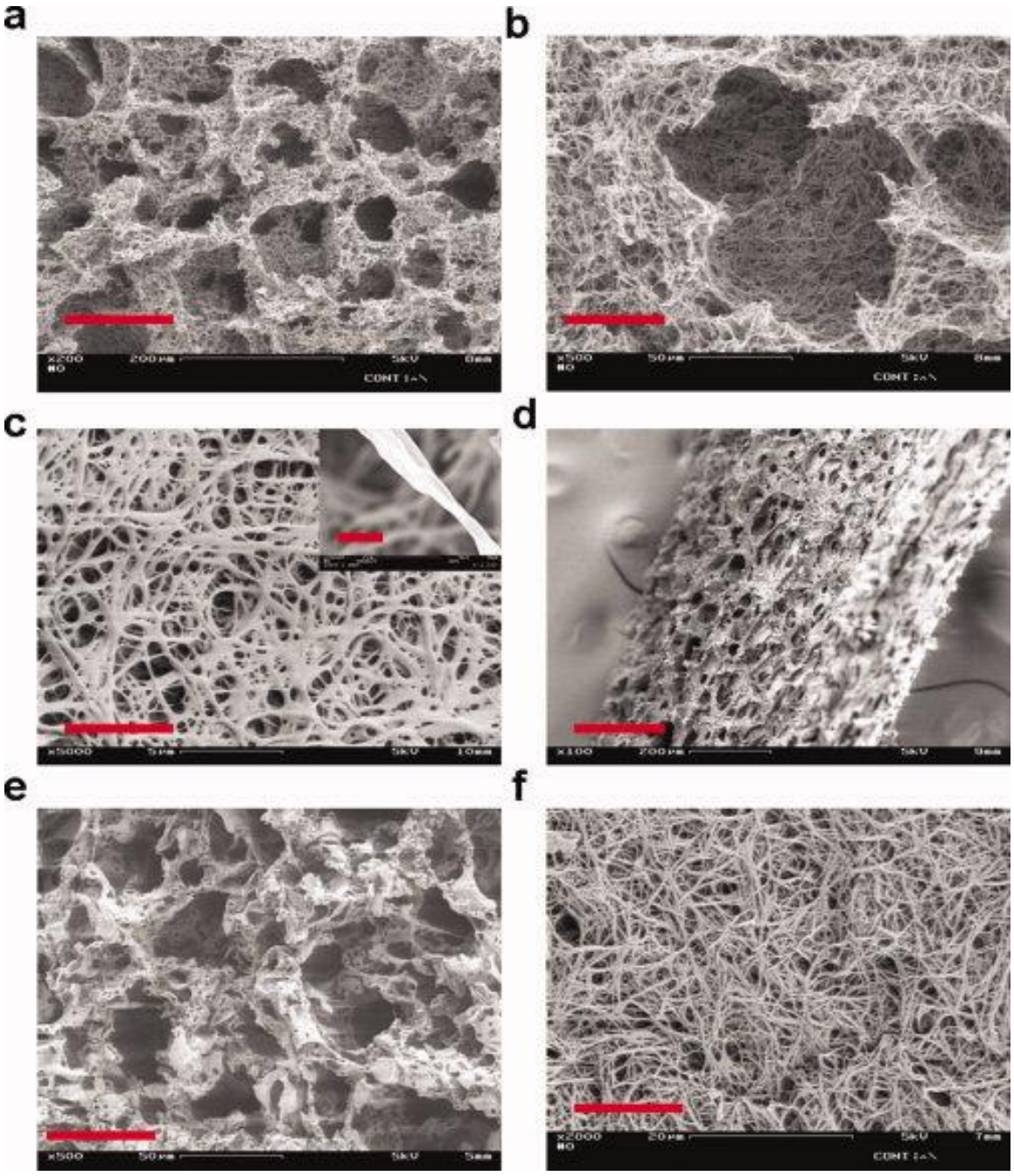

Figure 2.24**:** SEM micrographs of NFMP scaffold [152]:

Table 2.1 lists the advantages and disadvantages of the three types of scaffolds.

TABLE 2.1

ADVANTAGES AND DISADVANTAGES OF THREE TYPES OF SCAFFOLDS

Scaffold Type	Advantages	Disadvantages
Nano	• High mechanical strength • Ability to promote cell differentiation (neural) • Ability to promote 3D cell adhesion (fibroblast)	• Low porosity • Only 2D space for cell growth and interaction
Micro	• High porosity • 3D space for cell growth and interaction	• Low mechanical strength • Limited cell differentiation (neural) • Limited 3D cell adhesion (fibroblast)
NFMP	• High porosity • 3D space for cell growth and interaction • Ability to promote neural differentiation • Ability to promote 3D cell adhesion (fibroblast)	• Low mechanical strength

2.6.2 PCL Scaffolds

PCL is a semi-crystalline aliphatic polyester, which is of great interest as can be obtained by ring opening polymerization of a relatively cheap monomeric unit called ε-caprolactone. Its chemical structure is shown in Figure 2.25.

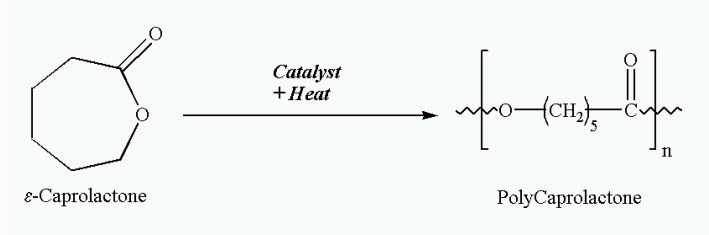

Figure 2.25: Chemical structure of PCL

PCL has the following properties:

- Low glass transition temperature (T_g = –60°C).
- High elastomeric properties that allow it be spun into fibers [26].
- Approved for use by the FDA since the 1970s for biomedical applications.
- Enhanced solubility in organic solvents.
- Can be processed at low temperatures.
- Long-term degradation properties (>24 months to lose total mass).
- Degrades slowly by hydrolysis and loses about 50% of its strength in eight weeks using an *in vitro* degradation test .
- Its degradation byproducts are non-toxic.
- Can be co-polymerized with various starches to reduce production costs and also encourage cell growth with the presence of a natural biopolymer.
- When blended with starch, shows an increased rate of non-isothermal crystallization.
- Attractive for biomedical applications that undergo extensive mechanical strain, such as orthopedic implants .
- because of its higher starch content, more susceptible to enzymatic degradation by proteinase K49 therefore, the rate of degradation can be tailored [186-189].

Izquierdo et al. presented a technique for producing controlled interconnected porous structures for application as a tissue engineering scaffold for chrondocytes (cartilage) and tested them for and cell adhesion, viability, proliferation, and proteoglycan (PG) synthesis. Cells cultured on PCL disks showed an adhesion similar to that of the polystyrene control (which allowed high levels of proliferation) [190].

Yoshimoto et al. investigated microporous, non-woven poly(ε-caprolactone) (PCL) nanoscaffolds made by electrostatic fiber spinning. The cell-polymer constructs were cultured with

osteogenic supplements under dynamic culture conditions for up to four weeks. Their study showed that the surfaces of the cell-polymer constructs were covered with multilayers of cells at four weeks. In addition, mineralization and type I collagen were observed at four weeks [191]. In another study, the surface properties of the PCL were tweaked to improve its hydrophilicity. In that study, alkaline hydrolysis of poly (ε-caprolactone) (PCL) nanofibrous scaffolds was carried out for different periods of time to increase the hydrophilicity of the scaffolds. Matrigel (gelatinous protein mixture secreted by mouse sarcoma cells) was attached covalently on the surface of an optimized four-hour hydrolyzed scaffold. Results of the cell proliferation assay and SEM studies showed that the covalently functionalized PCL/matrigel nanofibrous scaffolds promote the proliferation and neurite outgrowth of neural progenitor cells compared to PCL and hydrolyzed PCL nanofibrous scaffolds, providing suitable substrates for nerve tissue engineering [10].

2.7 Astrocytes

Astrocytes are "star-like cells" and the most numerous and diverse type of glial cells in the central nervous system. A typical morphological feature of astrocytes is their expression of intermediate filaments, which form the cytoskeleton. The main types of astroglial intermediate filament proteins are glial fibrillary acidic protein and vimentin. GFAP is commonly used as a specific marker for the identification of astrocytes, which are very heterogeneous in nature.

2.7.1 Functions of Astrocytes

Astrocytes perform the following functions:

- Maintain brain homeostasis.
- Store and distribute energy substrates.
- Control the development of neural cells.
- Constitute the blood-brain/blood-spinal cord barrier.

- Create the brain environment.
- Build up the micro-architecture of the brain parenchyma.
- Promote synaptogenesis and synaptic maintenance.

Since the importance of astrocytes has only been realized in the last couple of decades, their functions and mechanisms are not yet completely understood. Nevertheless, considerable progress has been made, and the functions of astrocytes as reported by various researchers have been explained in detail. A summary of these functions follows.

Definition of Brain's Micro-Architecture

Astrocytes are a major type of glial cells in the human CNS. Almost 90% of the body's cells are glia, and they play an essential role both structurally and physiologically. Each astrocyte extends processes that cover almost eight neuronal cell bodies, five blood vessels, and more than 100,000 synapses. Protoplasmic astrocytes are known to occupy a separate territory and create the micro-anatomical domains within the limits of their processes. Within these anatomical domains, the membrane of the astrocyte covers synapses and neuronal membranes. It also sends processes to cover the wall of the neighboring blood vessel with their endfeet. Astrocytes define the micro-architecture of the parenchyma by dividing the grey matter into relatively independent structural units in the mammalian brain. The astrocyte-neurons-blood vessel is known as a neurovascular unit [192-197].

Control of Extracellular Homeostasis

Astrocytes can control extracellular homeostasis in the brain. By multiple molecular cascades, they control concentrations of ions, neurotransmitters, and metabolites and regulate water movements. Neuronal activity leads to an increase in K^+ concentration from a resting level of about 3 mM to a maximum of 10–12 mM under physiological conditions and to higher values

under pathological conditions. A higher K^+ concentration in the extracellular space modulates neuronal activity. Astrocytes remove excess extracellular K^+ to maintain stability. Glial syncytia and aquaporine channels expressed in astrocytes play a role in water homeostasis in the brain [192, 194, 197-202] .

Removal of Excess Glutamate

Glutamate is the major excitatory neurotransmitter in the brain of all vertebrates. When glutamate is released for a long-time or in excess, it acts as a potent neurotoxin, triggering neuronal cell death in acute and chronic brain lesions. Astrocytes remove the bulk of glutamate from the extracellular space. They can accumulate almost 80% of the glutamate that is released, which is then removed by excitatory amino acid transporters (EAATs). Five types of EAATs are present in the human brain, two of which are expressed exclusively in astrocytes [203, 204].

Maintenance of Glutamatergic Neurotransmission

Astroglial glutamate transport is crucial for neuronal glutamatergic transmission by operating the glutamate-glutamine pathway. Glutamate that is accumulated by astrocytes is converted into glutamine. Glutamine is not sensed by neurotransmitter receptors and is not toxic. It can be safely transported to presynaptic terminals through extracellular space. It is converted back to glutamate after entering the neuronal compartment [192].

Control of Local Blood Flow and Metabolic Support for Neurons

Astrocytes integrate neural circuitry with local blood flow and metabolic support. The basal lamina of blood vessels is almost entirely covered by astrocyte endfeet, with one arm at the blood vessel and the other at the neuronal membrane, synapse, or axon. Increased activity of neurones triggers Ca^{2+} signals in astrocytes, which leads to the release of vasoactive agents that regulate local blood flow. It is still unknown if astrocyte activity leads to vasoconstriction or vasodilatation.

But astrocytes are the only cells in the brain that can synthesize glycogen, thus serving as an energy reservoir [192, 205-208].

Control and Maintenance of Synaptogenesis

Astrocytes regulate the formation, maturation, maintenance, and stability of synapses and hence control the connectivity of neuronal circuits. They secrete numerous chemical factors required for synaptogenesis. Synaptic formation depends on cholesterol formation, which is produced and secreted by astrocytes. This cholesterol can be converted into steroid hormones, which can act as synaptogenic signals. It is also induced by the expression of specific proteins, agrin and thrombin, which are essential for synapse formation. Subsequently, they control the maturation of synapses through several signaling systems that affect the postsynaptic density and synapse maturation such as the tumor necrosis factor-alpha (TNF-α) factor and the activity-dependent neurotrophic factor. They can also limit the number of synapses since astrocyte membranes can enclose the neuronal processes and thus compete with synapses. They are able to eliminate synapses in the CNS by secretion of certain factors or proteolytic enzymes, which demolish the extracellular matrix and reduce the stability of the synaptic contact [192, 206, 208-210].

Tripartite Synapse

In the gray matter, astrocytes are associated with neuronal membranes and synaptic regions, so that astroglial membranes completely or partially enwrap presynaptic terminals and postsynaptic structures. In the cerebellum, glial-synaptic relations are even closer, and almost all of synapses formed by parallel fibers on dendrites are covered by membranes of Bergmann glial cells, which enwrap between 2,000 and 6,000 synaptic contacts. The distance between the terminal structures of astrocytes and neuronal presynaptic and postsynaptic membranes is almost 1 μm;

therefore, astrocytes are exposed to neurotransmitters released from synaptic terminals. They have a complement of receptors very similar to that of their neuronal neighbor. In the cortex, both pyramidal neurons and neighboring astroglial cells express glutamate and purinoreceptors, whereas in the basal ganglia, neurons and astrocytes are sensitive to dopamine. The astroglial cell closely resembles the postsynaptic neuron [192].

Close morphological and functional relations between astrocytes and synapses lead to the concept of the "tripartite synapse," whereby synapses are built from three equally important parts: presynaptic terminal, postsynaptic neuronal membrane, and surrounding astrocyte. A neurotransmitter that is released from the presynaptic terminal activates receptors in both the postsynaptic neuronal membrane and the perisynaptic astroglial membranes, which results in the generation of a postsynaptic potential in the neuron and a Ca^{2+} signal in the astrocyte. It is difficult to determine if astrocytes actively participate in the ongoing synaptic transmission because their signals are on a much slower time scale compared to the rapid signaling of neurons. As a result, they are considered to be integrators or modulators [192, 195, 211-216].

Signaling in Glial Syncytia

Astroglial metabotropic receptors are coupled to intracellular signalling cascades, which provide glia with specific excitability mechanisms. The glial excitability is based on the excitability of the endoplasmic reticulum membrane containing Ca^{2+} release channels. Stimulation of astroglial metabotropic receptors induces the formation of $InsP_3$, which in turn triggers Ca^{2+} release from the endoplasmic reticulum, thus producing Ca^{2+} signals. These signals can cross cell-to-cell boundaries and propagate through astroglial syncytia. The mechanisms of generation and maintenance of intercellular Ca^{2+} waves are complex [192].

Concept of Gliotransmission

Astrocytes can release a variety of transmitters into the extracellular space, such as glutamate, adenosine triphosphate (ATP), gamma aminobutyric acid, and D-serine. Their mechanisms include diffusion through high-permeability channels (Cl^- channels), transporters, or Ca^{2+}-dependent exocytosis [192, 213, 216-219].

Astrocytes in Neuropathology

The pathological potential of neuroglia was already recognized at the end of the 19th to the beginning of the 20th centuries by prominent neuropathologists such as Carl Frommann, Franz Nissl, Alois Alzheimer, and Pio del Rio-Hortega. Astrocytes are an important part of the intrinsic brain defense system. Brain insults can trigger an evolutionary conserved astroglial defense response, generally referred to as reactive astrogliosis, which is essential for both limiting the areas of damage and for the post-insult remodeling and recovery of neural function [197, 220-222].

Astrocytes are involved in all types of brain pathologies from acute lesions (trauma or stroke) to chronic neurodegenerative processes (such as Alexander's disease, Alzheimer's disease, Parkinson's disease, multiple sclerosis) and psychiatric diseases. Recent studies have highlighted the role of astroglial degeneration and atrophy in the early stages of various neurodegenerative disorders, which may be important in cognitive impairment. Astrocytes play an important role in the progression and the outcome of neurological diseases [192].

2.7.2 Damage of Astrocytes

Some neurodegenerative diseases like ALS lead to loss of motor neurons due to mutations caused in the superoxide dismutase. Yamanaka et al. have shown that using mice carrying a deletable mutant gene diminished the mutant expression in astrocyte-delayed microglial activation and sharply slowed the disease progression. Their research indicated that mutant astrocytes are

viable targets for therapies for slowing the progression of the non-cell autonomous killing of motor neurons in ALS [223].

Oxidative Stress and Neurodegeneration

One of the trademarks of various neurodegenerative diseases and neuroinflammatory disorders is oxidative stress-induced CNS damage. Similarly, the natural aging process per se is associated with increased oxidative stress. Such oxidative stress can damage lipids, proteins and nucleic acids of cells, and power-house mitochondria, causing cell death in assorted cell types including astrocytes and neurons. Mitochondria are central neuronal organelles that play a vital role in neuronal life and death. Both mitochondrial dysfunction and proper function are essential components in neurodegeneration[224].

Neurodegenerative Diseases—Processes, Prevention, Protection, and Monitoring

It has been reported that astrocytes react rapidly to various neurodegenerative insults, thus leading to vigorous astrogliosis. This reactive gliosis is associated with the alteration in morphology and structure of activated astrocytes along with its functional characteristics [225] The astrocytic processes construct a bushy network surrounding the injury site, thus secluding the affected part from the rest of the CNS area. Subsequently, astrogliosis has been implicated in the pathogenesis of a variety of chronic neurodegenerative diseases, including Alzheimer's disease, Parkinson's disease, ALS, acute traumatic brain injury, stroke, and neuroinflammatory brain diseases

2.7.3 Role of Astrocytes after Injury

The role of astrocytes after an injury has been misunderstood for several years. It was initially assumed that astrocytes play a negative role following the event of injury, which inhibits

the regeneration and growth of neurons [226]. However, recent studies prove otherwise, and the steps involved following an injury are listed here:

- Cellular damage can result in the release of large amounts of ATP into the extracellular environment, because intracellular concentrations can reach 3–5 mM [227-229].
- Depending on the extracellular ATP concentration and subtype of astrocytic P2 receptor activated, astrocytes can modulate the TNF-α-mediated inflammatory response [227, 229] [226].
- TNF-α directly affects astrocytes, inducing a slow increase in intracellular Ca^{2+} and marked depolarization, and reducing glutamate-evoked rises in Ca^{2+},which would affect synaptic transmission indirectly [229, 230].
- Pro-inflammatory cytokines, such as IL-1 and TNF-α, can cause damage to BBB, release neurotoxins such as nitric oxide from the vascular endothelium, cause the up-regulation of adhesion molecules involved in the invasion of leukocytes (for example, intercellular cell-adhesion molecule-1), and induce vasogenic edema [229].
- Nucleosides and nucleotides released from dying cells might induce reactive astrogliosis, which involves striking changes in astrocyte proliferation and morphology [226, 227, 229, 231].
- This can be measured by increased expression of the astroglial-specific marker GFAP and the elongation of GFAP-positive processes [232].
- ATP stimulates proliferation of microglia and acts as a powerful chemoattractant to the site of brain injury [230, 233].

- In moderate situations (chemical lesions and mild injury), reversible aberrant hypertrophy of astrocytes occurs, which is marked by up-regulated GFAP without any significant proliferation [197, 234-236].
- In time, the severity of the injury increases, as the appropriate expansion of astrocytes both in terms of hypertrophy and proliferation gradually disrupt and distort the once well-organized tissues [197].
- This may lead to irreversible glial scarring, which is predominantly composed of reactive astrocytes, resident microglia, infiltrating macrophages, and ECM molecules. This feature has been thought to be inhibitory to repair and associated with dystrophicaxons [237, 238].
- Recent compelling research shows that reactive astrocytes protect injured tissues and cells in various ways [220, 239].
- One major benefit brought on by reactive astrocytes is the neuroprotection mediated by the degradation of amyloid-beta peptides [240] and the release of neurotrophic factors and growth supportive factors, such as brain-derived neurotrophic factor [241], ciliary neurotrophic factor (CNTF), and laminin [242].
- By clearing excitotoxic glutamate with increased expression of glial transporters such as the glutamate-aspartate transporter (GLAST) and glial glutamate transporter 1(GLT-1), reactive astrocytes protect the spared neurons from oxidative stress and NH^{4+} toxicity [9, 243-245].
- Moreover, selective proliferation of juxtavascular astrocytes repairs the integrity of the BBB and BSB [243] and restricts the spread of inflammation [116].
- In addition, astrocytes also stabilize the extracellular fluid and ion balance and reduce vasogenic edema after trauma. Hence, the sole ablation of activated astrocytes could lead

to impaired restoration of the BSB, increased demyelination, enhanced inflammatory response, severe neuronal death, and thereafter worse locomotion recovery after SCI [116, 237, 243, 246].

Glial scarring takes a considerable time to form a growth-blocking barrier, so it may not be the main reason for poor regeneration of the CNS. It is gradually being recognized that glial scarring is more likely to be a required physiological response for restoring the internal homeostasis of the CNS, which allows the cells to be replaced and the BSB to be restored by separating the remaining healthy tissue from the bleeding and necrotic primary lesion. This prevents the potential exacerbation of inflammatory response, cellular death, and tissue damage during the secondary injury [220, 226, 237].

2.7.4 Importance of Astrocyte Regeneration

According to research by Filous et al.[247], regeneration of injured adult CNS axons is inhibited by the formation of a glial scar. Immature astrocytes are able to support robust neurite outgrowth and reduce scarring. These researchers tried to test this effect on brain injuries. by transplanting these cells into brain-injured areas. They determined that alone, immature, but not mature, astrocytes had a limited ability to form bridges across the inhibitoriest outer rim. In turn, the astrocyte bridges promoted adult sensory axon regrowth across the gradient. The use of selective enzyme inhibitors revealed that mastrix metalloproteinase-2 (MMP-2) enabled immature astrocytes to cross the proteoglycan rim. They used adult rat brains to test the ability of matrix modification. When used alone, neither treatment was capable of promoting axonal regeneration. Their findings indicate that when faced with a minimal lesion, neurons of the basal forebrain can regenerate in the presence of a proper bridge across the lesion and when levels of chondroitin sulfate proteoglycans (CSPGs) in the glial scar are reduced [247].

During brain ischemia, impairment in astrocyte functions can critically influence neuron survival. Astrocyte functions that are known to influence neuronal survival include glutamate uptake, glutamate release, free-radical scavenging, water transport, and the production of cytokines and nitric oxide. Astrocyte surface molecule expression and trophic factor release influence long-term recovery after brain injury. This is because their behavior affects neurite outgrowth, synaptic plasticity, and neuron regeneration. The death or survival of astrocytes themselves may affect the ultimate clinical outcome and rehabilitation through their effects on neurogenesis and synaptic reorganization [248].

Astroglial cells are engaged in neurological diseases by determining the progression and outcome of neuropathological processes. According to some of the recent research, early stages of neurodegenerative processes are associated with the atrophy of astroglia, which causes disruptions in synaptic connectivity, misbalance in neurotransmitter homeostasis, and neuronal death through increased excitotoxicity. At later stages, astrocytes become activated and contribute to the neuroinflammatory component of neurodegeneration [249].

As mentioned previously, Cheng and Kisaalita [152] used three types of scaffolds—nanoscaffolds, microscaffolds, nanofiber micropore scaffolds—to study the differentiation of neural stem cells. The micro scaffolds and NFMP scaffolds exhibited significantly larger cell populations than the nanoscaffolds. This was probably due to the fact that the micropores within microscaffolds and NFMP scaffolds provided space for cells to infiltrate and grow in three dimensions. On the other hand, the nanopores in nanoscaffolds were too small for cells to infiltrate; therefore, the cells could only grow on the surface. The nanostructures within NFMP scaffolds induced partial neural differentiation and suppressed cell proliferation. To quantify the extent of neural differentiation, two intracellular markers were used: beta-tubulin III (Tuj) for neurons and

nestin for neural progenitors. A large number of cells from all three groups stained positive for both Tuj (red) and nestin (green) at 14 days into differentiation. According to the quantitative differentiation, the microscaffolds exhibited a significantly smaller percentage of Tuj positive cells, compared to the nanoscaffolds and NFMP scaffolds, which were indistinguishable from each other relative to the Tuj positive cell percentage. Moreover, Tuj positive neurites, which are four times longer than soma bodies, were found on the nanoscaffolds and NFMP scaffolds, while cells on the microscaffolds only developed short neurites [152].

2.7.5 Astrocyte Transplantation

Different types of astrocyte transplantation have been studied, from the early use of rodent immature astrocytes to the currently popular human glial-restricted precursor (GRP)-derived astrocyte (hGDA) with specifically identified phenotypes. In most transplantation methods, astrocytes are locally injected into the injured site at different times after injury. One of the earlier forms of astrocyte transplantation was performed in 1990 by Kliot et al. [250], who used embryonic astrocytes from the spinal cord, which was locally injected seven days after injury. This lead to the growth of injured dorsal root fibers with long-lasting terminals formed by regenerated fibers with limited inflammatory response. But their results were variable. Another research study in 1995 by Wang et al., who used cortical cells from the cerebral cortex of a new born rat, showed a reduction in scar tissue formation [251]. In 2004, Joosten et al. locally injected neonatal astrocytes into Wistar rats, which were able to regain subtle motor function in the hind legs [252]. The Proschel Laboratory has taken advantage of the ability to generate enriched populations of two distinct types of astrocytes from GRP cells. These astrocyte populations, referred to as GRP-derived astrocyte-BMP and GRP-derived astrocyte-CNTF (GDA^{BMP} and GDA^{CNTF}, respectively), differ in several properties, including their morphology, marker expression, and ability to support

neurite outgrowth. GDA^{BMP} has been likened to astrocytes found during normal development, while GDA^{CNTF} resembles reactive astrocytes formed in response to numerous CNS insults. Also, human GDA^{BMP} promotes neuronal survival, axonal growth, and recovery of volitional foot placement, while human GDA^{CNTF} does not [253, 254].

2.8 Spinal Cord Injury

The pathological progression of SCI is often separated into two types: primary and secondary, as shown in Figure 2.26. Primary injury consists of the initial trauma and local tissue injury caused by, for example, bone fracture, stretching, flexion, rotation, laceration, compression, or displacement of the spinal cord. Secondary injury involves the spread of damage from the original site to adjacent tissue through a series of events initiating from the trauma itself and having negative implications. The secondary injury can continue for several months after the primary injury. Secondary injury includes many mechanisms:

- Damage to blood vessels: This is especially prevalent in small vessels and results in ischemia (restriction of blood supply to tissues), thrombosis (local clotting or blood coagulation), and hypoxia (oxygen starvation) [11].
- Reactive oxygen species: These are produced during ischemia and contribute to oxidative stress. After cells' ability to protect themselves from oxidative stress using antioxidants comes to an end, proteins, nucleic acids, and lipids will oxidize and cause damage.
- Depolarization from primary damage: This causes voltage-dependent channels in the cells to open, resulting in a mass release of ions, edema, and intracellular Ca^{2+} overload. This calcium ion imbalance causes damage, inhibiting cellular respiration and stimulating lipases (lipid catabolism) and proteases (protein catabolism), which subsequently degrade important protein structures in the CNS.

- Immune cell recruitment: This leads to the disruption of synaptic connections, and axonal degradation, contraction, and demyelination[11].

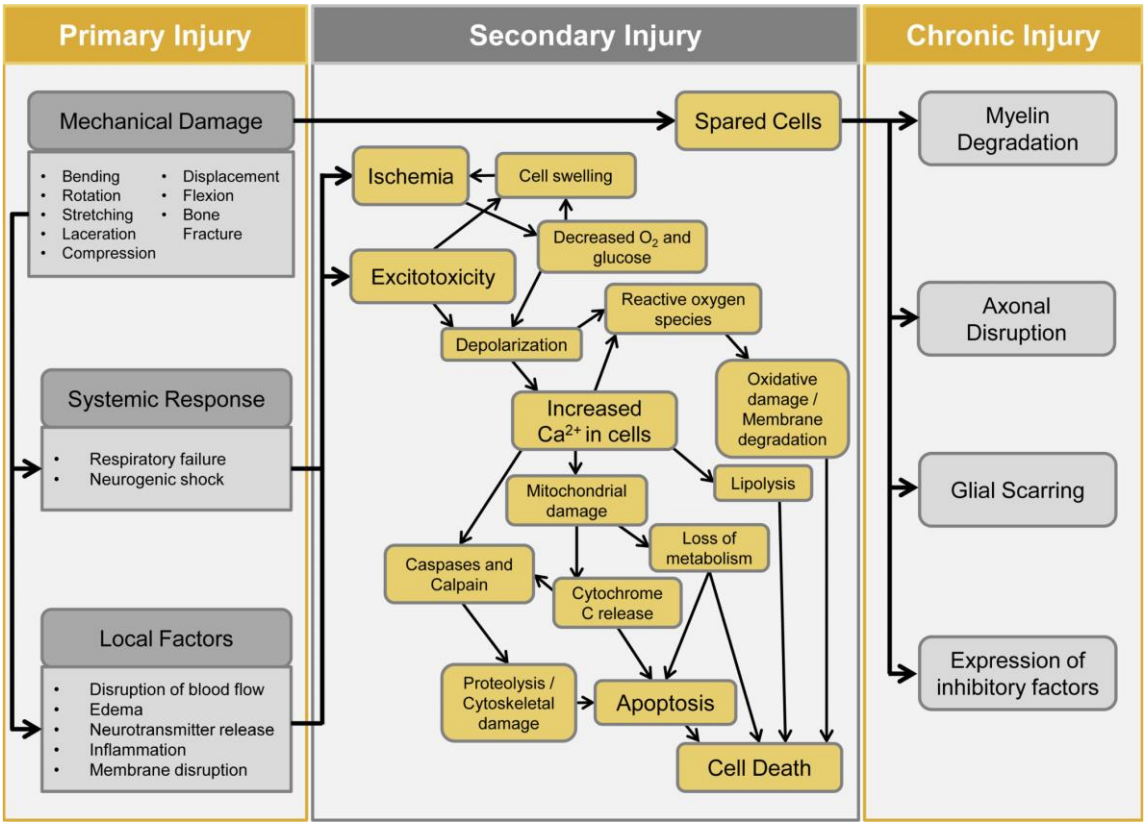

Figure 2.26: Pathophysiology of spinal cord injury showing pathological events during primary SCI, secondary SCI, and recovery phases [11].

CHAPTER 3

EXPERIMENT

For the purpose of simplicity, this experimental section has been divided into three major subsections, as shown in purple in Figure 3.1. Each section has its own set of characterizations (shown in blue in Figure 3.1), which are covered in Chapter 4.

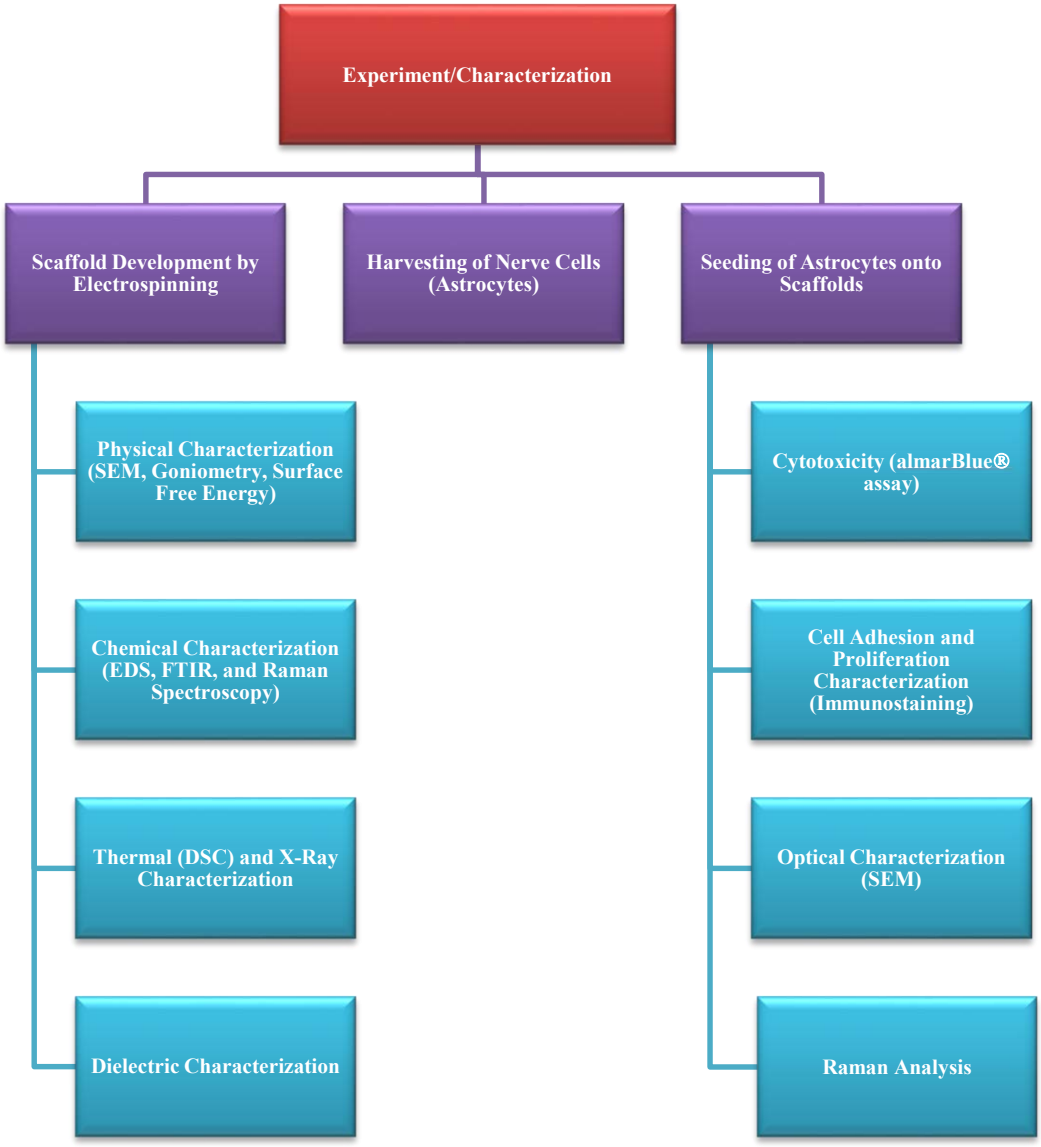

Figure 3.1: Diagram showing flow of experimentation and characterization performed in this study.

3.1 Fabrication of PCL-Based Scaffolds Embedded with Nanomaterials: Electrospinning Process

After several trial-and-error methods, four different types of nanofiber scaffolds were shortlisted in order to culture astrocyte cells. The trial-and-error experiments were performed to determine the appropriate solvent composition that can dissolve PCL completely and the appropriate solute-to-solvent ratio. The main requirement was to fabricate fibers of nanosize diameters and micron-size pores. According to some studies which were mentioned in the literature review in Chapter 2, a combination procedure (microsize pores/ nanosize fibers) provides the best environment for tissue culture since it closely mimics the extracellular matrix within the body. Four types of nanofiber scaffolds were created: (1) pure PCL scaffold, (2) PCL scaffold with graphene (0.05%, 0.1%, and 0.2% by weight), (3) PCL scaffold with carbon nanotubes (0.05%, 0.1%, and 0.2% by weight), and (4) PCL scaffold with fullerene (0.05%, 0.1%, and 0.2% by weight).

3.1.1 Materials and Apparatus Used to Fabricate Nanoscaffolds

The chemicals, shown in Figures 3.2 and 3.3, used to fabricate the scaffolds include the following:

- Polycaprolactone: $(C_6H_{10}O_2)_n$ molecular weight 70,000, pellets, $T_m = 60^{\circ}C$, $T_g = -60^{\circ}C$, Scientific Polymer Products Inc.
- Anhydrous acetonitrile: CH_3CN, 99.8%, boiling point = 82˚C, Sigma Aldrich #271004).
- Glacial ascetic acid: ≥ 99.7% w/w, boiling point = 117˚C, Fischer Scientific #A38212.
- Graphene: nanographene platelets, ≥ 98.48%, X-Y dimensions = ≤ 5 μm, Z dimension = 50–100 nm , ≤ 2.2 g/cc, Angstron Materials Inc. #N008-100-N.

- Carbon nanotubes: catalytic MWCNTs, 5–15 μm, 140 nm diameter, 0.2 g/cc, MER corporation.
- Fullerene (≥ 99.5%, spherical = 0.7–1 nm, clump of crystals = 3 nm, mol.wt 720.64 g/mol, 1.600 g/cc, SES Research # 600-9950.

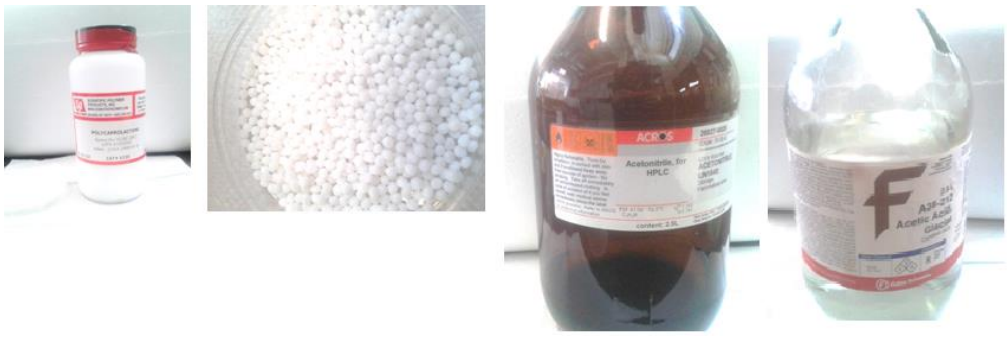

Figure 3.2: PCL, acetonitrile, and acetic acid used for electrospinning of nanoscaffolds.

Figure 3.3: Graphene, MWCNT, and fullerene used for electrospinning of nanoscaffolds.

The apparatus used to fabricate the scaffolds include the following:

- Magnetic stirrer
- Beakers and other glassware
- Heating plate
- Fume hood
- Sterile syringe (10 ml)
- Electrospinning tip

- Hot gun with glue
- Copperwire (1 mm in diameter)
- High DC power source
- Aluminum foil—collector
- Syringe dispenser
- Sterile containers
- Fiberglass insulating chamber

3.1.2 Procedure Used to Fabricate Nanoscaffolds

First, a solution of polycaprolactone mixed with acetic acid and acetonitrile (50:50 (v/v)) was made by magnetic stirring for 12–16 hours at 50˚C. The solvent-to-solute ratio for the mixture was 85:15 by weight. Parameters for the electrospinning process can be found in Table 3.1. The electrospinning process creates nanoscale fibers by applying a strong electric field in a viscous polymer solution that is injected at a constant feed rate though a needle charged with a high voltage. The liquid droplet surface coming off the nozzle elongates to form a dry polymer PCL-based nanofiber matrix. Fibers were collected on a stationary aluminum foil collector, placed at 25 cm from the infusion syringe with an infusion speed of 1 mL/h at 25 kV. Figure 3.4 shows the setup and syringe preparation for the electrospinning process.

TABLE 3.1

PARAMETERS IN ELECTROSPINNING PROCESS

Solute	Polycaprolactone (PCL)
Solvent	Acetonitrile + Acetic Acid (50/50 volume)
Solvent:Solute	85:15
Initial Temperature of Solution	50˚C
Volume of solution	8–10 ml
Infusion Speed	1 ml/hr
Electric Potential	25 kV
Distance between Electrodes	25 cm

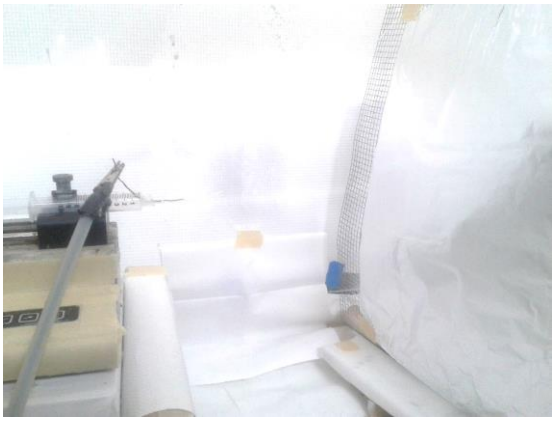

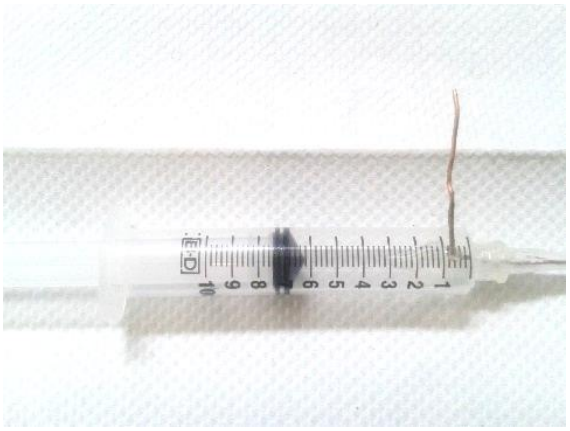

Figure 3.4: Setup (left) and syringe preparation (right) for electrospinning process.

3.2 Harvesting of Neonatal Rat Brain and Culture Astrocyte Glial Cells

For the purpose of this study, astrocyte cells were harvested from neonatal rats. The procedure for isolating the astrocytes was approved by the Institutional Animal Care and Use Committee and completed at the Department of Biological Sciences, Wichita State University, Wichita, KS [255].

3.2.1 Materials and Physical Apparatus Used to Harvest Astrocyte Glial Cells

The chemicals used for harvesting astrocyte glial cells are shown in Table 3.2.

TABLE 3.2

MATERIALS USED FOR HARVESTING ASTROCYTES

Coating on Cell Culture Plates	Mixed Glial Cell Isolation	Microglia Isolation	Maintenance of Cultures
70% ethanol	70% ethanol	70% ethanol	70% ethanol
Borate buffer	Minimum Essential Medium (MEM) culture media (Invitrogen) Gibco, Grand Island, NY	MEM culture media, (Invitrogen) Gibco, Grand Island, NY	Heat-inactivated horse serum (Invitrogen 26050070) Gibco, Grand Island, NY
Borax (71997) Sigma, 3050 Spruce Street, St. Louis, MO 63103	Dissociation media	Dissociation media	Heat-inactivated fetal bovine serum (Invitrogen 10082-147) Gibco, Grand Island, NY

TABLE 3.2 (continued)

Coating on Cell Culture Plates	Mixed Glial Cell Isolation	Microglia Isolation	Maintenance of Cultures
Poly-L-lysine (P-1274) Sigma 3050 Spruce Street, St. Louis, MO 63103	Heat-inactivated horse serum (Invitrogen 26050070) Gibco, Grand Island, NY	Heat inactivated horse serum (Invitrogen26050070) Gibco, Grand Island, NY	Penicillin/streptomycin (Invitrogen 15140-163) Gibco, Grand Island, NY
Autoclaved distilled water	Heat-inactivated fetal bovine serum (Invitrogen 10082-147) Gibco, Grand Island, NY	Heat-inactivated fetal bovine serum (Invitrogen 10082-147) Gibco, Grand Island, NY	MEM culture media (Invitrogen) Gibco, Grand Island, NY
MEM culture media (Invitrogen 11095) Gibco, Grand Island, NY	Penicillin/streptomycin (Invitrogen 15140-163) Gibco, Grand Island, NY	Penicillin/streptomycin (Invitrogen 15140-163) Gibco, Grand Island, NY	Phosphate-buffered saline (554781) BD Biosciences, San Diego, CA 92121
MEM with Earle's salts, modified for suspension cultures (S-MEM) (Invitrogen 11385) Gibco, Grand Island, NY	Trypan blue staining solution (T8154) Sigma	Trypan blue staining solution (T8154) Sigma	

The physical apparatus used for harvesting astrocyte glial cells is show in Table 3.3.

TABLE 3.3

EQUIPMENT USED FOR HARVESTING ASTROCYTES

Coating on Cell Culture Plates	Mixed Glial Cell Isolation and Micro Glial Cell Isolation	Maintenance of Cell Cultures
Autoclave	Autoclave	Autoclave
Six-well cell culture plate	Laminar-flow cell culture hood with UV light	Laminar-flow cell culture hood with UV light
Laminar-flow cell culture hood with UV light	CO_2 incubator (37°C, 95% room air/5% CO_2, 95% humidity)	CO_2 incubator (37°C, 95% room air/5% CO_2, 95% humidity)
Portable power pipette filler/dispenser	Dissecting microscope	Portable power pipette filler/dispenser
	Low-speed (60 rpm) stir plate	
	Low-speed centrifuge (<1000 × g) with swinging bucket rotor and 50-ml conical tube adapters	
	Portable power pipette filler/dispenser	
	Inverted phase-contrast microscope	
	Hemocytometer hand-held counter	

TABLE 3.3 (continued)

Disposable Tools Used during Process
Sterile pipettes, disposable borosilicate glass: 146 mm (5¾ inch) and 229 mm (9 inch)
Serological pipettes, cotton-plugged disposable borosilicate glass, 10 ml short length
Sterile disposable syringes: 5 ml
Syringe filter with 25 cm cellulose acetate membrane: 0.2 μm pore size
Sterile serological pipettes, cotton-plugged disposable polystyrene, individually wrapped: 1 ml, 5 ml, 10 ml, and 25 ml
Sterile vented cell culture flasks: 225 cm^2
Sterile dressing sponges: 4 × 3 inch
Sterile polystyrene centrifuge tubes: 15 ml
Sterile polypropylene tubes: 50 ml
Six-well cell culture plate
Non-Disposable Tools Used during Process
Dumont forceps (Pattern #5): 110 mm length, tip 0.1 × 0.06 mm, 2 each
Curved forceps: 4 inch length, full curve, 0.8 mm tip width, 2 each
Curves forceps: 4 inch length, full curve, 0.4 mm tip width, 2 each
Micro-dissecting scissors: 4 inch length, 25 mm angled blade, 3 each
Mayo scissors: 7 inch length, 50 mm curved blade
Beaker: 50 ml beaker
Stir bar: 25 mm length
Foil: to cover top prior to autoclaving
Pipettes: 5¾ inch Pasteur, 9 inch Pasteur, 10 ml glass serological
Surgical instrument tray
Autoclave

3.2.2 Procedure Used to Harvest Astrocyte Glial Cells

The protocol described here is composed of two continuous steps. The first step focuses on dissecting rat cortices, and the second step entails the dissociation of glial cells including astrocytes, microglia, and a small amount of oligodendrocytes.

Step 1: Dissection of Neonatal Rat Cortices

1. Gently hold and rinse the head and neck of the rat with 70% ethanol.
2. Decapitate the head onto a sterile gauze pad using sterile curved scissors. Place the body in the biohazard plastic bag for disposal. Place the surgical apparatus in 70% ethanol between decapitations to avoid contamination.

3. Use sterile fine-angled dissecting scissors to cut the skin as well as skull at a slight upward angle from the foramen magnum to the eyes along the midline. Use extra caution to avoid damaging the brain cortices.
4. With the 0.8-mm-tip curved forceps, sever the olfactory bulbs at the anterior part and the spinal cord at the posterior part of the brain. Gently move forceps with a slight back angle pulling up the brain, in order to separate the whole brain from the skull base.
5. Place the brain in Hanks' Balanced Salt Solution in a 100 mm Petri dish on ice, and observe the separated brain under the dissecting microscope.
6. Gently slip one side of the 0.4-mm-tip curved forceps under the cortices on either side of the brain so the forceps sits astride the brain.
7. Gently move the forceps from side to side and with a slight back angle pull up from the cortices, in order to separate the cortices from the rest of the brain.
8. With Dumont forceps, gently tease away the meninges coverings on the cortical surface without damaging it.
9. Flip over the cortices to expose the underside of the tissue to remove any extra tissues.
10. Once each cortex is dissected, place them in a sterile 50 ml conical tube containing 10 ml of Spinner-modified Minimum Essential Medium (S-MEM) plus antibiotics on ice.

Step 2: Dissociation of Glial Cells

1. Isolate cerebral cortexes from the brains of neonatal rats after they are sacrificed.
2. Triturate the cortex tissues gently through a 5 mL syringe with a needle.
3. Pass the tissue suspension through a 70 mm nylon cell strainer, and collect the flow-through with a 50 mL conical tube.
4. Culture the isolated cells were cultured for about 7–14 days (Figure 3.5).

5. After reaching confluency, shake the cultures to remove macrophages and progenitor cells.
6. Culture the adherent astrocytes for the study on nanofibers.

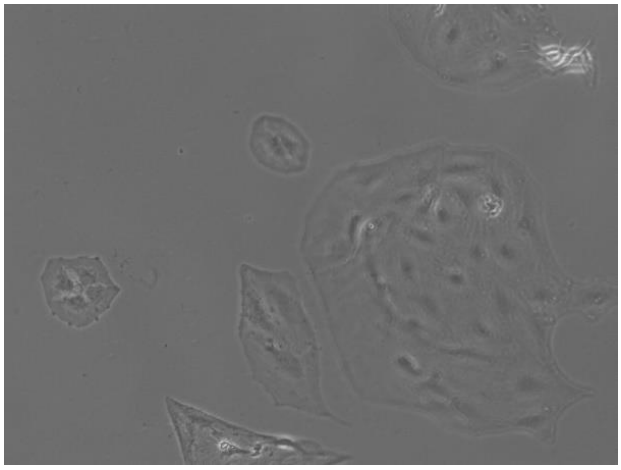

Figure 3.5: Optical microscopy of astrocyte cells.

3.3 Seeding of Astrocyte Cells onto PCL-Based Nanoscaffolds

3.3.1 Materials and Apparatus Used to Seed Astrocyte Cells onto PCL Nanoscaffolds

The chemicals used to seed astrocyte cells onto PCL scaffolds include the following:

- Dulbecco's Modified Eagle Medium (DMEM) solution
- Ethyl alcohol
- Phosphate-buffered saline (PBS)
- Trypsin

The physical apparatus used to seed astrocyte cells onto PCL scaffolds include the following:

- 24-well plate
- Silicone O-rings
- Sharp blade/scissors
- Tweezers

- Incubator
- Sterile fume hood
- Centrifuge
- Hemocytometer
- Optical microscope

Figure 3.6 shows a 24-well plate used to prepare samples for cell seeding.

Figure 3.6: Sample preparation for cell seeding in 24-well plate.

3.3.2 Procedure Used to Seed Astrocyte Cells onto PCL Nanoscaffolds

1. Secure the electrospun fibers to the bottom of a 24-well plate, first by cutting four circular replicates of each fiber type and attaching them to the bottom of the well plate with a silicone O-ring.
2. Spray the well plate with ethyl alcohol to prevent contamination. Retrieve the cell culture containing the astrocytes from the incubator and change the medium by adding fresh PBS. Rinse the cells gently to remove the excess serum, and then add PBS again using the automatic pipet. (NOTE: before using any biological medium, ensure that it is at 37^{o}C.)
3. Add about 2 ml of trypsin to the cell culture, ensuring that the trypsin covers the base of the container because it releases the cells from the bottom of the plate.

4. After five minutes, view the cell culture under the microscope to ensure that all cells are detached from the bottom. Do not prolong the exposure of the cells to trypsin, since they are capable of dissolving the cell wall and killing the cells.
5. After ensuring that all cells are detached, add DMEM to neutralize the trypsin. Using the automatic pipet, agitate the solution, ensuring no air bubbles are formed.
6. Add the cell solution to a centrifuge tube and centrifuge at about 650 rpm for 4–5 minutes, keeping in mind that the rpm and the time are critical, as high rpms and prolonged times may destroy the cells.
7. Note that the cells form a white residue at the bottom of the centrifuge tube, and pipet out the top medium that is devoid of the cells.
8. Re-suspend the cell concentrate by adding 500 µl to 1 ml of fresh DMEM from the centrifuge, and mix this to obtain a homogeneous solution.
9. Use a sterilized (using water and ethanol) hemocytometer (cell counter slide) to count the cells.
10. Add about 10 µl of the re-suspended cell solution to the hemocytometer (4 x 4 grid), count the cells in the first row, and multiply this number by 4. For more accuracy, count the cells in the entire 4 x 4 grid. This number gives an estimate of the cell concentration.
11. Add 50,000 cells to each well.
12. Top each well with 500 µl of fresh DMEM, in order to provide nutrition to the seeding cells.
13. Change the DMEM every 3–4 days to provide constant nutrition to the cells.

CHAPTER 4

CHARACTERIZATION METHOD, RESULTS, AND ANALYSIS

4.1 Morphology and Surface Characterization of Electrospun Fibers

4.1.1 Contact Angle and Work of Adhesion

Precise characterization of solid material surfaces plays a vital role in research and product development in many industrial and academic areas. Wettability and surface energy is an important aspect to be analyzed for implant applications. A static sessile drop method employing a goniometer (CAM 100, KSV Instruments Ltd., Helsinki, Finland) was used to capture the image of a liquid drop and record its shape as a function of time. This image was captured at the rate of ten frames per second with ten repetitions. Only results having a standard deviation of less than 2 degrees were considered. A FireWire connectable CCD camera with 50 mm optics was used.

The density of water (1g/cc) is comparable to the density of extracellular fluid within the body, which is mainly blood (1.06 g/cc); hence, water was used as the liquid for this characterization. The drop image was analyzed with a profile fitting method in order to determine contact angle and surface tension. The contact angle, ranging from 1° to 180° was measured using this instrument with an accuracy of ±0.1°. The software used curve fitting based on the Young-Laplace equation. A schematic diagram of the goniometer setup is shown in Figure 4.1.

The shape of the drop depends on the surface tension of the liquid, gravity, and the density difference between the liquid (water) and substrate (electrospun scaffold) and the surface free energies. Basically, the three phases—solid (scaffold-S), liquid (water drop-L), and gaseous (ambient air-G)—are in thermodynamic equilibrium. The interfacial energies among the three phases, as shown in Figure 4.2, are as follows:

γ_{SG}: Interfacial energy between solid and gas

γ_{SL}: Interfacial energy between solid and liquid

γ_{LG}: Interfacial energy between liquid and gas

Young's equation can be denoted by

$$\text{Cos}\,\theta = \frac{\gamma_{SG} - \gamma_{SL}}{\gamma_{LG}} \qquad (4.1)$$

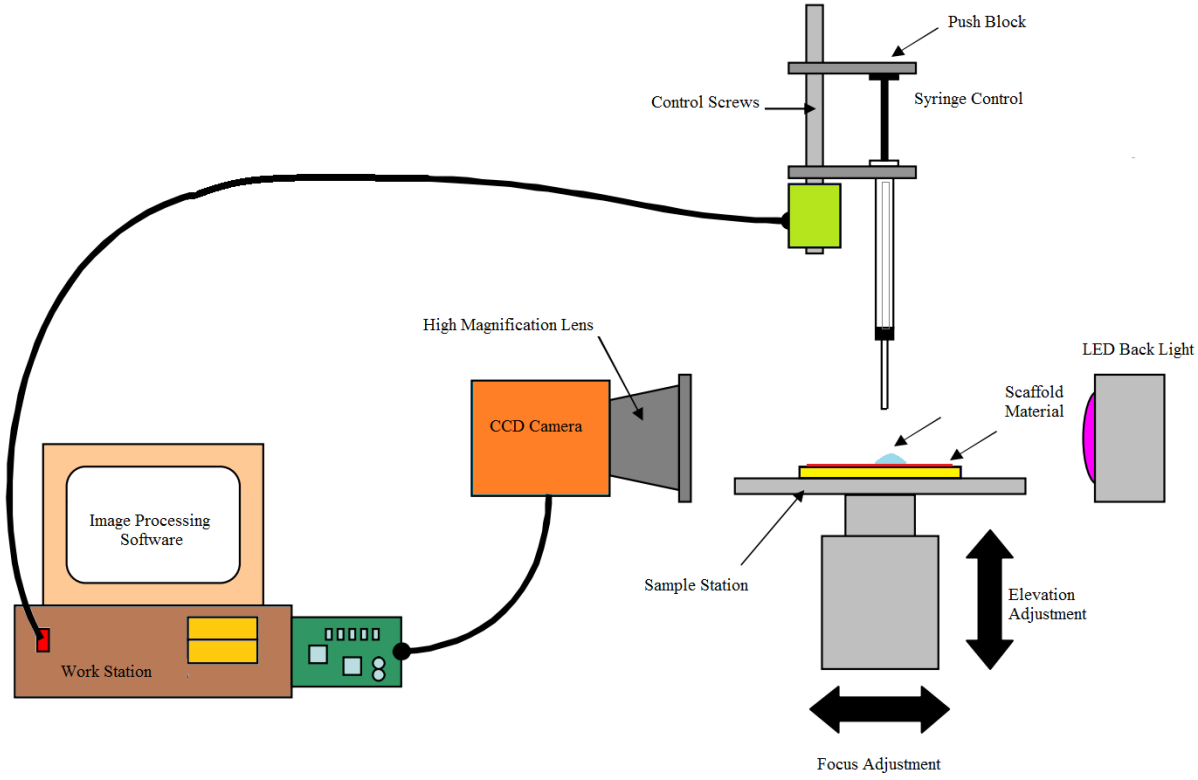

Figure 4.1: Schematic showing the working of a basic goniometer

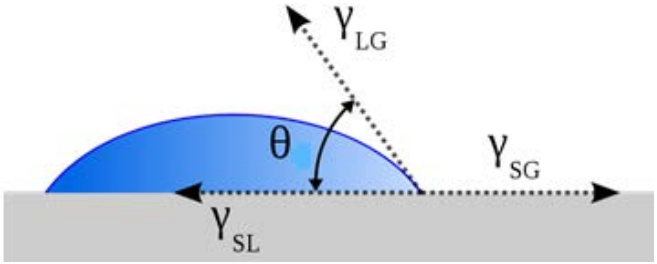

Figure 4.2: Interfacial energies among the three phases.

From the tests, it was found that the PCL scaffold in general is hydrophobic with a contact angle of 110° (Figure 4.3). The literature shows that the contact angle of PCL fiber varies from 70º to 120º. The process of electrospinning is known to increase the hydrophobicity of fibers. The water-repellent properties of PCL electrospun materials are due to their rough, rippled surfaces, which trap air between the ripples. This trapped air prevents liquids such as water from penetrating the ripples, forcing it to remain perched on top as intact droplets [10, 256-258] .

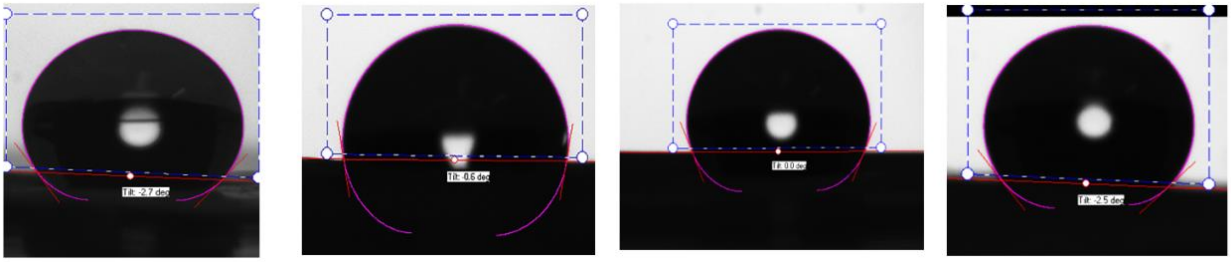

Figure 4.3: Contact angle results from PCL, PCL-fullerene 0.2%, PCL-CNT 0.2%, and PCL-graphene 0.2%.

According to the Royal Society of Chemistry, scientists have proven that hydrophobic materials act as an excellent medium for drug delivery over an extended period of time. The hydrophobicity lowers the degradation kinetics and increases the time for hydrolysis, thereby increasing the time for cell attachment before degradation [259, 260]. The effect of adding nanomaterials to PCL nanofibers is shown in bar graphs in Figures 4.4 and 4.5.

In general, the trend shows that with an increase in percentage of nanomaterials, the contact angle increases. But with fullerene, the contact angle has a marginal effect and is lower than that of pure electrospun PCL.

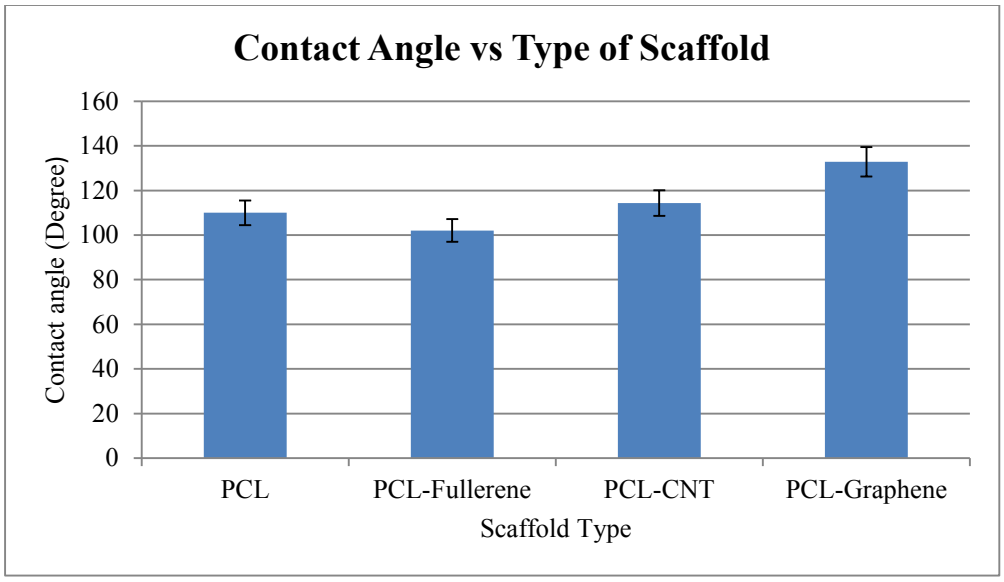

Figure 4.4: Effect of type of nanoparticle on contact angle.

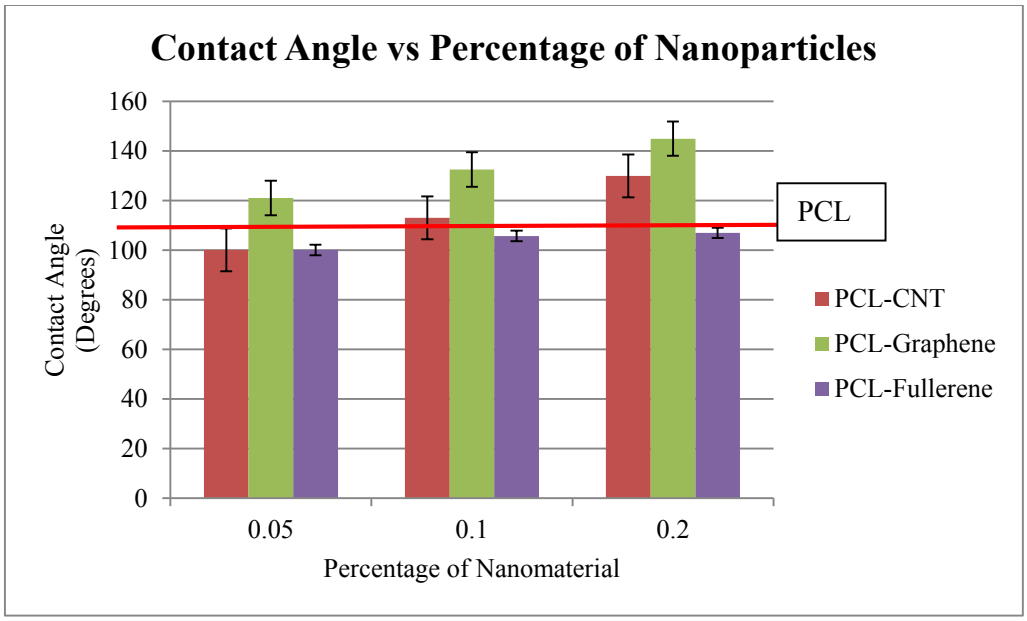

Figure 4.5: Dependence of nanoparticle concentration on contact angle.

In order to fully understand the significance of contact angle, the work of adhesion between the solid- PCL scaffold and the liquid-water was calculated. As shown previously in equation (4.1), the surface free energy of the solid is described by using the contact angle θ, interfacial tension between the solid and gas γ_{SG}, interfacial tension between the solid and the liquid γ_{SL}, and

interfacial tension between liquid and gas γ_{LG}. Thermodynamic adhesion is the work required to separate the surfaces into two new surfaces. The equation for the work of adhesion can be written as

$$W_{Adhesion} = \gamma_A + \gamma_B - \gamma_{AB} \tag{4.2}$$

where γ_A is the surface tension of phase A, γ_B is the surface tension of phase B, and γ_{AB} is the interfacial tension between two phases. Now, if the other phase is solid and the other liquid, then equation (4.2) can be written as

$$W_{SL} = \gamma_{LG} + \gamma_{SG} - \gamma_{SL} \tag{4.3}$$

Equations (4.1) and (4.3) can be combined into Young-Dupré equation:

$$W_{SL} = \gamma_{LG}(1 + \cos\theta) \tag{4.4}$$

From the data sheet, it is known that the surface tension of pure water (γ_{LG}) at 25ºC is 7.2 N/m, or the surface energy density is 7.2 J/m^2. The work of adhesion for different scaffolds is shown in Table 4.1. Adhesion is the tendency of dissimilar particles or surfaces to cling to one another. An alternate way of looking at surface energy is to relate it to the work required to cleave a bulk sample, thus creating two surfaces. Hence, the work of adhesion provides an estimate of the surface energy.

TABLE 4.1

WORK OF ADHESION OF PCL-BASED NANOSCAFFOLDS AT VARIOUS CONCENTRATIONS

Concentration (%)	**PCL-Graphene (x 10^{-2} J/m^2)**	**PCL-CNT (x 10^{-2} J/m^2)**	**PCL-Fullerene (x 10^{-2} J/m^2)**
0.05	3.6	5.9	5.9
0.1	2.1	4.1	5.8
0.2	1.52	2.5	5.6

With an increase in the percentage of nanomaterials, the work of adhesion decreases. Nanoparticles act as points of defects/impurities within the electrospun scaffold, which may

contribute to the decrease in surface adhesion. Also, the work of adhesion for the PCL scaffold itself without any nanoparticle inclusion was calculated to be 5.09J/m^2. PCL infused with fullerene showed an increase in adhesion. Adhesion itself is governed by a number of factors, such as the presence of a chemical bond, presence of a hydrogen bond, surface roughness, presence of entrapped air molecules, impurities, thickness of fiber diameter, and type of nanomaterial. The interaction of different factors can be quite complex. Adhesion also depends on the fiber diameter. Lower fiber diameters show lower adhesion and hence higher hydrophobicity. Lower fiber diameters increase the density of nanoscale ripples on the surface. The literature shows that the contact angle of water on a fullerene coating is around 91.5°. The carbon wafers coated with fullerenes were assessed by using the expanded Fowkes method, derived from Owens-Wendt theory [261, 262].

Carbon nanotubes are known to show a highly hydrophobic character with contact angles between 144° and 176°. The orientation of the CNTs plays a very important role in the work of adhesion. On average, the contact angle is around 115° [263]. According to Shin et al., the contact angle of water on graphite is 90°–95°, and they suggested a contact angle of 127° for graphene [264]. The interactive potential energy between water and graphene-based substrates is the main contribution to the work of adhesion of water, with a relative magnitude that is independent of the number of graphene layers. They believe that the remaining contribution is entropic in nature and is connected to fluctuations in the water substrate interaction energy. Similarly, according to Taherian et al., who reported a contact angle of 120°, the wetting properties of graphene are not sensitive to the number of layers. The hydrophobic surface becomes more hydrophobic when microstructured [265].

4.1.2 Scanning Electron Microscopy

The morphology of the nanoscaffolds was analyzed by using scanning electron microscopy. A ZEISS SIGMA VP scanning electron microscope (Carl Zeiss Microscopy, LLC, Thornwood, NY) (Figure 4.6) and energy dispersive spectroscopy (EDS) were used in this study. The SEM images were used to measure the fiber diameter using NIH ImageJ software (National Institutes of Health, Bethesda, MD). Very thin layers of fibers were attached to carbon stubs and coated with 1.5 μm of gold to improve conductivity and imaging under a vacuum.

Figure 4.6: Scanning electron microscope.

To quantify the fiber diameter, 150 fibers from each type of fiber were measured using ImageJ software and an average was taken. The fiber diameters of the nanoscaffolds, tabulated in Table 4.2, vary from 80 nm to 200 nm with PCL-fullerene > PCL-CNT > PCL > PCL-graphene. From the SEM images shown in Figure 4.7, it is clear that the electrospinning process is suitable for fabricating a nearly ideal tissue engineering scaffold. By carefully controlling the process parameters, it is possible to control the fiber diameters within a certain range. The high surface area and extracellular-like physical environment provided by nanofibers compared to that of other

non-fibrillar surfaces may have led to an increase in cellular attachment and the observed cell polarity.

TABLE 4.2

FIBER THICKNESS OF NANOSCAFFOLDS

Scaffold	Average Fiber Thickness (nm)
PCL	123.2
PCL-Graphene	116.73
PCL-CNT	165.1
PCL-Fullerene	186.55

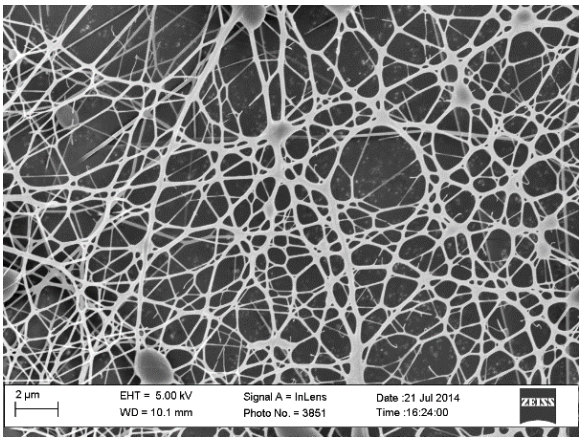

(a) PCL Nanoscaffold

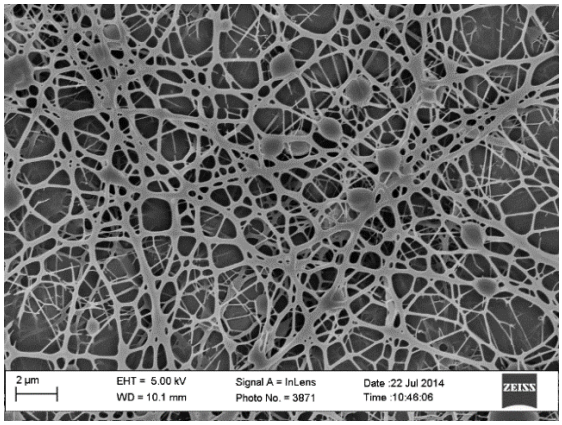

(b) PCL-CNT 0.1%

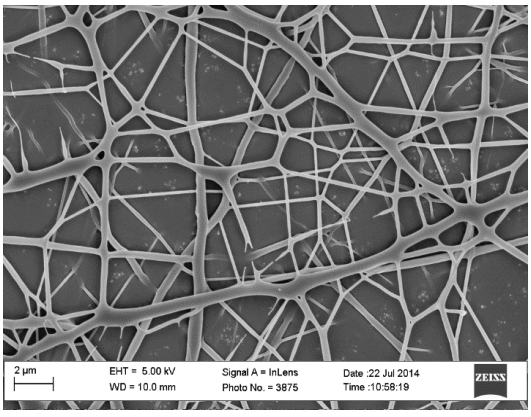

(c) PCL-CNT 0.2%

Figure 4.7 SEM images of nanoscaffolds fabricated by electrospinning process: (a) PCL, (b) PCL-CNT 0.1%, (c) PCL-CNT 0.2%, (d) PCL-graphene 0.05%, (e) PCL-graphene 0.1%, (f) PCL-graphene 0.2%, (g) PCL-fullerene 0.2%.

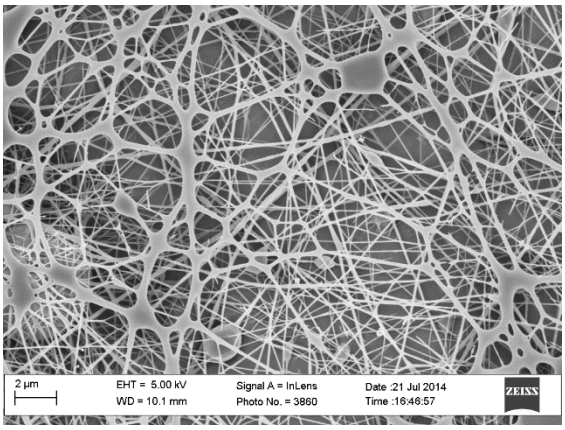

(d) PCL-Graphene 0.05%

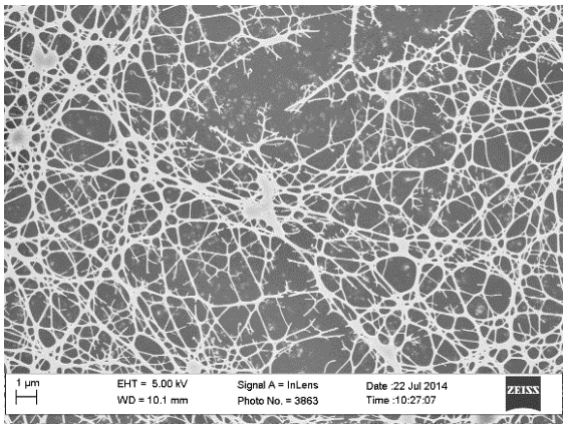

(e) PCL-Graphene 0.1%

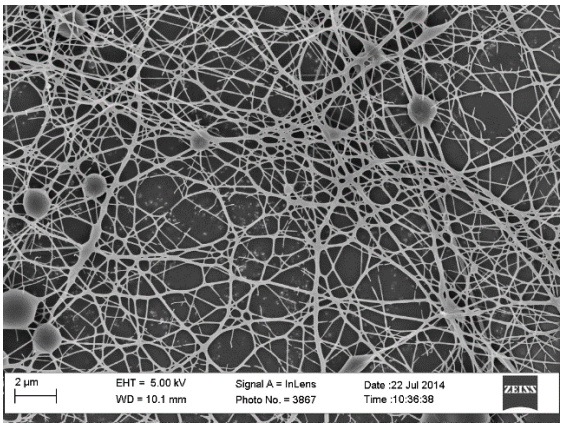

(f) PCL-Graphene 0.2%

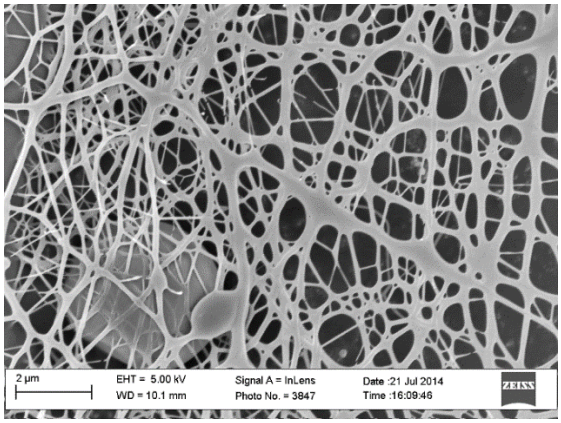

(g) PCL-Fullerene 0.2%

Figure 4.7: (continued)

Almost all biological structures, human tissues, and organs are deposited onto nanofibrous forms or structures. All of them are characterized by well-organized hierarchical fibrous structures realigning on a nanometer scale. The basic architecture of nerve tissue from the brain or spinal cord very closely resembles that of an electrospun scaffold. Cheng and Kisaalita [152], introduced the concept of dual-scale scaffold, wherein the microporous structure facilitated cell infiltration and multi-cellular organizations in the pores, and the nanofibrous structures promoted cell differentiation and a more in-vivo-like cell-matrix adhesion. The scale of the porosity of these scaffolds has not been confirmed; nevertheless, the nanoscale of the fiber diameters are confirmed.

For cells to grow through the scaffold architecture, it is necessary for the scaffolds to have a minimum pore size of 10 μm. In reviewing the SEM images, the pore sizes seem to be on a much smaller scale, and there is a possibility that the cell growth might be restrained to only the top layer. It can be hypothesized that the increased strength of random fibers results from more compactness of nanofibers in the web, which can assist them to withstand higher loadings. Bi-polar and tri-polar extensions with spindle-shaped morphology are characteristics of astrocytes. Hence, random fiber alignment might prove to be beneficial for cell adhesion growth and proliferation [266].

4.2 Compositional Characterization of Nanoscaffolds Using Spectroscopy

4.2.1 Energy Dispersive X-Ray Spectroscopy

Information about atomic bonds and the structure of molecules comes by studying their interaction with light (electromagnetic radiation). Different regions of the electromagnetic spectrum provide different kinds of information as a result of such interactions. Backscattered electron images in the SEM display a compositional contrast that results from different atomic number elements and their distribution. EDS allows one to identify what those particular elements are and their relative proportions (for example, atomic percent [at%]). Elemental analysis and chemical characterization was done using the ZEISS SIGMA VP scanning electron microscope. The results of EDS spectral analyses of PCL, PCL-graphene 0.2%, PCL-CNT 0.2% and PCL-fullerene 0.2% are shown in Figure 4.8. The gold that appears here is because of the gold coating on the samples to improve the image quality. Some of the electrospun fibers contain blobs, and spectral analysis was performed on both the fibers and the blobs, as there is no compositional difference between the two. Results from the EDS are shown in Table 4.3.

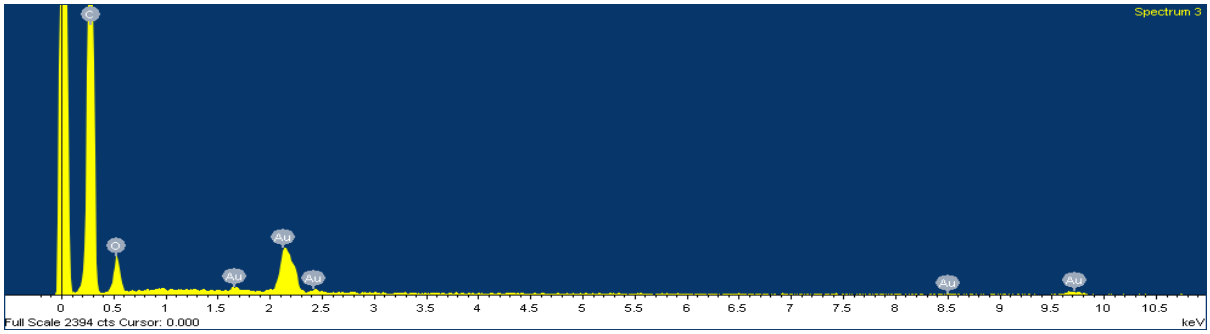

(a) PCL Nanoscaffold

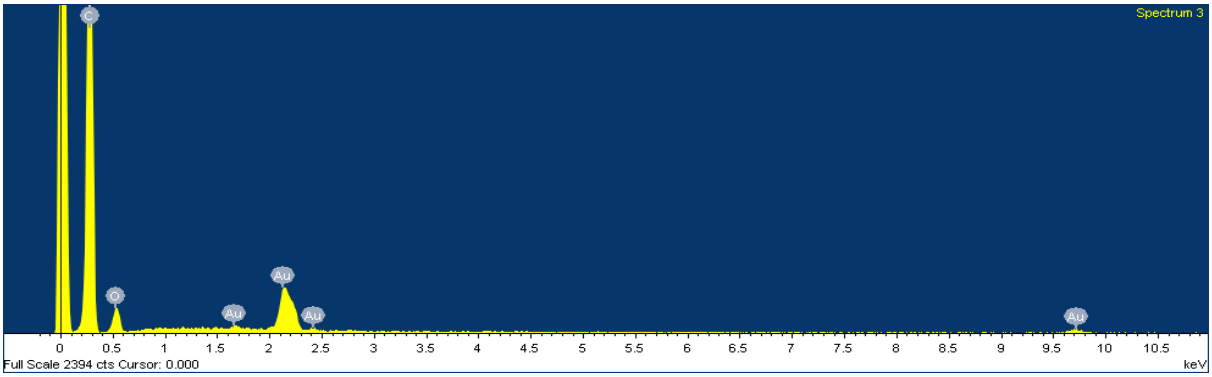

(b) PCL-Graphene 0.2%

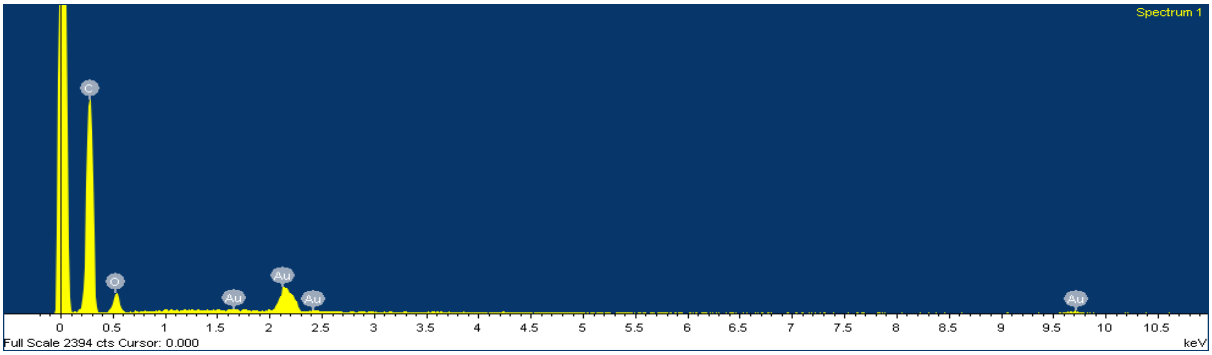

(c) PCL-CNT 0.2%

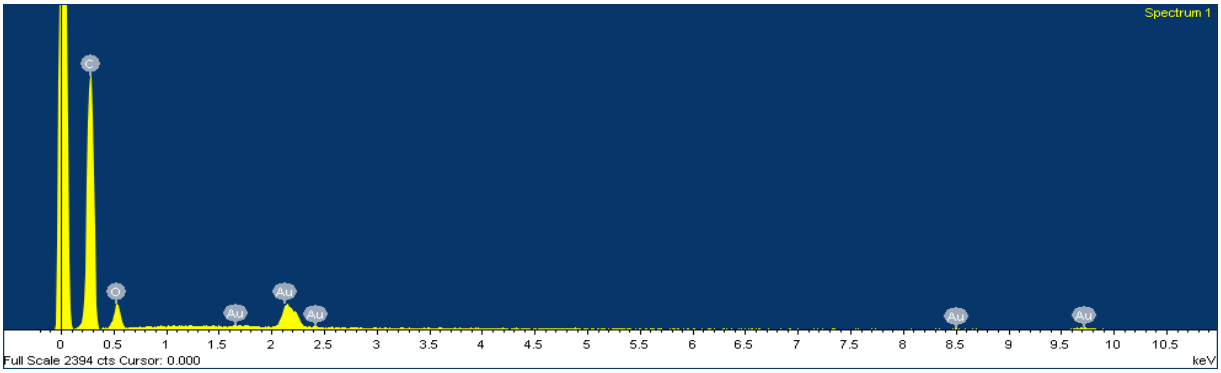

(d) PCL-Fullerene 0.2%

Figure 4.8: EDS results of analysis of nanoscaffolds: (a) PCL, (b) PCL-graphene 0.2%, PCL-CNT 0.2%, PCL-fullerene 0.2%.

TABLE 4.3

EDS RESULTS

Material	Carbon (wt%)	Carbon (at%)	Oxygen (wt%)	Oxygen (at%)
PCL	73.02	88.50	15.24	13.86
PCL-Graphene 0.2%	75.21	90.89	12.73	11.55
PCL-CNT 0.2%	72.74	85.94	17.41	15.44
PCL-Fullerene 0.2%	71.47	86.31	15.24	13.82

From the EDS results, it is clear that the nanoparticles were not contaminated with heavy metals that are usually used as catalysts during their production. It was important to confirm this because most of the toxicity of nanoparticles is caused by the presence of small amounts of nano-sized heavy metals. EDS result also shows that the elemental composition on the scaffolds is primarily carbon and oxygen, both of which are compatible with biological systems. Further analysis about the type of bonds can be done using Fourier transform infrared (FTIR) spectroscopy The trace amounts of gold resulted from the samples being gold coated to improve the resolution.

4.2.2 Fourier Transform Infrared Spectroscopy

The FTIR spectroscopy technique serves the purpose of identifying unknown substances. They are widely used to study bond types. In addition, since FTIR spectrometers can be hyphenated to chromatography, the mechanism of chemical reactions and the detection of unstable substances can be investigated with such instruments. Figure 4.9 shows the FTIR results of the analysis of nanoscaffolds. Figure 4.9(a) shows the FTIR results of a PCL fiber. The results obtained were in accordance with established results. Prominent peaks can be observed at 2944, 2864, 2150, 2022, 1710, 1418, 1365, 1293, 1240, 1174, 1107, 1046, 961, and 732 cm^{-1}. Of these, 2944 shows the C-H stretch, the long 1710 shows the carbonyl stretch, 1471 shows C-H scissoring, 1240 shows the C-O stretch, and 961 and 732 show the C-C stretch.

From Figure 4.9(b) prominent fullerene peaks can be observed at 525, 574, 1179, and 1427 cm^{-1}. Fullerene has a very high symmetry. In spite of having 174 vibrational degrees of freedom for each C60 molecule, the icosahedral symmetry of the fullerene gives rise to a number of degenerate modes, so only 46 frequency modes are expected for this molecule. Of these, four are infrared active, 10 are Raman active, and the remaining are optically inactive. The 525 and 574 peaks are associated with radial motion of the carbon atoms, and peaks 1179 and 1427 are associated with tangential motion. [267]

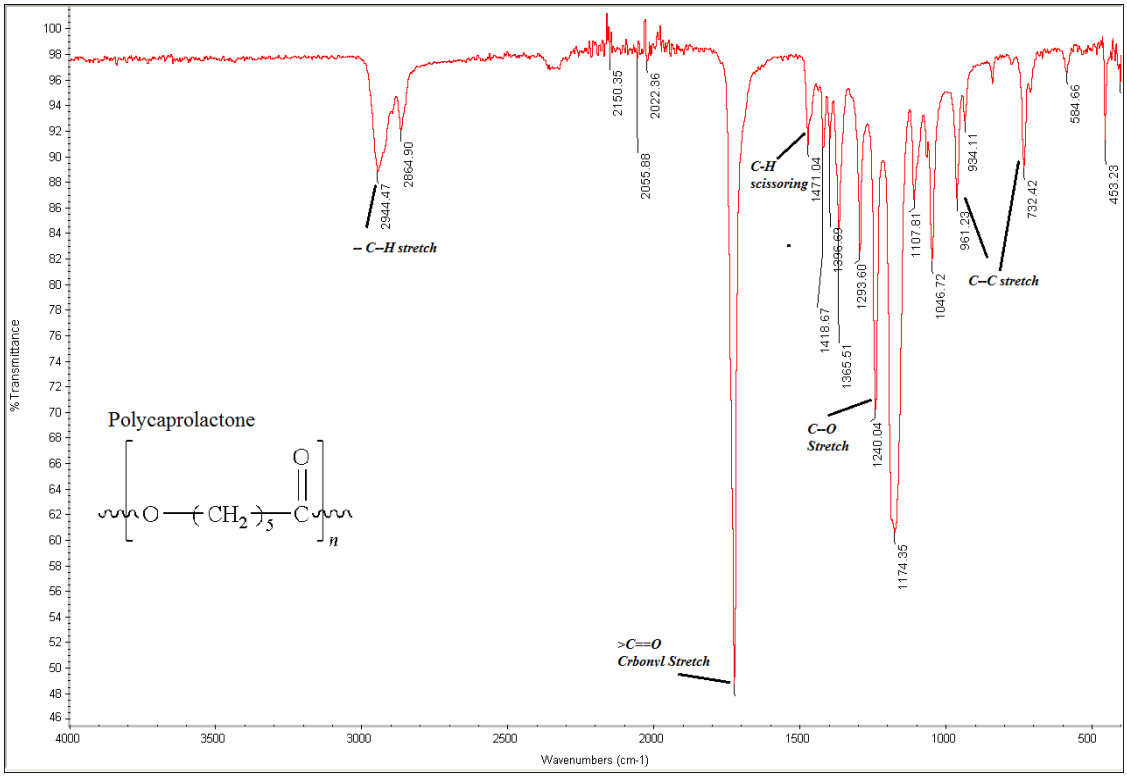

(a) PCL

Figure 4.9: FTIR results of analysis of nanoscaffolds: (a) PCL, (b) fullerene, (c) PCL-fullerene, (d) PCL-CNT, and (e) PCL-graphene.

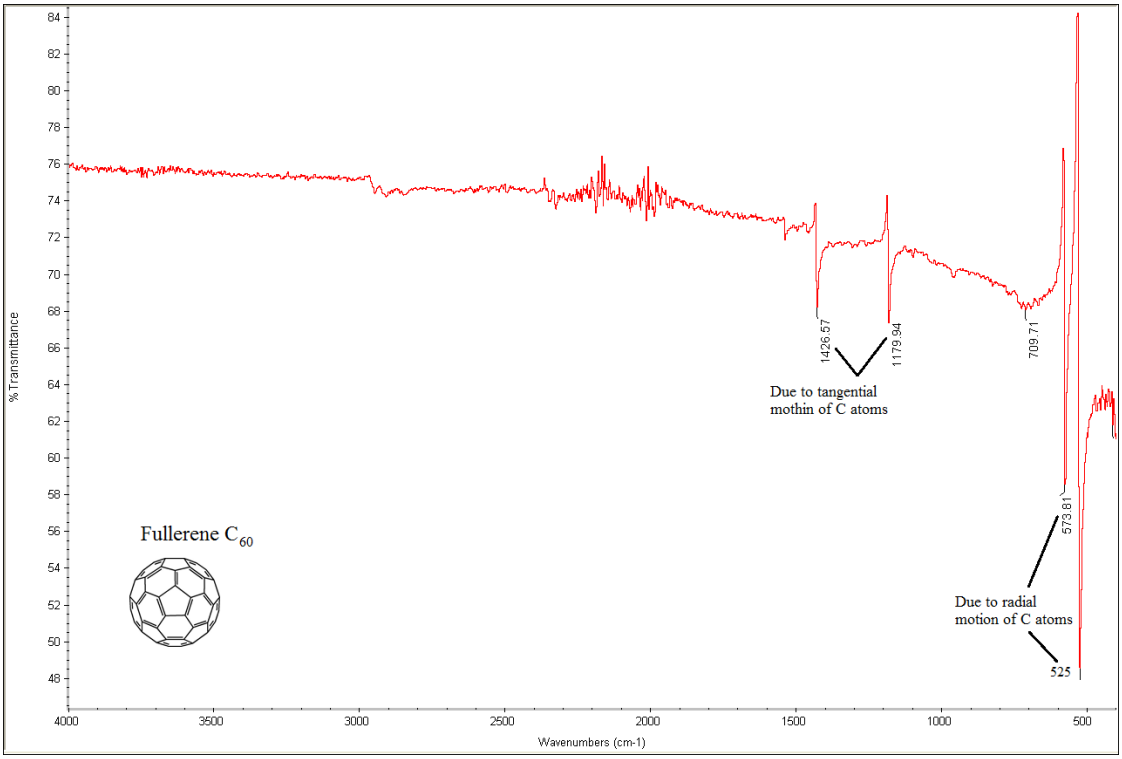

(b) Fullerene

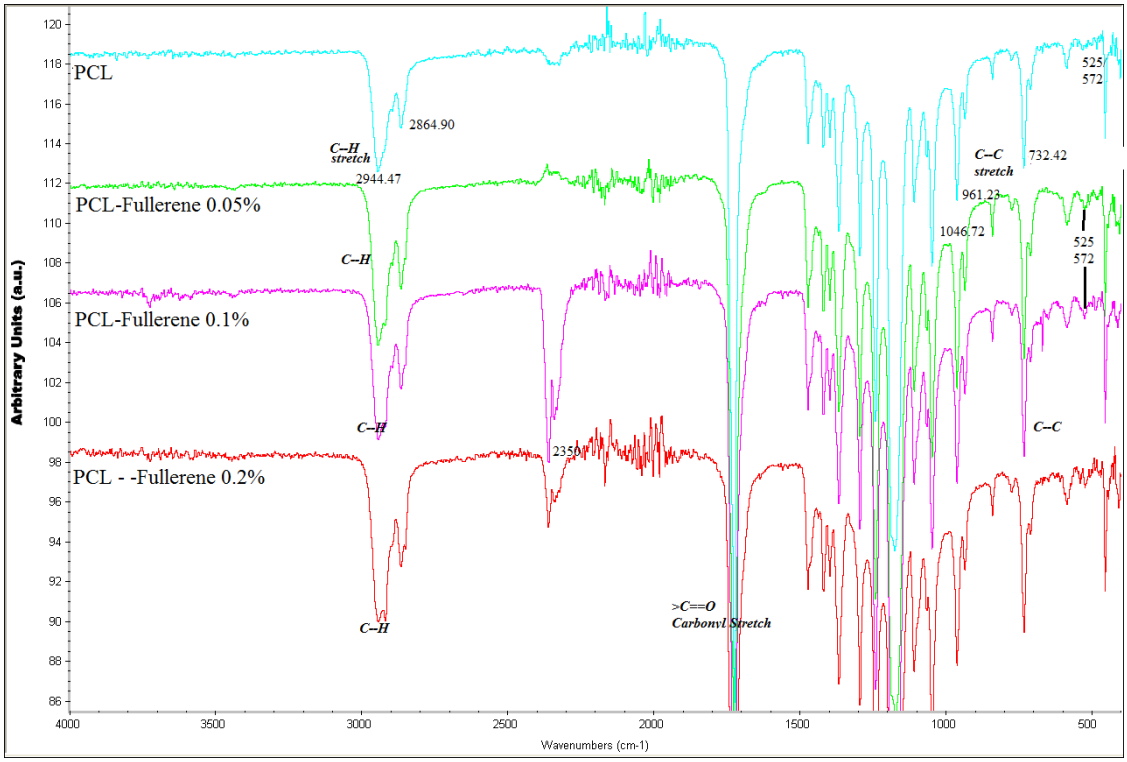

(c) PCL-Fullerene

Figure 4.9: (continued)

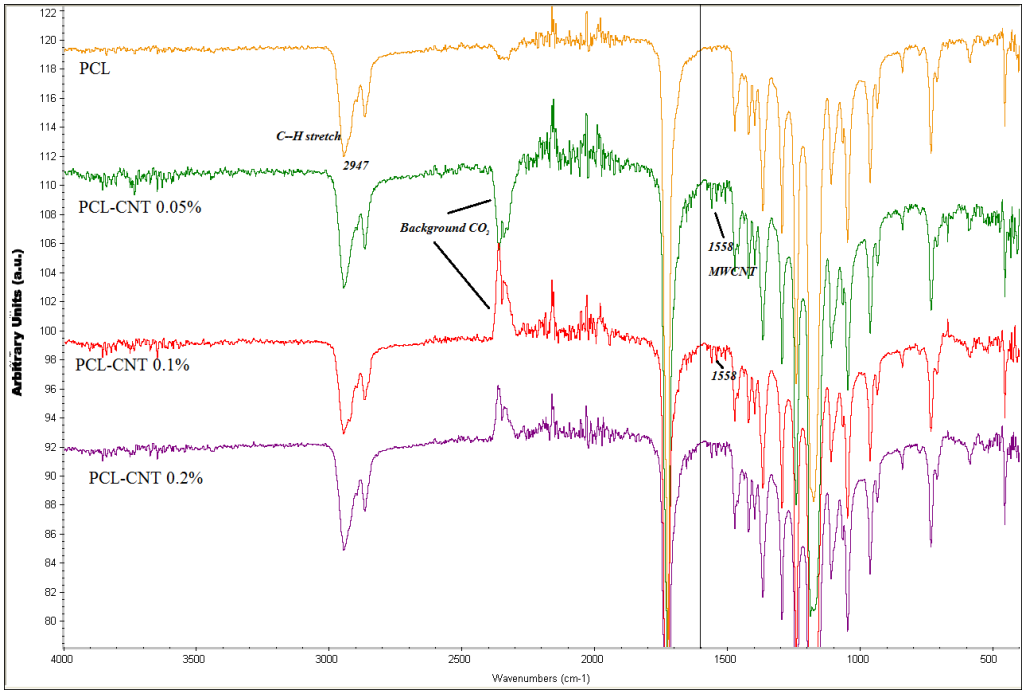

(d) PCL-CNT

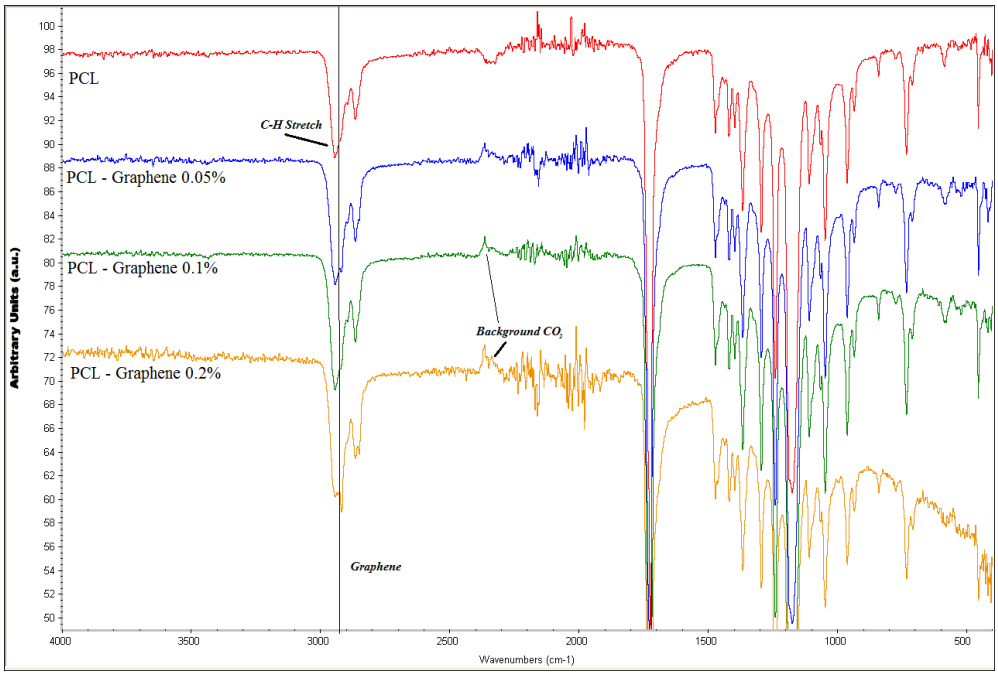

(e) PCL-Graphene

Figure 4.9: (continued)

Figure 4.9(c) shows an increase in the C-H stretch with the increase in fullerene concentration at 2944 and 2864. The C-C stretch at 732.42 also seems to increase. Small peaks at

525 and 572, which were not present in the original PCL, also emerge [267]. Figures 4.9(c) and 4.9(d) show an extra peak at 2350, which is actually background CO_2. According to Park et al.[80], pristine MWCNTs show up at around 1560. In Figure 4.9(d) peaks that were initially not present in PCL show up in the subsequent PCL-CNT scaffolds, confirming the presence of CNT [80, 268]. Figure 4.9(e) shows the FTIR analysis of PCL-graphene scaffolds. According to Naebe et al.[269] , pristine graphene shows up in the 2900 region. With the increase in percentage of graphene, the peak at 2930 keeps increasing [269]. From Figure 4.9(e), the length of the C-H stretch increases at 2944 and 2864, whereas the C-C stretch increases at 732. The FTIR analysis confirms the presence of nanomaterials in the scaffolds.

4.3 Thermal and X-Ray Characterization of PCL-Based Nanoscaffolds

According to the literature, the degree of crystallinity may play an important role in cell compatibility, adhesion, growth, and proliferation. Polycaprolactone is a semicrystalline polymer, and the fabrication process, operation parameters, and presence of carbon-based nanomaterials may alter their degree of crystallinity. Non-isothermal crystallization behavior is an important thermal property of semi-crystalline polymers, since most processing techniques are melt-based and actually occur under non-isothermal conditions, and the resulting physical properties including bio-degradability are strongly dependent on the morphology formed and the extent of crystallization. In this experiment, the degradation kinetics was not studied; however, an educated guess based on the degree of crystallinity could be made. The literature indicates, in separate instances, that the higher crystallinity of PCL/PGA (polygycolide) films manufactured by compression molding are suitable for the growth of fibroblasts, whereas amorphous PCL/PGA films support the growth of osteoblasts. Highly crystalline hydroxylapatite showed higher proliferation rates, whereas lower crystallinity showed enhanced cell attachment in human

fibroblasts. A higher percentage of crystallinity in the PHB/PHBV (polyhydroxybutyrate/poly 3-hydroxybutyrate-co-3-hydroxyvalerate) mixture encouraged higher proliferation of Schwann cells (peripheral nerve cells). The effects of crystallinity of the scaffold on the cells of the central nervous system are known. Crystallinity of the PCL polymer in electrospun scaffolds were characterized by wide-angle x-ray diffraction (WAXD) and differential scanning calorimetry (DSC) methods [266, 270, 271] .

4.3.1 Differential Scanning Calorimetry

DSC determines the heat flow rate associated with thermal changes that can be measured as a function of temperature and time. Thermal properties were evaluated under a nitrogen atmosphere using a differential scanning calorimeter (Q2000, TA Instruments), 10°C/min heating and cooling rates, and a heating temperature range of 0–500°C. The nitrogen flow rate was 50 ml/min. Specifications about the accuracy are provided in Table 4.4.

TABLE 4.4

SPECIFICATIONS OF Q2000 DSC APPARATUS (copyright TA instruments)

Temperature Accuracy	± 0.1° C
Temperature Precision	± 0.01° C
Temperature Range (with cooling accessory)	-180 to 725 °C
Calorimetric Precision (indium metal)	± 0.05%
Calorimetric Reproducibility (indium metal)	± 0.05%
Sensitivity	0.2 µW
Baseline Curvature with Tzero (-50 to 300° C)	10 µW
Baseline Reproducibility with Tzero	± 10 µW
Indium Height/Width Ratio	60 mW/°C

The degree of crystallinity (Xc) was assessed using Universal Analysis (TA Instruments) software by analyzing the melting curves. This was calculated as $\Delta H_m/\Delta H_m^o$, where ΔH_m is the enthalpy of melting of electrospun PCL fibers, and ΔH_m^o is the enthalpy of melting of fully

crystalline PCL, which is 136.08 J/g. A schematic diagram of a differential scanning calorimeter is shown in Figure 4.10.

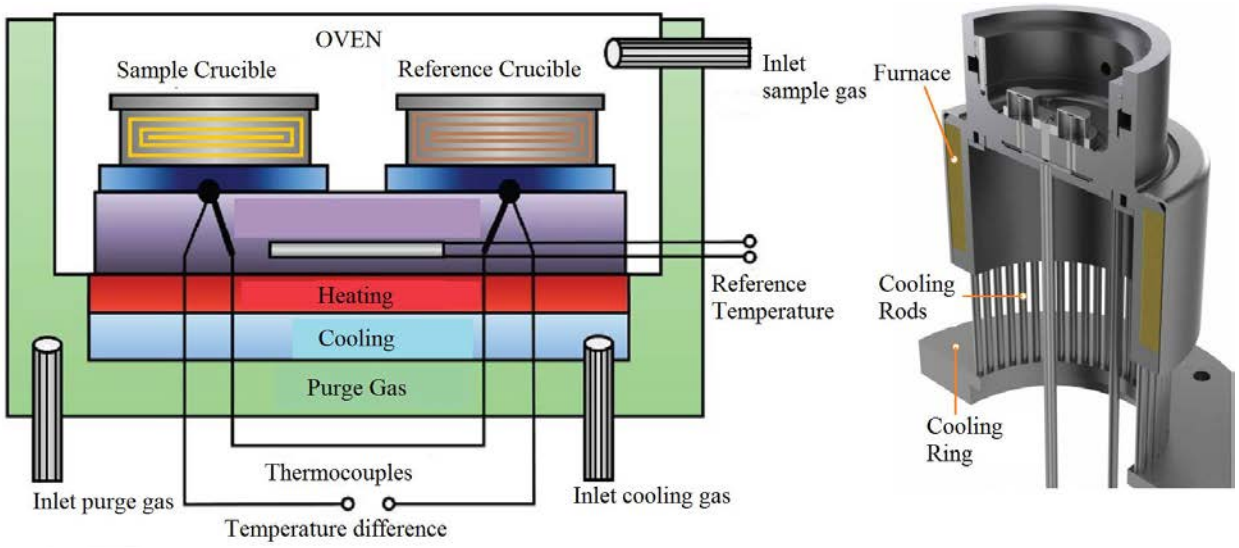

Figure 4.10: Schematic diagram of a differential scanning calorimeter.

Thermal analysis may be the most routine and simplest method for evaluating crystallinity, but this method also has a disadvantage—the melting enthalpy of the fully crystalline polymer ΔH_m^o must be accurately known. DSC results revealed a slightly broad melting peak, which is typical of semi-crystalline materials. The onset of the melting point according to the material safety data sheet for the PCL pellet sample used for this study is 60°C. Polymeric materials melt over a range of temperature. As heat is added to the solid, the molecules acquire energy, and when there is enough energy to overcome the intermolecular forces previously binding them together (in this case, covalent bonds of several repeating units "mers"), they melt. Considering the fact that it was processed by electrospinning method where the lattice arrangement is further disrupted, the net onset of melting point is reduced from 60ºC to 54.3ºC for pure PCL (Table 4.5). Because of the increase in randomness and low thermal conduction, the energy that is absorbed does not penetrate the solid instantaneously. It can be seen in Table 4.5 and Figure 4.1 that the addition of nanomaterials seems to add to the disorganization by further weakening the lattice; hence, the

melting process begins at lower temperatures in the range of 52–55°C. The end of the melting process for pure PCL electrospun fibers is 64.4°C and for PCL-CNT, PCL-fullerene, and PCL-graphene is 63.61, 65.51, and 64.95°C, respectively. These temperatures vary within the 1.4% range [272, 273].

The same reason can be attributed to the change in percent crystallinity and the latent heat of fusion. Looking at the percentage of crystallinity and latent heat of fusion, also tabulated in Table 4.5, a discernible trend can be seen in the overall decrease in the values following the addition of nanomaterials into the PCL. The crystallinity of pure PCL was the highest, which was about 68.45%, with the latent heat of fusion at 93.14J/g. The addition of nanomaterials into the polymer solution resulted in a further decrease in crystallinity in the following order: PCL > PCL-CNT > PCL-fullerene > PCL-graphene. In order to address potential uncertainties in the crystallinity determination due to peak broadening, x-ray diffraction (XRD) analysis was undertaken.

TABLE 4.5

THERMAL ANALYSIS OF PCL-BASED NANOSCAFFOLDS

	Melting Point Range (°C)	**Latent Heat of Fusion (J/g)**	**Crystallinity (Xc%)**
PCL	54.3–64.4	93.14	68.45
PCL + CNT	52.28–63.61	87.02	63.94
PCL + Graphene	52.61–64.95	76.91	56.51
PCL + Fullerene	53.67–65.51	84.44	62.05

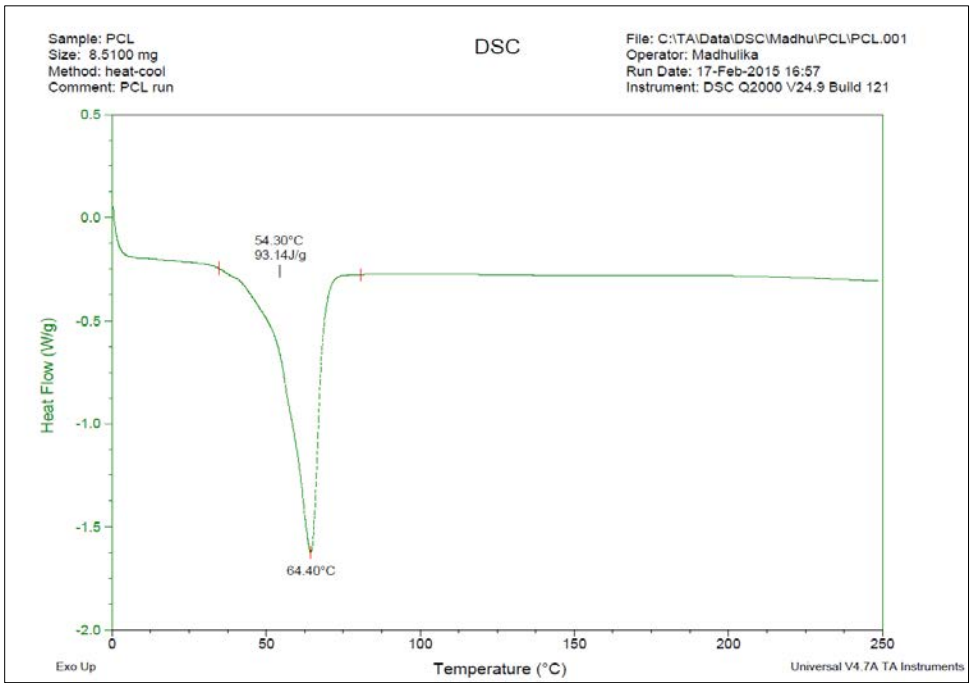

(a) PCL

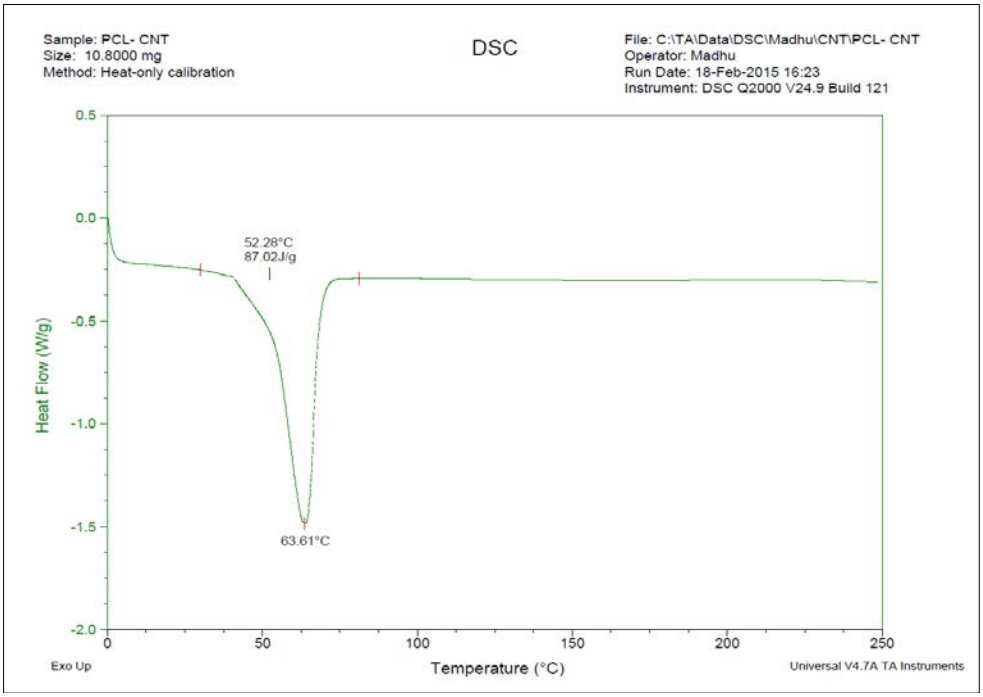

(b) PCL-CNT

Figure 4.11: Thermal analysis curves for nanoscaffolds: (a) PCL, (b) PCL-CNT, (c) PCL-fullerene, (d) PCL-graphene.

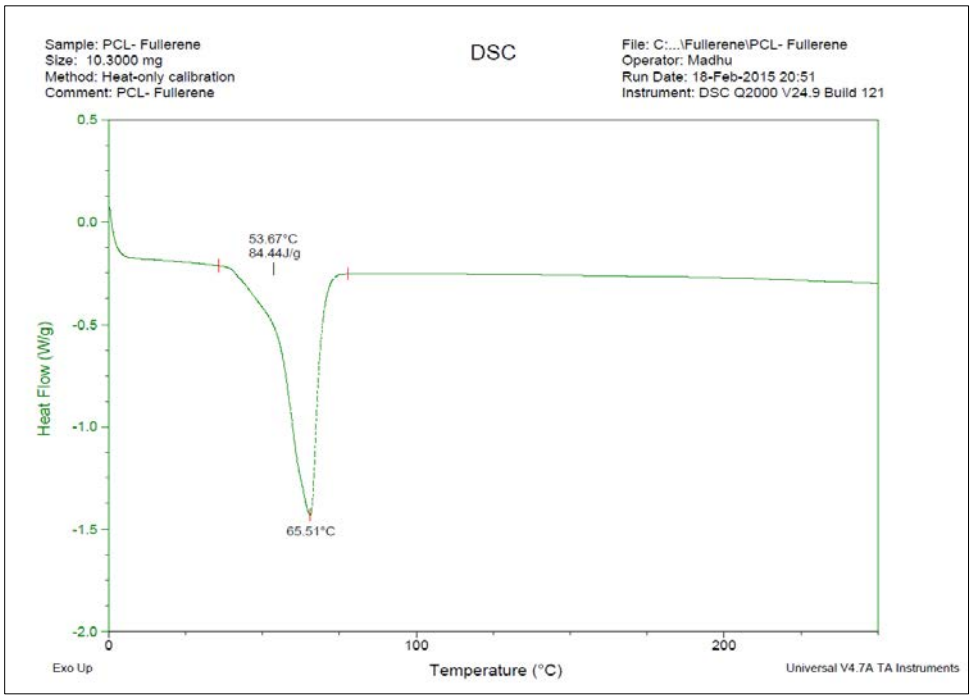

(c) PCL-Fullerene

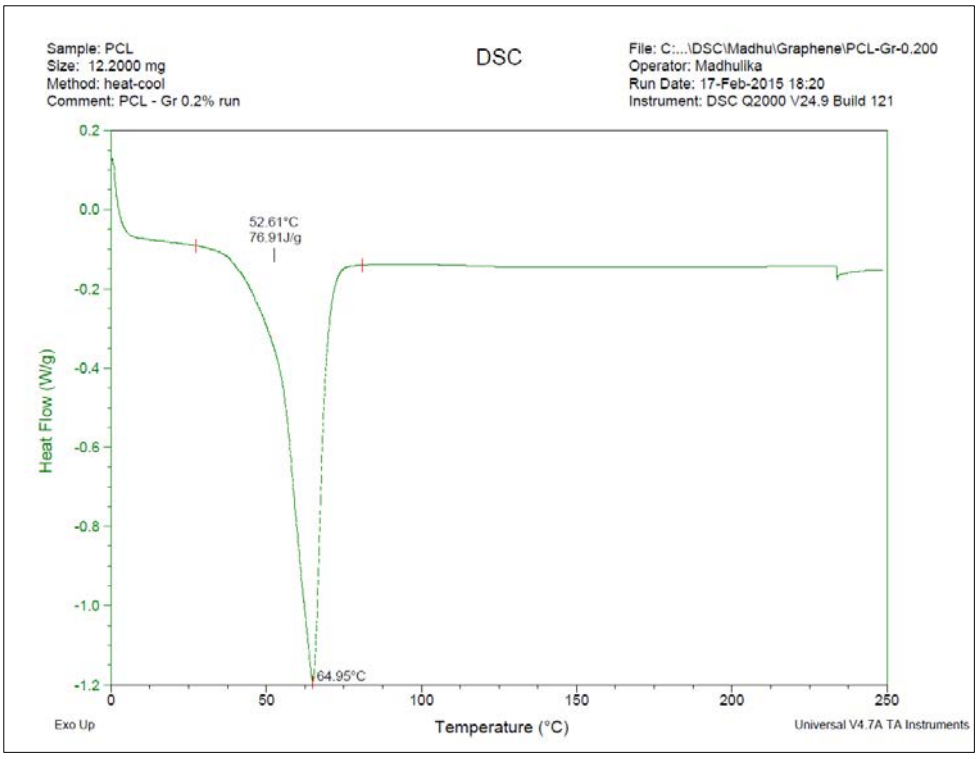

(d) PCL-Graphene

Figure 4.11: (continued)

4.3.2 Wide-Angle X-Ray Diffraction

Crystallinity of the polymeric fibers in the electrospun membranes was evaluated using WAXD. Measurements were carried out with a fixed-anode X-ray generator (Rigaku, Geigerflex, 40 kV and 30 mA) with Cu Kα radiation (λ = 0.1542 nm) with 2θ ranging from 10° to 35°. The specimen was prepared by attaching few layers of PCL fiber material onto glass slides. The purpose of using a multilayer was to make the specimen opaque in order to prevent the possibility of the rays passing through the material onto the glass slide. X-rays are produced by bombarding a metal target (usually Cu and Mo) with a beam of electrons emitted from a hot filament (often tungsten). The incident beam ionizes electrons from the K-shell (1s) of the target atom, and X-rays are emitted as the resultant vacancies are filled by electrons dropping down from higher energy levels—L (2P) or M (3p) levels. This gives rise to Ka and Kb lines, which are characteristic of the type of target material. In this case for the Cu target, the Kα radiation was 1.5417 Å. As shown in the graph in Figure 4.12, β has a higher energy than α because β refers to the energy difference from two jumps and α from one jump. It should be noted that the intensity is a measure of the probability of the number of electrons jumping from one level to the other and not a measure of energy. The wavelength is the measure of energy [274].

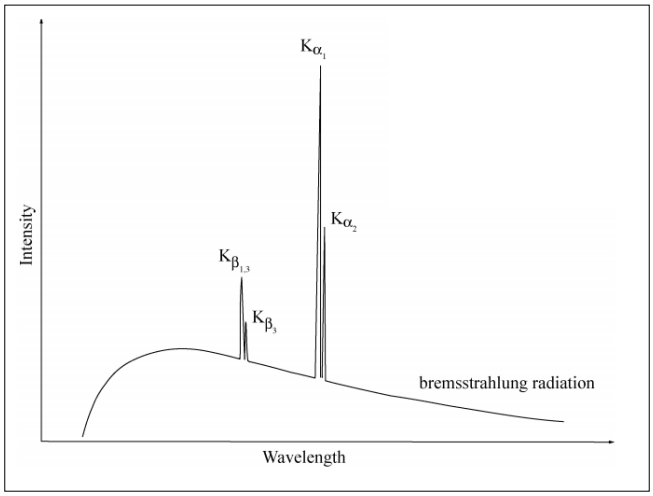

Figure 4.12: Graph showing K_a and K_b characteristic peaks with bremsstrahlung radiation.

The WAXD pattern for a semicrystalline PCL nanoscaffold, shown in Figure 4.13, indicates diffraction at angles. 21.52° and 23.94°. The XRD pattern has a slight background signal. PCL itself is semi-crystalline, and the process of electrospinning has been reported to reduce crystallinity, which leads to some short-/medium-range order. The XRD pattern is a superposition of the amorphous and crystalline phase. The amorphous phase adds a slight hump to it. However, it does not affect the absolute intensities of the crystalline phase and the peak position.

The geometric characteristics of an XRD graph can give considerable information about the type of crystal, crystallinity, distance between adjacent reflecting planes, crystalline size, strain, phase diffraction feature, etc. Although accuracy of some of the information that can be gathered is still controversial, much can be inferred from the graphs [275]

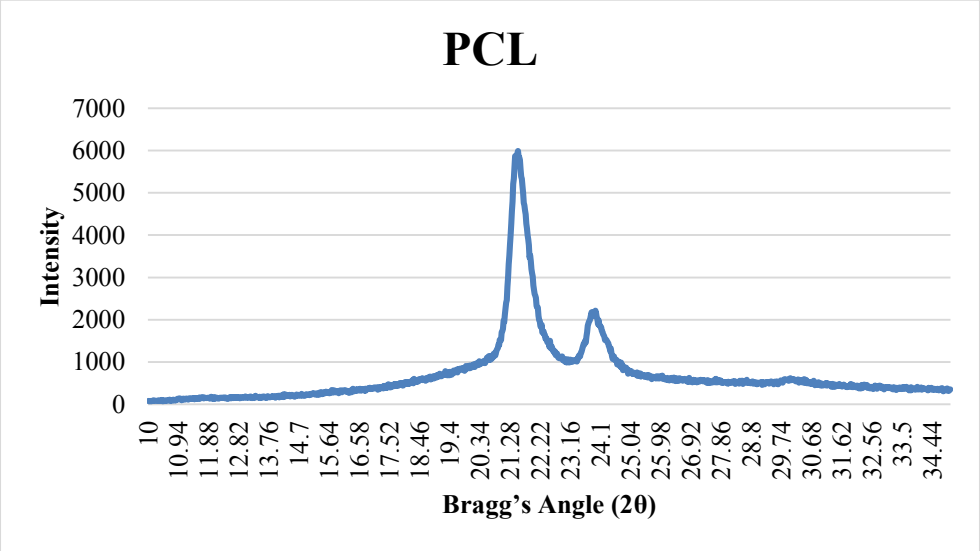

Figure 4.13: XRD pattern for pure PCL nanoscaffold.

By using the XRD indexing method, the pattern can be indexed to the orthorhombic crystal system (Figure 4.14), i.e., the higher the symmetry, the easier it is to index the pattern and have fewer lines than are in the pattern. Bragg's equation gives the path difference between the two reflected rays, as shown in Figure 4.15 and can be expressed as

$$n\lambda = 2d\text{Sin}\theta \tag{4.5}$$

where λ is the wave length, θ is the angle between the incident ray (Bragg angle) and the surface of the crystal, and d is the distance between two adjacent planes of the same orientation. When n is a whole number, constructive interference occurs.

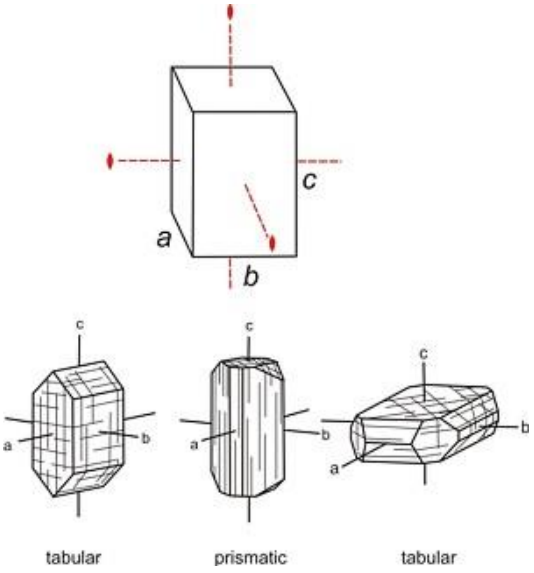

Figure 4.14: Orthorhombic crystal system

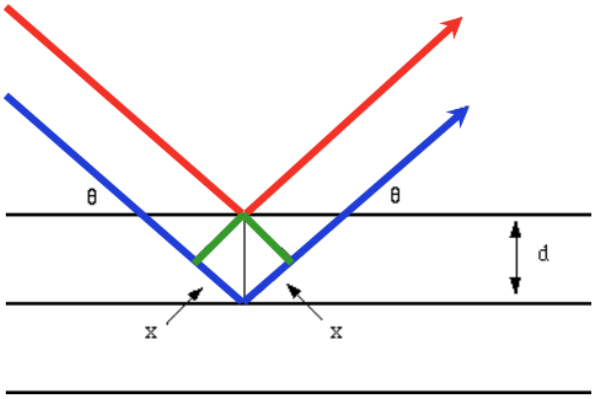

Figure 4.15: Bragg's law

The d values were calculated for the (110) and (200) planes for PCL, which came to be 0.41 nm and 0.37 nm, respectively. This d can be used to calculate the lattice parameters (a,b,c) of an orthorhombic crystal structure (where a ≠ b ≠ c and α = β = γ = 90°) and is given by

$$\frac{1}{d^2} = \frac{h^2}{a^2} + \frac{k^2}{b^2} + \frac{l^2}{c^2} \tag{4.6}$$

where, h,k,l are the lattice parameters. The Scherrers formula relates the size of sub-micron particles of crystallites to the broadening of a peak in a diffraction pattern [274, 276]. It is given by

$$\tau = \frac{K\lambda}{\beta Cos\theta} \tag{4.7}$$

where τ is the mean size of the ordered (crystalline) domains, K is a dimensionless shape factor whose value varies from 0.62 to 2.08 depending on the shape of the crystalline but on an average it is rounded off to 1, and β is the line broadening at half the maximum intensity. The WAXD apparatus itself can contribute to peak broadening; hence, it is important to subtract instrumental line broadening, in radians, from the actual values in the graph. This quantity is also sometimes denoted as $\Delta(2\theta)$. According to the calculations, the average size of the crystallite varied from 12.6 to 13.1 nm. A complete account of crystallite size τ, interplanar distance d, and intensity ratio is given in Table 4.6.

TABLE 4.6

XRD ANALYSIS RESULTS

	(110) Plane			**(200) Plane**			
	Bragg Angle at Max Intensity (°)	**d_{110} (nm)**	**τ_{110} (nm)**	**Bragg Angle at Max Intensity (°)**	**d_{200} (nm)**	**τ_{200} (nm)**	**Intensity Ratio (I_{110}/I_{200})**
PCL	21.52	0.413	12.60	23.94	0.372	13.19	2.71
PCL+ Fullerene	21.4	0.425	19.06	23.78	0.374	18.53	2.35
PCL+ Graphene	21.5	0.413	10.56	23.82	0.374	11.45	2.13
PCL + CNT	21.32	0.427	15.95	23.68	0.386	13.66	2.46

From Table 4.6, it can be seen that the presence of nanoparticles either marginally changes or does not change the value of d, which means that nanoparticles do not affect the lattice parameters, thus implying that they occupy the interstitial spaces. The nanoparticles seem to have a pronounced effect on the crystallite size. The presence of carbon nanotubes increases the crystallite size, whereas the presence of graphene decreases the crystallite size. Although it is possible to attribute these differences to the differences in morphologies of these nanoparticles, the exact mechanism and the reason can be very complicated to comprehend. The concept of crystallite size measurement itself is a very complex concept. Scherrer's formula is based on the assumption that all the crystallites are close to the spherical shape and are of the same size. This

formula is inversely proportional to the peak width at half maximum. A number of factors contribute to the peak width. Apart from crystallite size, the size distribution, instrumental profile, presence of micro strain, solid solution inhomogeneity, and temperature treatments contribute to peak broadening. The broadening of a single diffraction peak is the product of crystallite dimensions in the direction perpendicular to the planes that produced the diffraction peak. Microstrains are very common in nanocrystalline materials. Various factors can contribute to micro strains: non-uniform lattice distortions, dislocations, antiphase domain boundaries, grain surface relaxation, and faulting. XRD is poorly designed to facilitate the analysis of crystallites with a broad or multimodal size distribution.

By examining Table 4.6 and the graph in Figure 4.16, a slight peak shift to the left can be observed. This change is not related to phase change or composition change. This means that the lattice parameter is increasing. Several reasons can lead to peak shifts, including increase in number of defects, increase in residual strain, etc. The intensity ratio gives the ratio of intensities of (110) and (200) planes. The maximum ratio between intensities of the (110) and (200) planes is for pure PCL and the minimum ratio is for PCL-graphene. A decrease in the intensity of the (110) plane peak relative to that of the (200) plane peak was observed on the fibers electrospun with nanomaterial inclusions. This is indicative of a change in crystallographic texture (i.e., preferred orientation). The intensity ratio of the (110)/(200) plane peaks for the electrospun PCL fibers was 2.71. For the electrospun PCL-graphene fibers, this ratio was reduced to 2.13. The ratio is an indication of crystallinity. Here the crystallinity follows the trend PCL > PCL-CNT > PCL-fullerene > PCL-graphene, and this is in accordance with the results from the thermal analysis (DSC) [275-279].

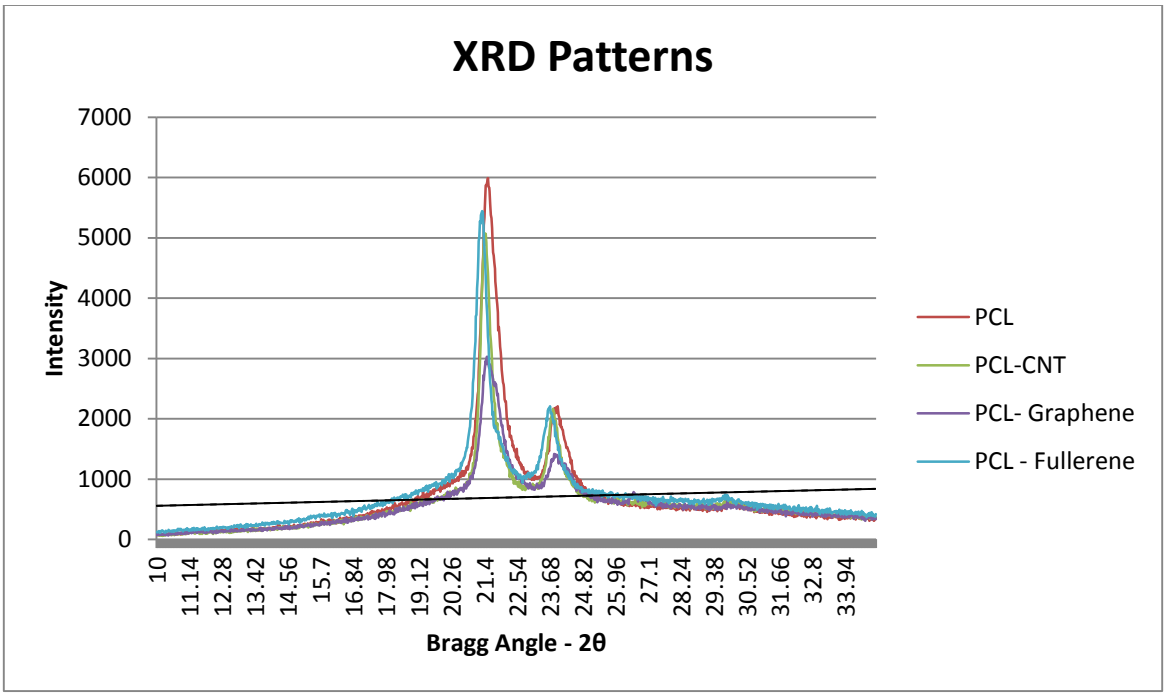

Figure 4.16: XRD patterns for nanoscaffolds: PCL, PCL-CNT, PCL-graphene, and PCL-fullerene.

4.4 Dielectric Characterization of PCL-Based Nanoscaffolds

In order to perform electrical characterization, it is very important to first understand the basic mechanism of electrical conduction in a nervous system. Axons are responsible for the transmission of information between different points of the nervous system, and their function is analogous to the wires that connect different points in an electric circuit. Despite the similarity in overall function, the basic mechanism is quite different. In an electrical circuit, the wire maintains both ends at a constant electrical potential difference, and the current is caused by movement of the electrons due to this difference against a certain resistance. On the other hand, the axon, which is a part of a cell (biological), separates its internal medium from the external medium with a plasma membrane and the signal conducted, which is due to the transient potential difference that appears across this membrane. The membrane is made up of a lipid bilayer and has channels for the passage of ionic species in and out of cell. This causes a potential difference, or membrane potential, which is the result of ionic gradients and produces ionic currents perpendicular to the

membrane. These ionic currents lead to a regeneration of the membrane potential changes in a different region of the axon, which gives rise to longitudinal currents due to the temporary closing of local ionic current circuits.

The dielectric constant is defined as the ratio of a capacitance induced by two metallic conductor plates that hold an insulating material in between them. Dielectric constant values are calculated from the capacitance C measurements. Basically, the dielectric constant ε represents the standard unit of force (in units of Newtons) acting across a distance (in units of meters) against charged particles (in units of Coulombs). The parameter ε basically does not define capacitance as much as it defines the strength of the force one charged particle exerts on another at a distance. The practical importance of studying and measuring a dielectric constant within a biological system is because it makes life possible. Amino acids, which are the building blocks of life, have a peculiar property called amphotericity. In an aqueous medium, they can be a base, an acid, or both at the same time (Figure 4.17) [280-284] .

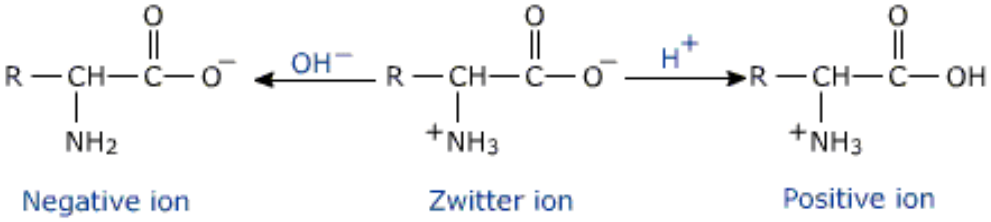

Figure 4.17: Zwitter ion character of peptides

When amino acids are formed into long chains to make proteins, enzymes, and other molecules, the exposed electrical charges in the individual amino acids of the chain attract or repel each other and cause the chain to curl up into different shapes, even controlling the Na+, K+ gates—the membrane potential. The ε is always at play and constantly changes. The manipulation of εr locally at the molecular level is one of the fundamental mechanisms of life. The exact values are so complex they are difficult to comprehend. The effect of nanoparticles in the dielectric

constant of PCL was measured using an automatic capacitance bridge, which has a resolution of 0.8aF (Figure 4.18).

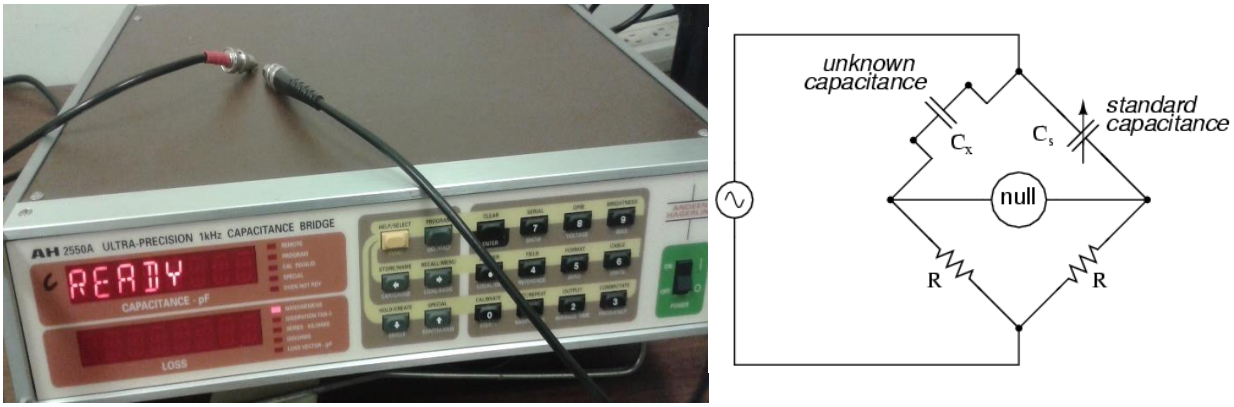

Figure 4.18: Apparatus and circuit diagram showing working of capacitance bridge.

The PCL electrospun fibers without nanomaterials showed a dielectric constant of 2.13, which is very close to the values previously reported. PCL-CNT and PCL-fullerene showed an average dielectric constant of 2.49, and PCL-graphene showed an average dielectric constant of 3.93. The dielectric constant increased with the increase in percent of nanomaterials. In the case of PCL-graphene, this increased from 2.05 to 6.54 when the concentration was increased from 0.05% to 0.2%, as shown previously in Figure 4.13. [285, 286], whereas the increase for the other two was marginal.

The conductivity in CNT and graphene nanoparticles depends on their orientation and level of dispersion. At certain orientations and dimensions, they may show a ballistic phenomenon, and at other orientations, they may act as insulators. Hence, it is difficult to quantize and generalize their behavior. The mechanism of conduction in such scenarios cannot be generalized based on the existing knowledge of macromaterials.

4.5 Cytotoxicity Measurement of PCL-Based Nanoscaffolds Using almarBlue® Assay

The viability and proliferation of the PCL-based nanoscaffolds were studied by monitoring their metabolic activity using the alamarBlue® assay (Pierce Biotechnology, Rockford, IL). Cell

viability can be monitored by numerous methods. The alamarBlue® cell viability reagent functions as a cell health indicator by using the reducing power of living cells to quantitatively measure the proliferation of various human and animal cell lines. When cells are alive, they maintain a reducing environment within the cytosol of the cell. Resazurin, the active ingredient of alamarBlue® reagent, is a non-toxic, cell-permeable compound that is blue in color and virtually non-fluorescent. Upon entering cells, resazurin is reduced to resorufin, a compound that is red in color and highly fluorescent. Viable cells continuously convert resazurin to resorufin, increasing the overall fluorescence and color of the media that surrounds the cells. It is known to have several advantages over other viability assays (MTT). It is quantitative, has high sensitivity and linearity (detects as few as 50 cells), exhibits robust performance, is fast and simple without cell lysis, can be used for a wide variety of cells, and is economical and safe [142, 287, 288].

To perform this assay, the films of dense electrospun nanofibers were cut into round shapes and placed in 24-well plates to cover the bottom of the wells. The cells, with a density of 50,000 cells/well, were cultured for four days and then incubated with DMEM containing 10% (v/v) alamarBlue® reagent for two hours. Absorbance was measured at wavelengths of 570 and 600 nm in a microplate reader (Synergy MxMonochromator-Based Multi-Mode Microplate Reader, Winooski, VT). The cell viability was tested for the batch containing the maximum percentage (0.2%) of nanoparticles. It was assumed that if the samples passed the viability test at 0.2%, they would pass the test for 0.05% of nanoparticles.

From Figure 4.19, it can be seen that the viability varied between 95% and 100%. In the case of PCL-graphene, viability was a little over 100%, which means that the cells proliferated more than what they did in the absence of the nanoscaffold, which signifies that it has very low toxicity. To confirm this, further analysis was done.

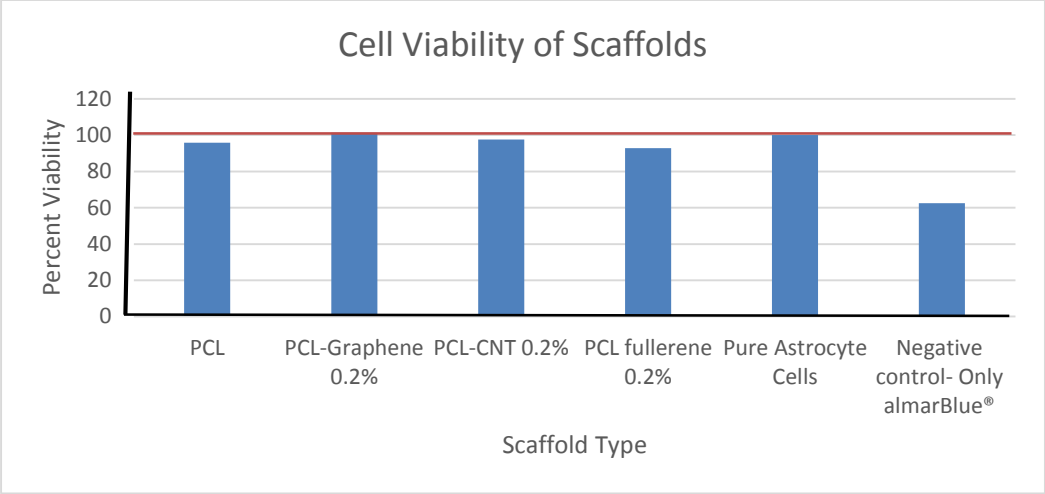

Figure 4.19: Cell viability of nanoscaffolds at 0.2% concentration.

4.6 Histological Studies of Astrocytes on PCL-Based Scaffolds by Immunostaining

4.6.1 Rhodamine Phalloidin and Hoechst Stains

The cytoskeleton of eukaryotic cells is composed of a series of filamentous structures, including intermediate filaments, actin filaments, and microtubules. Actin which is basically a multifunctional protein, participates in many important cellular processes, including muscle contraction, cell motility, cell signaling, cytokinesis, and the formation and maintenance of cell junctions and cell shape. Immunofluorescent staining has been most frequently used to study cytoskeletal components. However, it is also possible to fluorescently label isolated cytoskeletal proteins, especially phalloidin, to label F-actin of the cytoskeleton by acting as a polymerization enhancer. Phalloidin labelled with different fluorophores is available. The choice of the specific fluorophore should depend on whether phalloidin labelling for actin is part of a double-label experiment. In general, rhodamine labels are more resistant to photo-bleaching and can be subjected to longer exposures required for finer structures. The Hoechst stain is also used as a nucleic acid stain, which is popular cell-permeant nuclear counterstain that emits blue fluorescence when bound to dsDNA. This dye is often used to distinguish condensed pycnotic nuclei in

apoptotic cells and for cell-cycle studies [289, 290]. For this experiment, the red dye (Rhodamine Phalloidin) was used to view the astrocytes, and the blue stain (Hoechst) was used to stain the DNA. The following procedure was used:

1. First, the rhodamine phalloidin (red dye) was stabilized according to instructions provided in the packaging, and 500 µl of 100% methanol was added. This solution can be stored in a freezer at –20˚C for six months.
2. Then two solutions were prepared and added to a well: (a) a 1:1000) ratio of a Hoechst:PBS solution), and (b) 150 µl of PBS + 2 µl of rhodamine phalloidin reagent).
3. The medium from the well was removed and gently rinsed with PBS.
4. Triton, a wetting agent, was added for about 2–5 minutes to improve the permeability of the membrane to the dye. Then the mediumwas removed and rinsed with PBS.
5. The PBS was removed, and orange dye was added to each well and kept for an hour.
6. At the end of one hour, the orange dye was removed, and 100 µl of Hoechst stain was added for five minutes. Then the sample was removed, PBS was added, and the sample was viewed under a microscope (Figure 4.20).

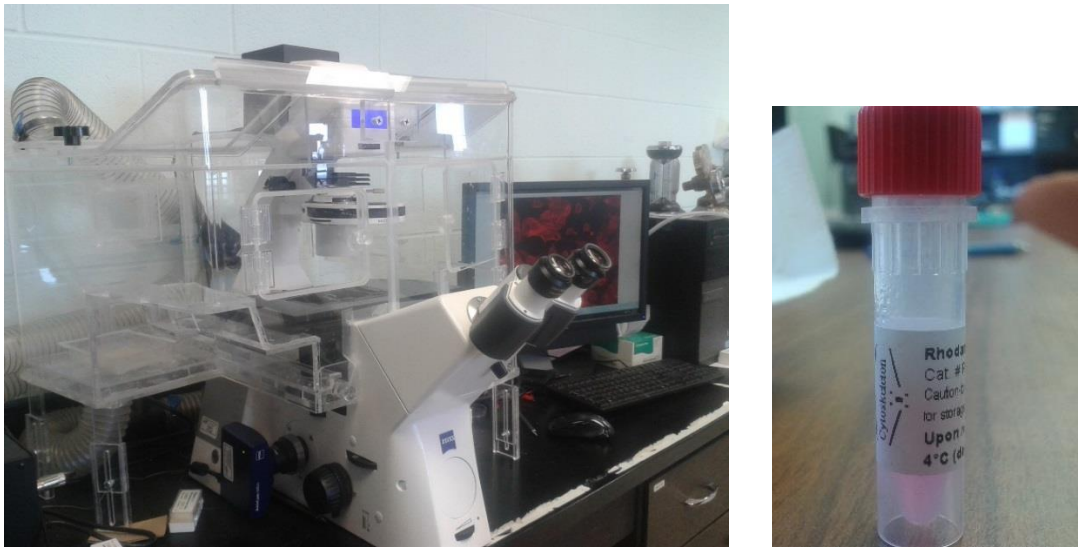

Figure 4.20: Carl Zeiss fluorescence microscope (left) and rhodamine phalloidin dye (right).

The immunostaining images shown in Figure 4.21 clearly confirm the growth of astrocytes on all the nanoscaffolds. Astrocytes stained with rhodamine phalloidin show a cytoplasmic presence of the actin filament. Filopodia protruding from cell margins (arrows) stain brightly for actin. These images clearly show the extent of cell growth. To measure the extent of cell growth and proliferation, a separate proliferation test must be performed [279, 280]

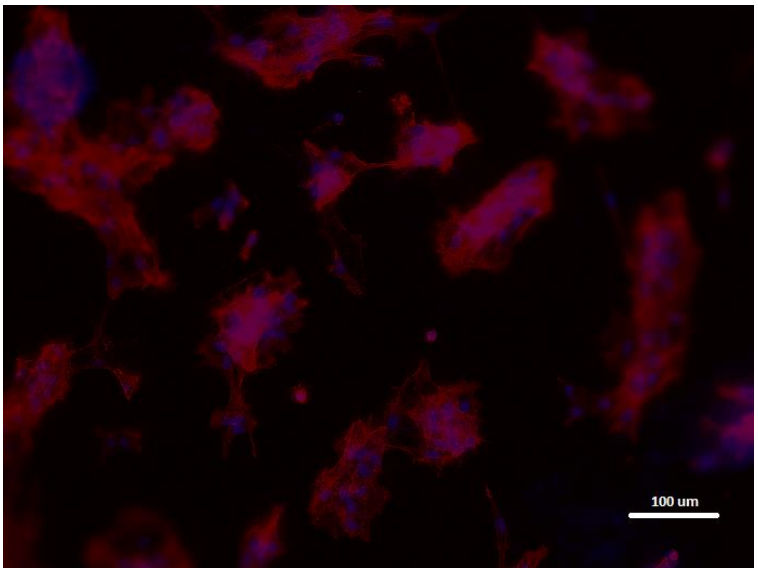

(a) PCL

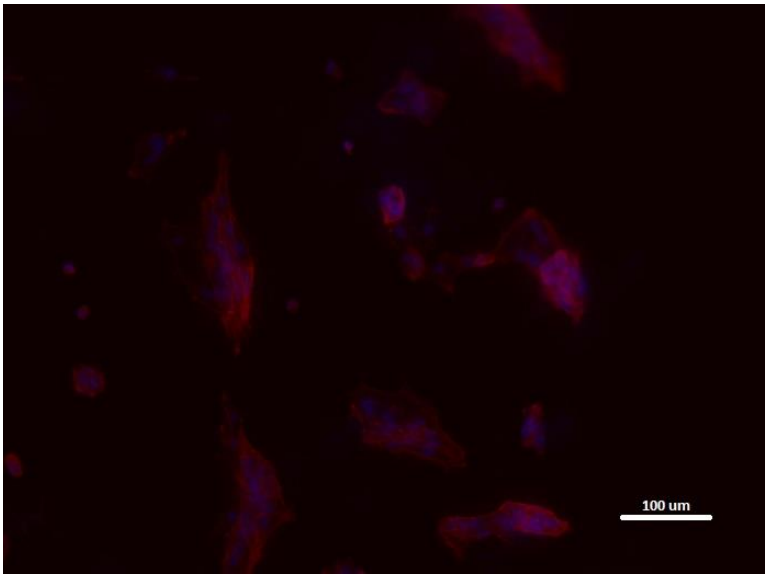

(b) PCL-Graphene

Figure 4.21: Fluorescence microscopic images of astrocytes with rhodamine phalloidin and Heochst dyes on nanoscaffolds: (a) PCL, (b) PCL-graphene, (c) PCL-CNT, (d) PCL-fullerene

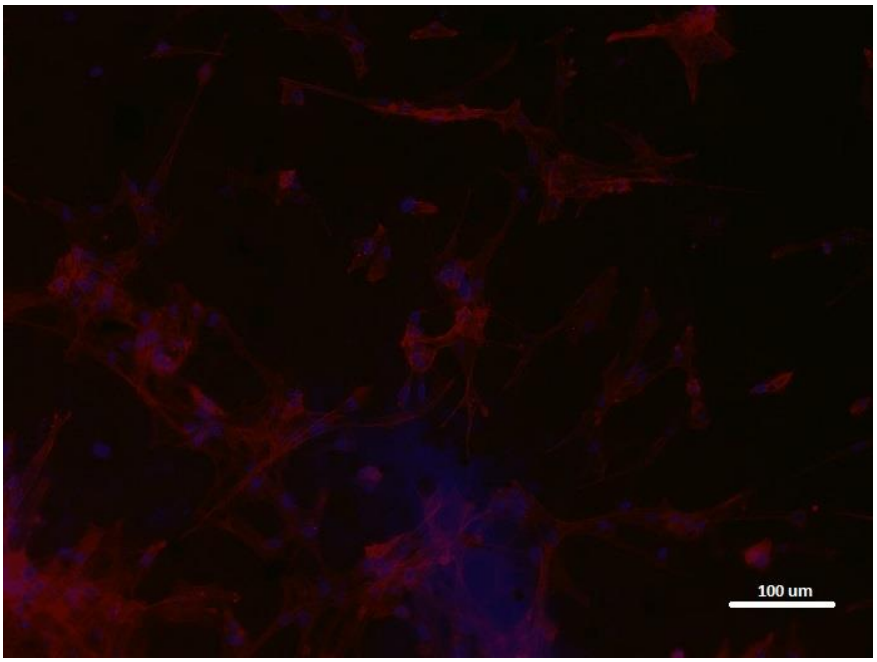

(c) PCL-CNT

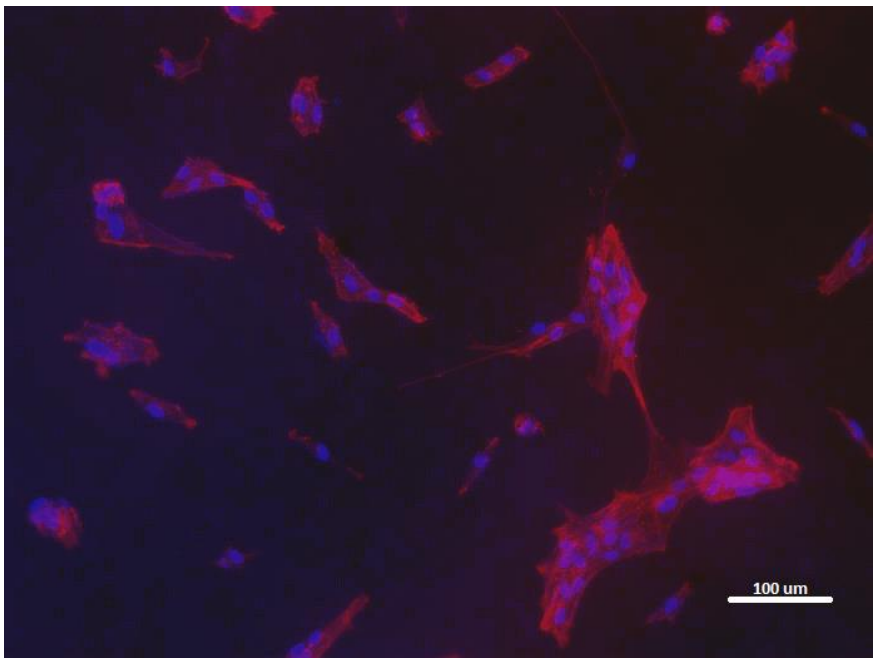

(d) PCL-Fullerene

Figure 4.21: (continued)

4.6.2 Anti-GFAP Antibody

Establishing the cellular identity in vivo of adult multipotent neural progenitors is fundamental to understanding their biology. It is well established that the glial fibrillary acidic protein is the principal 8–9 nm intermediate filament in mature astrocytes of the central nervous system. This recognition came over a decade ago then GFAP was valued as a prototyper antigen in nervous tissue identification and was established as a standard marker for research [291, 292]. GFAP is important in modulating astrocyte motility and shape by providing structural stability to astrocytic processes. In astrogliosis following an injury, there is an increase in GFAP content. In addition to the major application of GFAP antisera for routine use in astrocyte identification in the CNS, the molecular cloning of a mouse gene in 1985 opened a new and rich realm for GFAP studies. These include antisense, null mice, and numerous promoter studies. Studies showing that mice lacking GFAP are hypersensitive to cervical spinal cord injury caused by sudden acceleration of the head have provided more direct evidence for a structural role of GFAP.

Alexander disease is a rare disorder of the central nervous system of unknown etiology. Infants with Alexander disease develop physical and cognitive health retardation, leading to death usually within the first decade. The pathological hallmark of all forms of Alexander disease is the presence of Rosenthal fibers, cytoplasmic inclusions in astrocytes that contain the intermediate filament protein GFAP in association with small heat-shock proteins. A primary alteration/mutation in GFAP gene is responsible for Alexander disease. Recently GFAP has become more widely used in studying neurogenesis, CNS injury, disease, and development by using GFAP expressing progenitor cells, [291-293].

The cells were double labelled using the anti-GFAP antibody marker and the Hoechst marker. The purity of the astrocyte culture was determined immunocytochemically with the anti-GFAP antibody (an astrocytic marker, AutogenBioclear, Calne, UK). The cells were fixed in 4% paraformaldehyde and then incubated with anti-GFAP (all at 1:200 dilutions) and visualized under the microscope.

The images shown in Figure 4.22 indicate multipolar morphologies of the astrocytes. They show a large number of DNA strands. The histological studies can suggest either fibrous or protoplasmic astrocytes, but this method is a general antibody label and is not very effective in differentiating between these two types of astrocytes. It has been reported that many mature astrocytes in healthy CNS tissue do not express detectable levels of GFAP and that GFAP expression by astrocytes exhibits both regional and local variability that is dynamically regulated by a large number of inter- and intra-cellular signaling molecules [197, 294-296].

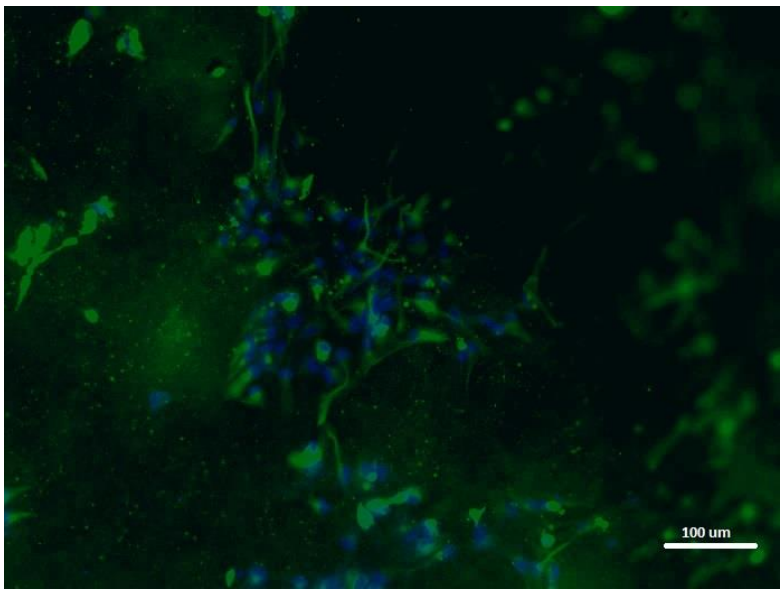

(a) PCL

Figure 4.22: Fluorescence microscopic immunostaining images of astrocytes with anti-GFAP antibody and Hoechst dyes on nanoscaffolds: (a) PCL, (b) PCL-graphene, (c) PCL-CNT, (d) PCL-fullerene, (e) culture plate (without nanoscaffolds)

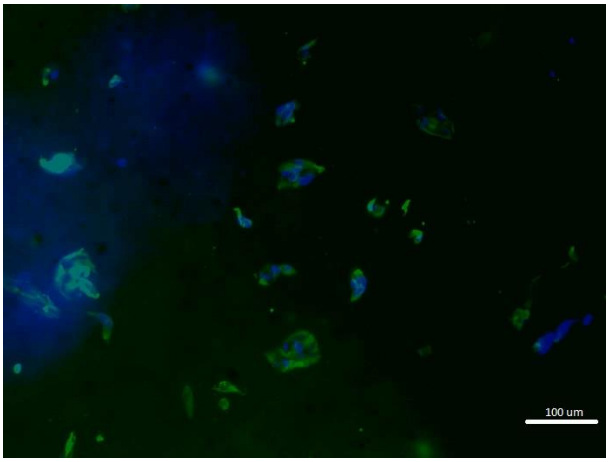

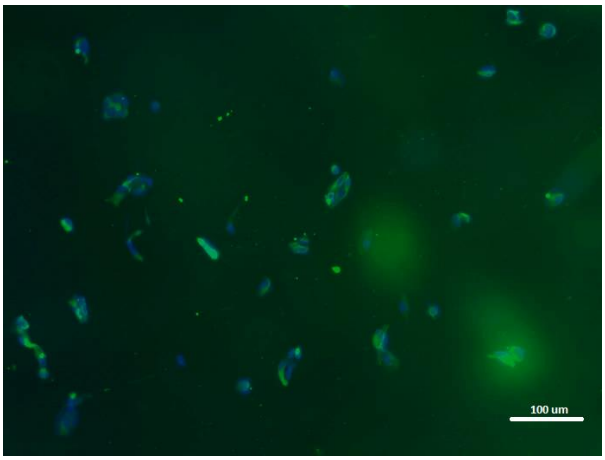

(b) PCL-Graphene

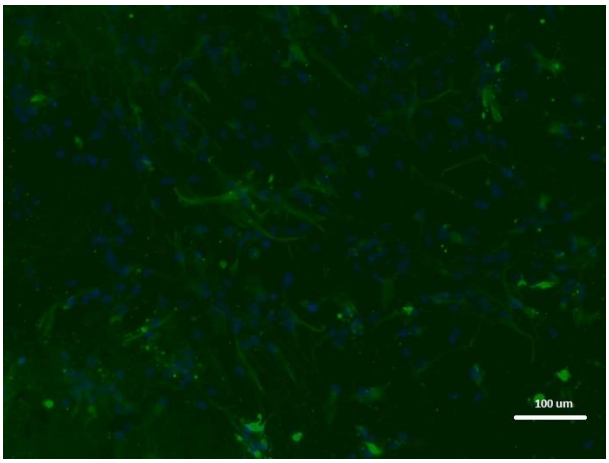

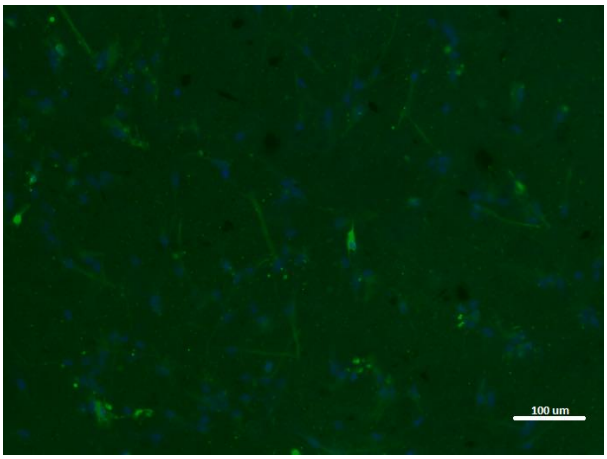

(c) PCL-CNT

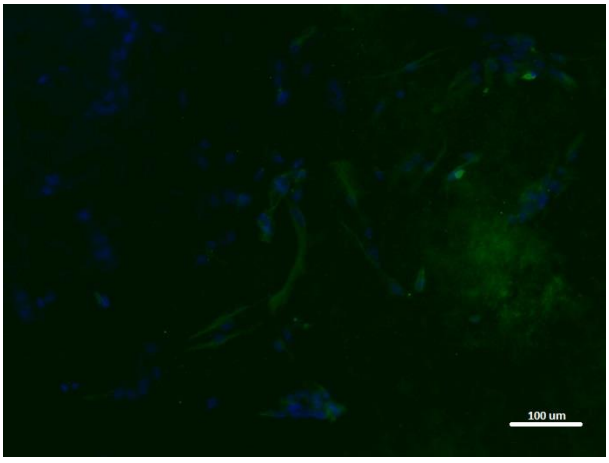

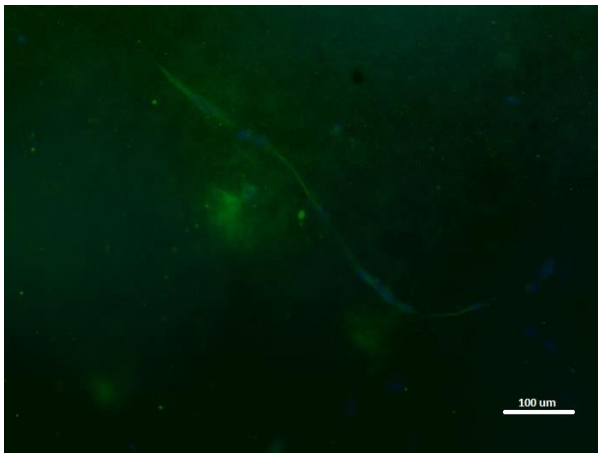

(c) PCL-Fullerene

Figure 4.22: (continued)

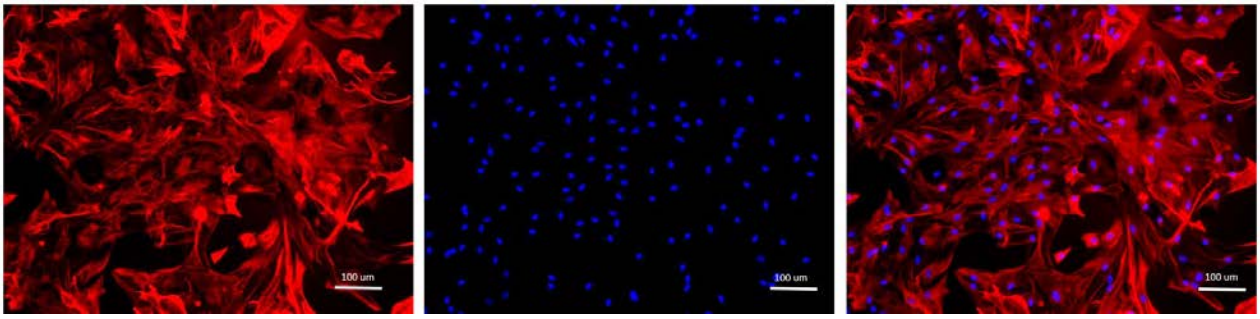

(e) Culture Plate (without Nanoscaffolds)

Figure 4.22: (continued)

4.7 Morphological Study of Astrocytes on PCL-Based Scaffolds Using SEM

The nanofibers with astrocytes were washed with PBS and placed in 2% glutaraldehyde-PBS for two hours. Then the samples were dehydrated with graded ethanol or acetone solutions in water—30%, 50%, 70%, 80%, 90%, 96%, and 100%—for 5 to 15 minutes, each followed by chemical dehydration in the last step. The nanoscaffolds were air dried and subsequently coated with gold to increase the conductivity of the increased contrast. Then the astrocyte morphology and the nanofibers were analyzed using SEM images.

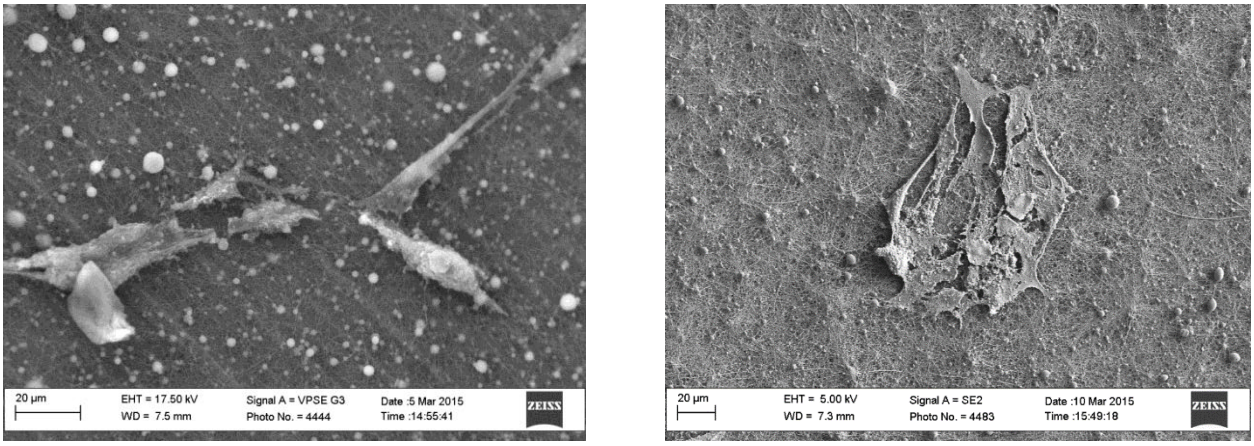

(a) PCL

Figure 4.23: SEM images of astrocytes on nanoscaffolds: (a) PCL (b) PCL-graphene, (c) PCL-CNT, (d) PCL-fullerene.

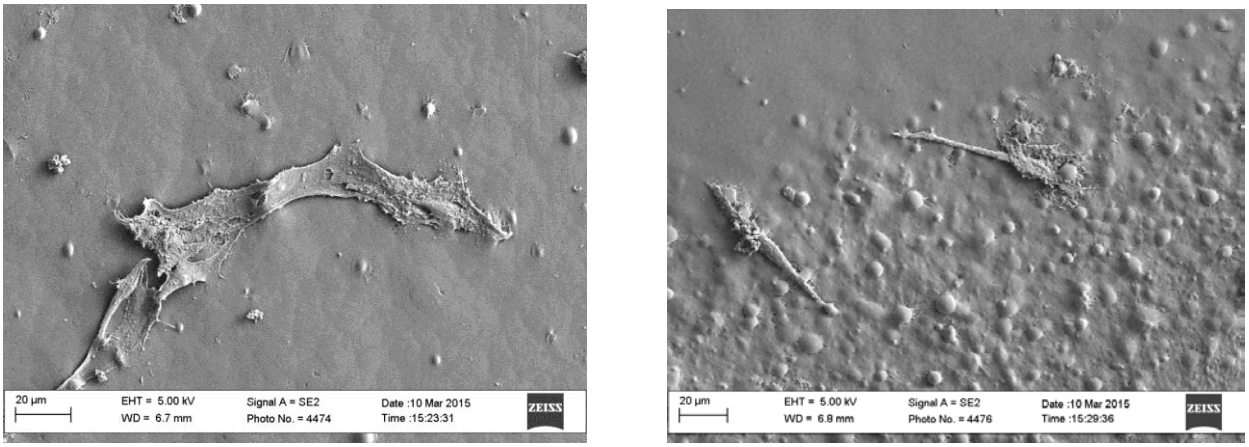

(b) PCL-Graphene

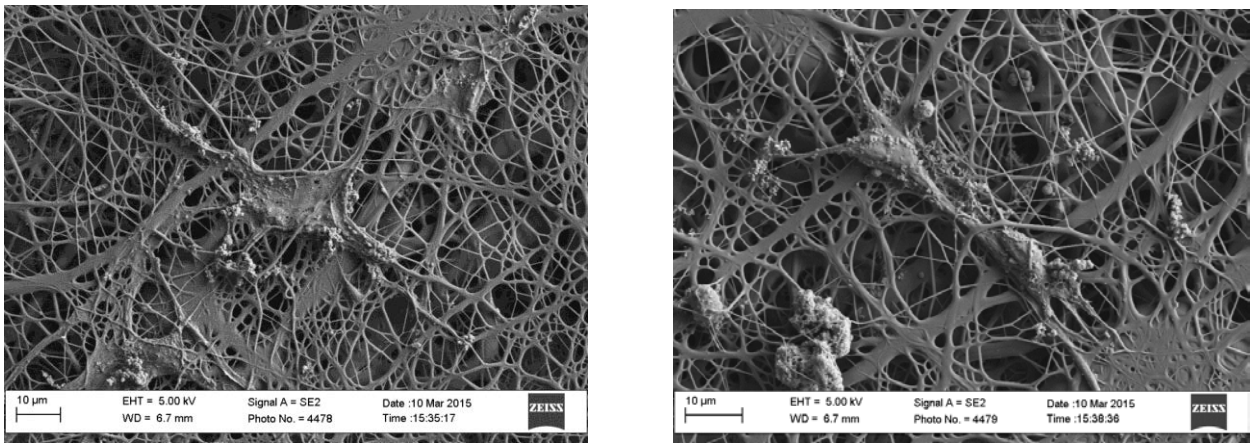

(c) PCL-CNT

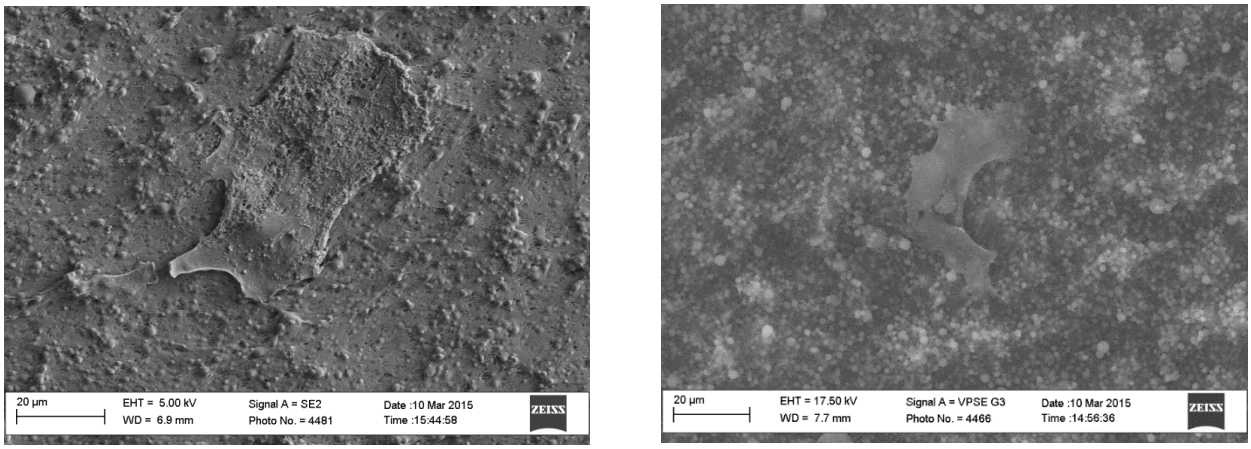

(f) PCL-Fullerene

Figure 4.23: (continued).

The gold coating that was done on top of the nanoscaffolds is responsible for the poor visibility of the fibrous texture. In addition, the magnification is much lower, which reduced the resolution of the individual fibers. Nevertheless, SEM studies confirm the formation of astrocytes and show their morphology. The astrocytes were successfully grown on all scaffold types.

4.8 Raman Spectroscopy to Analyze Neuroglial Signals

Spectroscopy has emerged as one of the central tools for biomedical applications and has made substantial progress in the field of clinical evaluation. Research has been more focused on Raman spectroscopy since this method is comparatively straightforward, reproducible, and noninvasive to tissue, and only small amounts of material with minimum sample preparation are required. In addition, it provides molecular-level information allowing for the investigation of functional groups, bonding types, and molecular conformations, etc. In vibrational spectra, the spectral bands are molecule specific and provide unique information about the biochemical composition. Raman offers some advantages over IR spectroscopic techniques. Since water is a weak scatterer, aqueous solutions can be measured [297, 298]. The XploRA^{TM} PLUS by Horiba Scientific (Figure 4.24) was used for Raman spectral analysis using a 532 nm laser.

Figure 4.24: XploRA^{TM} PLUS by Horiba Scientific used for Raman analysis.

Figure 4.25 presents preliminary data on the feasibility of using Raman microspectroscopy to assess cell growth on the nanofiber environment. Figure 4.25(a) presents a Raman spectral profile of the plain nanofiber matrix with no cells—there are no Raman spectral peaks. Figure 4.25(b) presents the Raman spectral profile of the nanofiber matrix with cells—there are Raman spectral peaks. Raman spectroscopy was able to detect a spectral signature of the cells growing on the nanofiber matrix. In studies related to spectroscopic techniques, it is strongly believed that both the reliable experimental procedure and characterization of spectral peak positions and their assignment along with accurate peak detection and definition are of crucial importance. Figure 4.26 shows the Raman spectra of PCL electrospun fibers. The Raman spectrum of PCL shows the characteristic peaks at 1,726 cm^{-1} (ν C=O), 1,060 cm^{-1} and ,1106 cm^{-1} (skeletal vibration/ stretching), 1,281–1,305 cm^{-1} attributed to wCH_2 groups, 1,415–1,470 cm^{-1} attributed to δCH_2, and 912 cm^{-1} attributed to the *v* C–COO bond.

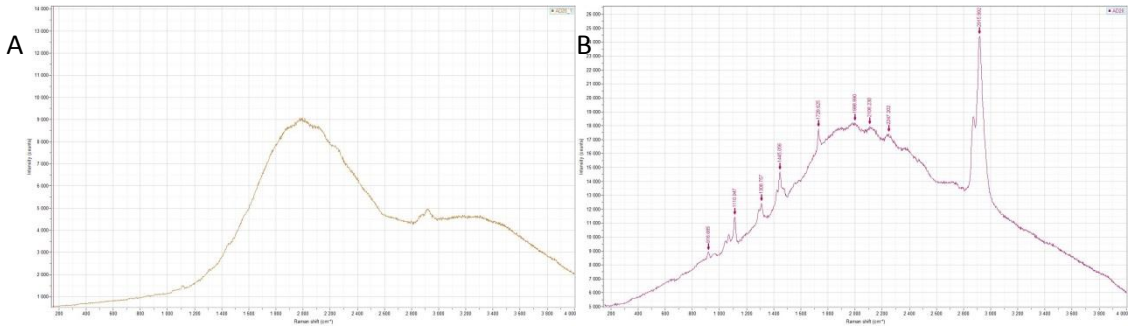

(a) (b)

Figure 4.25: Raman microspectroscopy: (a) nanofiber matrix with no cells, (b) nanofiber matrix with cells growing.

This data is in agreement with results from Kister et al. [278] and Foggia et al. [290]. A comparison of the peaks on all PCL-based nanoscaffold types as shown in Figure 4.27, indicates that the peak positions are the same but the intensities are different. There is a change in the intensities at 1,045 cm^{-1} and 1,106 cm^{-1} corresponding to skeletal stretching. The 1,281 and 1,415

cm^{-1} intensities of the CH_2 groups and the C=O stretch at 1,726 cm^{-1} show different intensities [299, 300].

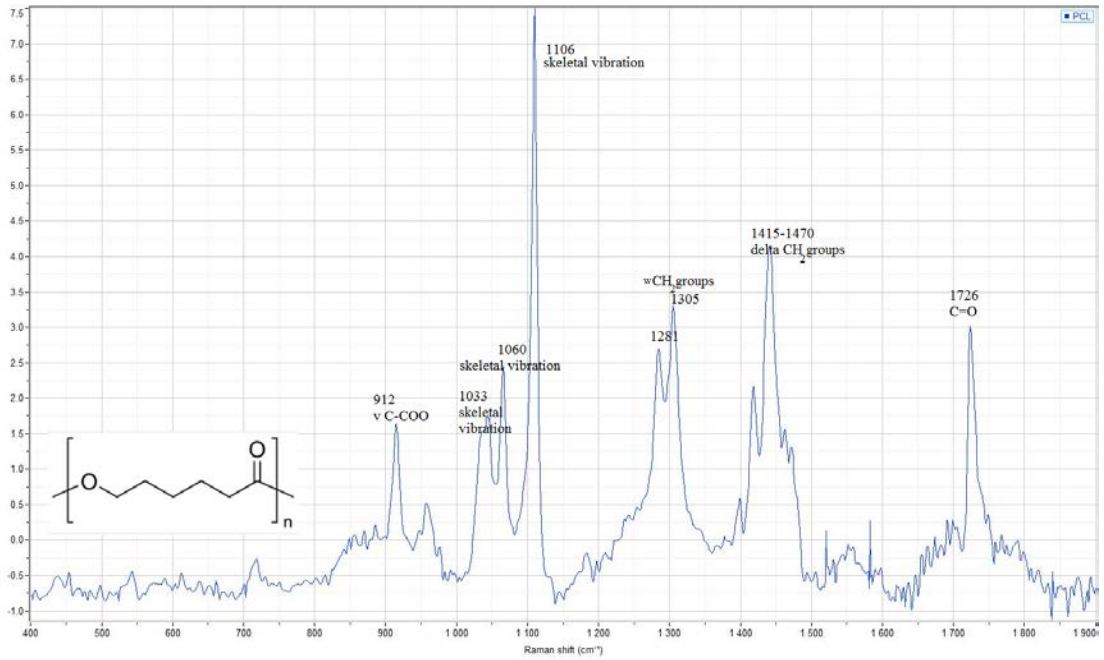

Figure 4.26: Raman microspectroscopy of electrospun PCL fibers.

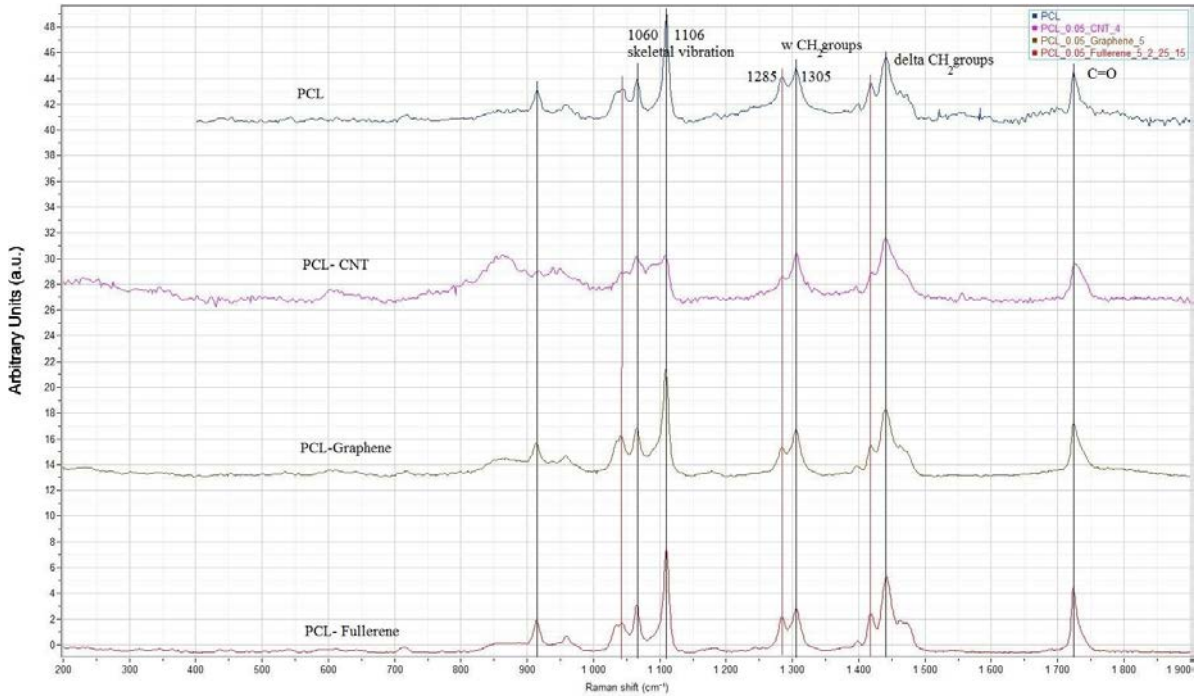

Figure 4.27: Raman microspectroscopy of electrospun nanoscaffolds: PCL, PCL-CNT, PCL-graphene, and PCL-fullerene scaffolds.

According to Taddei et al., the I1305/I1285 intensity ratio between the bands at 1,305 and 1,285 cm-1 is a marker of crystallinity. There is a discernible change in their ratios for different scaffolds on a relative scale but may quantitatively be vague [291, 292].

Figure 4.28 shows a comparison of the Raman spectra of the fullerene nanoscaffold with and without astrocytes, which indicates a significant difference in the spectra. Most of the signature peaks that are found in the PCL-fullerene scaffold (C-COO, skeletal vibration, CH_2 groups, C=O bonds) have become insignificant, and in contrast, the peaks at 274, 495, and 1465 cm^{-1} have become more prominent. Since astrocytes are associated with white matter of the brain, these signals were compared to existing research on Raman spectra for the white matter. According to Kohler et al. [301], fatty acid unsaturation and high cholesterol content was reported in white matter having peaks at 1,470 cm^{-1}. This data matches with the peak shown in Figure 2.8. However, it was difficult to assess the spectra for all scaffolds due to reduced visibility of astrocytes under normal optical conditions and the lack of contrast between the imperfections and the astrocytes. The assessment of the cell growth was complicated due to imperfections in the electrospinning process. This area could be further analyzed in the future.

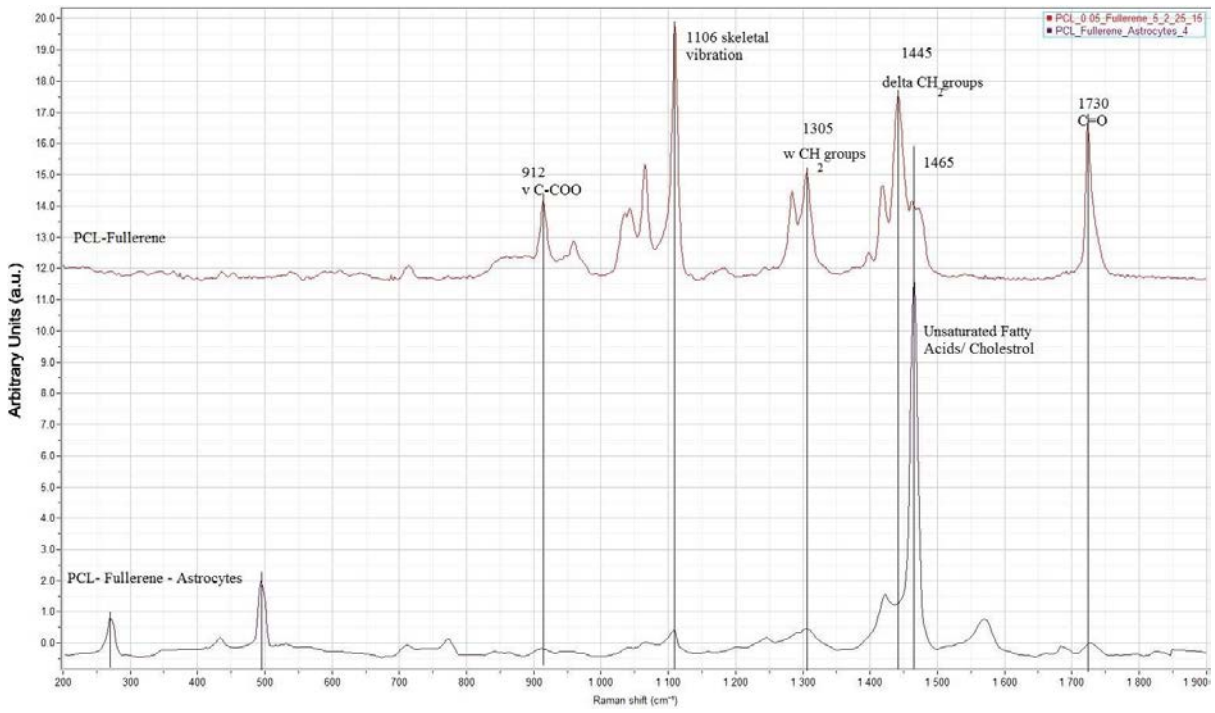

Figure 4.28: Raman microspectroscopy of electrospun PCL-fullerene scaffolds with and without astrocytes.

CHAPTER 5

CONCLUSION

The human central nervous system is a unique challenging structure that can be used to induce healing via different treatments. Nanomedicine shows a great potential for targeting and treating various causes of damage. Astrocytes, which until the last couple of decades were considered to be nothing more than supportive cells with rather negative implications, have been identified as one of the key cells that assist neurons in a variety of complex essential functions, including synaptic transmission and information processing. There has been a shift from endogenous treatment methods to exogenous treatment methods. Scaffolds have the capacity to provide structural support for regeneration, guiding and supporting cell growth from migration or transplantation. Nanomaterials, due to their chemistry and the size can, in certain favorable conditions, assist in cell regeneration and healing, and also provide unique therapeutic effects. Artificial PCL scaffolds with three types of nanomaterial inclusions—namely carbon, graphene, and fullerene were successfully fabricated. Nanomaterial scaffolds were modified to resemble the extracellular matrix by using the electrospinning process.

Contact angle tensiometry tests showed that all scaffolds in general displayed a hydrophobic tendency. The process of electrospinning is known to further increase the hydrophobicity. The process of electrospinning traps air within the ripples of fibers, which in turn prevents water from penetrating the surface. This is seen as a positive outcome because the hydrophobicity lowers the degradation kinetics and increases the time for hydrolysis, which in turn increases the time for cell attachment. With the increase in the percentage of graphene and CNT, the contact angle increased. Fullerene specifically did not seem to have much effect on the contact and also seemed to reduce it by a marginal amount. The work of adhesion was calculated from the

surface free energy values and the contact angle measurements. Graphene had the lowest value (1.52×10^{-2} J/m^2). The work of adhesion is governed by several factors, one of which is the fiber diameter. Lower fiber diameters reduce the work of adhesion.

SEM analysis on the scaffolds confirmed that graphene had the lowest fiber diameters. In general, scaffolds with nanoscale diameters were successfully fabricated, with diameters ranging from 80 to 200 nm. This feature is close to the actual architecture within the central nervous system.

Cytotoxicity has always been one of the main concerns when using nanomaterials. In most cases, the presence of heavy metal impurities in nanomaterials, which are unfiltered during catalytic production, causes cytotoxicity. The compositional characteristics of nanoscaffolds were analyzed by different spectroscopic techniques for two reasons: first, to confirm that no heavy metal impurities were present, and second, to confirm the presence of nanomaterials in the PCL scaffolds. EDS results confirmed that the primary composition of the scaffolds was only carbon and oxygen and that the nanomaterials were not contaminated with heavy metals. The average C% was 73.1% (by weight) and the average O_2 % was 15.1% (by weight). FTIR spectroscopy results confirmed nanomaterial inclusion in varying amounts by changes in the intensity of C-H peaks according to the percentage of nanomaterial present.

The degree of crystallinity has been known to affect cell adhesion, growth, and proliferation. And different levels of crystallinities have been known to favor certain types of cells and not favor the others. However, higher crystallinity has been known to favor the proliferation of Schwann cells. DSC and WAXD were used to characterize crystallinity. DSC results showed that the onset of melting temperature of PCL scaffold as compared to PCL pellets was reduced by 8ºC. The presence of nanomaterials further reduced the onset melting temperature of the PCL

scaffolds by 1–2ºC. The PCL scaffold showed the highest latent heat of fusion at 93.14J/g and a crystallinity of 68%, followed by PCL-CNT, PCL-fullerene, and PCL-graphene scaffolds. The WAXD pattern showed peaks at 21.52 and 23.94 degrees which was indexed to (110) and (200) planes of orthorhombic crystal system. The distance between adjacent (110) and (200) planes was 0.41 nm and 0.37 nm, and the crystallite sizes for all the scaffolds varied from 13 nm to 18 nm. Crystallinity was assessed by taking the intensity ratios of the (110) and (200) planes. Again, PCL had the highest crystallinity followed by PCL-CNT, PCL-fullerene and PCL-graphene. The dielectric constant was calculated, and graphene gave the highest dielectric constant values of around 3.93.

The almarBlue® assay was used to perform toxicity tests on the cells. The cell-cultured scaffolds showed a very high viability—from 95% to 100%. High viability is of utmost importance for successful cell culture. Immunostaining methods were employed to test the type of cell. First, the rhodamine phalloidin test confirmed a cytoplasmic presence of the actin filament, and the anti-GFAP antibody immunostaining method confirmed the presence of astrocytes. Although the number of astrocyte cells was not quantized, by looking at the immunostaining images, all scaffold types favored astrocyte growth, but PCL and PCL-CNT seemed to have maximum proliferation. This can be attributed to several factors such as favorable fiber diameters, high latent heat of fusion, high crystallinity, high viability, etc. SEM analysis confirmed astrocyte adhesion on the scaffolds. Raman analysis was used to study the Raman spectra of astrocytes. These results were consistent with the existing results from the spectra of white matter of the brain at 1,465 cm^{-1}

CHAPTER 6

FUTURE STUDIES

To begin, the injury mechanism related to the spinal cord itself is very complex and needs a thorough understanding. Also, astrocyte transplantation also needs considerable research, and their effects in blocking or promoting axonal regrowth under different circumstances need to be examined. To succeed in the battle with spinal cord injury, there is an urgent need to develop astrocyte transplantation, not only to replace the loss of astrocytes after injury but also support axonal regeneration. To achieve optimal therapeutic effects, it is important to elevate our understanding of astrocytes.

The already-established concept of glial scarring as an impediment to axonal regeneration dominates the research into eliminating scar components with degrading enzymes or specific antibodies. Although tissue scarring blocks axonal regrowth after injury, especially during the chronic phase, it protects residual axons from further damage during the acute phase by sealing the lesion site and regulating the immune activity. The primary concept of astrocytes needs to change. A defining feature of astrocytes is that their phenotypes and functions are determined by interactions among their intrinsic properties and the local cues that vary with injury type, severity, and timing of transplantation. Growth characteristics of different types of astrocytes need to be studied.

It has been researched that in order to achieve the best effects, a combination of both neuroprotection and regeneration treatments should be employed. This two-pronged approach would work to decrease the amount of regeneration necessary by sparing the maximum amount of tissue, then to repair this hidden damage, resulting in a maximally healed and functional spinal cord.

Nanoparticles have demonstrated their ability to increase the bioavailability of neuroprotective therapies to the spinal cord after injection. Improvements in delivery have the capability of improving clinical outcomes by reducing the required dosages and systemic toxicity of current treatments. They can also act as delivery vehicles for other drugs that may improve upon current standards. Besides improving the bioavailability, some nanomaterials, such as fullerenes and carbon nanotubes, also have innate neuroprotective attributes. Polymeric nanoscaffolds also have demonstrated promising results in both and *in vivo* and *in vitro* testing. Some were able to show the formation of blood vessels, significant progression of motor fibers through the lesion site, and recovery of function. All these attributes have been developed and tested with varying degrees of success, but the success rate needs to increase. Some nanoparticles have demonstrated exciting and significant behavioral or electrical functional recovery. They also show other intriguing prospects, but more research must be directed toward validation. Research needs to be done on the design, and the shape of the device would vary depending on its final application: it could consist of a film that could wrap the nerve bundles, a sponge-like scaffold in which neurites could be extended, or fiber bundles that could physically and functionally replace the injured tissue.

While *in vitro* testing can give an indication of the abilities of the nanomaterial, *in vivo* testing is essential for establishing a clinical value. Comparative treatment studies involving several different markers for functional recovery may be an important next step in identifying treatments in order to move forward with further development and clinical testing. More experimental studies are necessary to outline the pre-clinical issues of nanoparticle-based devices, such as their *in vivo* biodegradability or biostability, their functional performance, and their potential long-term toxicity. Tests must also include checking for vascular support and recovering

conduction. Eventually tests must be conducted to ensure that results can be achieved even in a chronic case rather than an acute case. It is necessary to use diverse animal models of SCI to provide compelling experimental data to demonstrate the therapeutic efficacy of nanomaterials and astrocyte transplantation. To date, mostly rodent models have been investigated to test the experimental therapy.

Although there is a great deal of work to be done in this area, especially with successful integration of directional, chemical, biological, and structural cues in a non-invasive manner, a great deal of progress has been realized in a few short years, and this advancement will only continue.

REFERENCES

LIST OF REFERENCES

[1] V. G. Coronado, L. Xu, S. V. Basavaraju, L. C. McGuire, M. M. Wald, M. D. Faul, "Surveillance for traumatic brain injury-related deaths--United States, 1997-2007," *MMWR Surveillance Summaries,* vol. 60, pp. 1-32, May 6 2011.

[2] C. Harrison-Felix, C. Pretz, F. M. Hammond, J. P. Cuthbert, J. Bell, J. Corrigan, "Life Expectancy after Inpatient Rehabilitation for Traumatic Brain Injury in the United States," *Journal of Neurotrauma,* Nov 4 2014.

[3] E. Zaloshnja, T. Miller, J. A. Langlois, and A. W. Selassie, "Prevalence of long-term disability from traumatic brain injury in the civilian population of the United States, 2005," *Journal of Head Trauma Rehabilitation,* vol. 23, pp. 394-400, Nov-Dec 2008.

[4] M. J. DeVivo, B. K. Go, and A. B. Jackson, "Overview of the national spinal cord injury statistical center database," *Journal of Spinal Cord Medicine,* vol. 25, pp. 335-8, Winter 2002.

[5] C. H. Tator, "Review of treatment trials in human spinal cord injury: issues, difficulties, and recommendations," *Neurosurgery,* vol. 59, pp. 957-82; discussion 982-7, Nov 2006.

[6] A. V. Molofsky, R. Krencik, E. M. Ullian, H. H. Tsai, B. Deneen, W. D. Richardson, , "Astrocytes and disease: a neurodevelopmental perspective," *Genes & Development,* vol. 26, pp. 891-907, May 1 2012.

[7] E. K. Zirm, *Die Welt als Fühlen; eine naturphilosophische Studie für Fachleute und Laien*. Leipzig, Wien,: F. Deuticke, 1937.

[8] Z.-M. Huang, Y. Z. Zhang, M. Kotaki, and S. Ramakrishna, "A review on polymer nanofibers by electrospinning and their applications in nanocomposites," *Composites Science and Technology,* vol. 63, pp. 2223-2253, 11// 2003.

[9] Y. Chen and R. A. Swanson, "Astrocytes and brain injury," *Journal of Cerebral Blood Flow & Metabolism,* vol. 23, pp. 137-49, Feb 2003.

[10] L. Ghasemi-Mobarakeh, M. P. Prabhakaran, M. Morshed, M.-H. Nasr-Esfahani, and S. Ramakrishna, "Electrospun poly(ε-caprolactone)/gelatin nanofibrous scaffolds for nerve tissue engineering," *Biomaterials,* vol. 29, pp. 4532-4539, 12// 2008.

[11] J. Y. Tyler, X. M. Xu, and J. X. Cheng, "Nanomedicine for treating spinal cord injury," *Nanoscale,* vol. 5, pp. 8821-36, Oct 7 2013.

[12] H. W. Kroto, J. R. Heath, S. C. O'Brien, R. F. Curl, and R. E. Smalley, "C60: Buckminsterfullerene," *Nature,* vol. 318, pp. 162-163, 11/14/print 1985.

[13] A. Hirsch, "The Chemistry of Fullerenes," *WILEY-VCH Verlag GmbH,* pp. 2-7, 2008.

[14] M. Prato, "[60] Fullerene chemistry for materials science applications," *Journal of Materials Chemistry,* vol. 7, pp. 1097-1109, Jul 1997.

[15] J. L. Delgado, M. A. Herranz, and N. Martin, "The nano-forms of carbon," *Journal of Materials Chemistry,* vol. 18, pp. 1417-1426, 2008.

[16] E. Y. Kolyadina, L. A. Matveeva, P. L. Neluba, and V. V. Shlapatskaya, "Physical properties of C-60 fullerene nanostructures," *Materialwissenschaft Und Werkstofftechnik,* vol. 44, pp. 144-149, Feb-Mar 2013.

[17] R. M. Ahmed and S. M. El-Bashir, "Structure and Physical Properties of Polymer Composite Films Doped with Fullerene Nanoparticles," *International Journal of Photoenergy,* 2011.

[18] S. Bosi, T. Da Ros, G. Spalluto, and M. Prato, "Fullerene derivatives: an attractive tool for biological applications," *European Journal of Medicinal Chemistry,* vol. 38, pp. 913-23, Nov-Dec 2003.

[19] T. Mashino, K. Shimotohno, N. Ikegami, D. Nishikawa, K. Okuda, K. Takahashi, "Human immunodeficiency virus-reverse transcriptase inhibition and hepatitis C virus RNA-dependent RNA polymerase inhibition activities of fullerene derivatives," *Bioorganic & Medicinal Chemistry Letters,* vol. 15, pp. 1107-1109, Feb 15 2005.

[20] R. Bakry, R. M. Vallant, M. Najam-ul-Haq, M. Rainer, Z. Szabo, C. W. Huck,, "Medicinal applications of fullerenes," *Intrnational Journal of Nanomedicine,* vol. 2, pp. 639-49, 2007.

[21] S. Marchesan, T. Da Ros, G. Spalluto, J. Balzarini, and M. Prato, "Anti-HIV properties of cationic fullerene derivatives," *Bioorganic & Medicinal Chemistry Letters,* vol. 15, pp. 3615-3618, Aug 1 2005.

[22] P. Back, B. P. Braeckman, and F. Matthijssens, "ROS in aging Caenorhabditis elegans: damage or signaling?," *Oxidative Medicine & Celularl Longetivity,* vol. 2012, p. 608478, 2012.

[23] A. Bratic and N. G. Larsson, "The role of mitochondria in aging," *Journal of Clinical Investigation,* vol. 123, pp. 951-7, Mar 1 2013.

[24] M. J. Jackson, "Strategies for reducing oxidative damage in ageing skeletal muscle," *Advanced Drug Delivery Reviews,* vol. 61, pp. 1363-8, Nov 30 2009.

[25] G. Nguyen and A. Torres, "Systemic antioxidants and skin health," *Journal of Drugs & Dermatology,* vol. 11, pp. e1-4, Sep 2012.

[26] D. M. Small, J. S. Coombes, N. Bennett, D. W. Johnson, and G. C. Gobe, "Oxidative stress, anti-oxidant therapies and chronic kidney disease," *Nephrology (Carlton),* vol. 17, pp. 311-21, May 2012.

[27] D. Harman, "Free Radical Theory of Aging: An Update," *Annals of the New York Academy of Sciences,* vol. 1067, pp. 10-21, 2006.

[28] E. Hernandez-Marin, A. Galano, and A. Martinez, "Cis Carotenoids: Colorful Molecules and Free Radical Quenchers," *Journal of Physical Chemistry B,* vol. 117, pp. 4050-4061, Apr 18 2013.

[29] S. Alcaro, S. G. Chiodo, M. Leopoldini, and F. Ortuso, "Antioxidant Efficiency of Oxovitisin, a New Class of Red Wine Pyranoanthocyanins, Revealed through Quantum Mechanical Investigations," *Journal of Chemical Information and Modeling,* vol. 53, pp. 66-75, Jan 2013.

[30] M. Leopoldini, N. Russo, and M. Toscano, "Gas and liquid phase acidity of natural antioxidants," *Journal of Agricultural and Food Chemistry,* vol. 54, pp. 3078-3085, Apr 19 2006.

[31] P. Krusic, E. Wasserman, P. Keizer, J. Morton, and K. Preston, "Radical reactions of C60," *Science,* vol. 254, pp. 1183-1185, 1991.

[32] I. C. Wang, L. A. Tai, D. D. Lee, P. P. Kanakamma, C. K. F. Shen, T. Y. Luh,., "C-60 and water-soluble fullerene derivatives as antioxidants against radical-initiated lipid peroxidation," *Journal of Medicinal Chemistry,* vol. 42, pp. 4614-4620, Nov 4 1999.

[33] B. C. Yadav, and Ritesh Kumar, "Structure, properties and applications of fullerenes," *International Journal of Nanotechnology and Applications,* pp. 15-24, 2008.

[34] V. A. Chistyakov, Y. O. Smirnova, E. V. Prazdnova, and A. V. Soldatov, "Possible Mechanisms of Fullerene C-60 Antioxidant Action," *Biomed Research International,* 2013.

[35] Q. H. Liu, Q. J. Cui, X. J. Li, and L. Jin, "The applications of buckminsterfullerene C-60 and derivatives in orthopaedic research," *Connective Tissue Research,* vol. 55, pp. 71-79, Apr 2014.

[36] N. Gharbi, M. Pressac, M. Hadchouel, H. Szwarc, S. R. Wilson, and F. Moussa, "[60]Fullerene is a powerful antioxidant in vivo with no acute or subacute toxicity," *Nano Letters,* vol. 5, pp. 2578-2585, Dec 2005.

[37] R. Injac, M. Perse, M. Cerne, N. Potocnik, N. Radic, B. Govedarica, "Protective effects of fullerenol C-60(OH)(24) against doxorubicin-induced cardiotoxicity and hepatotoxicity in rats with colorectal cancer," *Biomaterials,* vol. 30, pp. 1184-1196, Feb 2009.

[38] Y. N. Yamakoshi, T. Yagami, S. Sueyoshi, and N. Miyata, "Acridine adduct of [60]fullerene with enhanced DNA-cleaving activity (vol 61, pg 7237, 1996)," *Journal of Organic Chemistry,* vol. 62, pp. 4885-4885, Jul 11 1997.

[39] S. Foley, C. Crowley, M. Smaihi, C. Bonfils, B. F. Erlanger, P. Seta, "Cellular localisation of a water-soluble fullerene derivative," *Biochemical and Biophysical Research Communications,* vol. 294, pp. 116-119, May 31 2002.

[40] S. Foley, A. D. M. Curtis, A. Hirsch, M. Brettreich, A. Pelegrin, P. Seta, "Interaction of a water soluble fullerene derivative with reactive oxygen species and model enzymatic systems," *Fullerenes Nanotubes and Carbon Nanostructures,* vol. 10, pp. 49-67, 2002.

[41] T. Y. Zakharian, D. A. Engler, and L. J. Wilson, "Studies on transfection and DNA interactions of positively charged fullerene derivatives," *Abstracts of Papers of the American Chemical Society,* vol. 230, pp. U507-U509, Aug 28 2005.

[42] P. G. Rasmussen, T. S. Fabre, P. A. Beck, M. J. Eissa, J. Escobedo, and R. M. Strongin, "The reaction of [60] fullerene with 2-diazo-4,5-dicyanoimidazole," *Tetrahedron Letters,* vol. 42, pp. 6823-6825, Sep 24 2001.

[43] T. Yamada, D. Y. Jung, R. Sawada, A. Matsuoka, R. Nakaoka, and T. Tsuchiya, "Effects intracerebral microinjection and intraperitoneal injection of [60]fullerene on brain functions differ in rats," *J Nanosci Nanotechnol,* vol. 8, pp. 3973-80, Aug 2008.

[44] A. A. Tykhomyrov, V. S. Nedzvetsky, V. K. Klochkov, and G. V. Andrievsky, "Nanostructures of hydrated C60 fullerene (C60HyFn) protect rat brain against alcohol impact and attenuate behavioral impairments of alcoholized animals," *Toxicology,* vol. 246, pp. 158-65, Apr 18 2008.

[45] L. L. Dugan, E. G. Lovett, K. L. Quick, J. Lotharius, T. T. Lin, and K. L. O'Malley, "Fullerene-based antioxidants and neurodegenerative disorders," *Parkinsonism & Related Disorders,* vol. 7, pp. 243-246, Jul 2001.

[46] T. D. Dugan LL, Du C, Lobner D, Wheeler M, Almli CR, Shen CKF, Luh TY, Choi DW, Lin TS, *Proceedings of the National Academy of Sciences.,* vol. 94, 1997.

[47] H. Jin, W. Q. Chen, X. W. Tang, L. Y. Chiang, C. Y. Yang, J. V. Schloss, , "Polyhydroxylated C(60), fullerenols, as glutamate receptor antagonists and neuroprotective agents," *Journal of Neuroscience Research,* vol. 62, pp. 600-7, Nov 15 2000.

[48] X. Liu, W. C. Guan, and W. S. Ke, "C-60-based ebselen derivative: Synthesis by Bingel cyclopropanation and enhanced antioxidative and neuroprotective activity," *Journal of the Brazilian Chemical Society,* vol. 18, pp. 1322-1328, 2007.

[49] M. Srikanth, "In vitro cytotoxicity tests of nanomaterials on 3T3 and l929 cancerous cells," Wichita State University, 2012.

[50] G. D. Nielsen, M. Roursgaard, K. A. Jensen, S. S. Poulsen, and S. T. Larsen, "In vivo biology and toxicology of fullerenes and their derivatives," *Basic & clinical pharmacology & toxicology,* vol. 103, pp. 197-208, 2008.

[51] V. Dhawan, N. Mahajan, and S. Jain, "Role of C-C chemokines in Takayasu's arteritis disease," *International Journal of Cardiology,* vol. 112, pp. 105-11, Sep 10 2006.

[52] C. Y. Usenko, S. L. Harper, and R. L. Tanguay, "Fullerene C60 exposure elicits an oxidative stress response in embryonic zebrafish," *Toxicology and Applied Pharmacology,* vol. 229, pp. 44-55, May 15 2008.

[53] S. Iijima and T. Ichihashi, "Single-Shell Carbon Nanotubes of 1-Nm Diameter," *Nature,* vol. 363, pp. 603-605, Jun 17 1993.

[54] D. S. Bethune, C. H. Kiang, M. S. Devries, G. Gorman, R. Savoy, J. Vazque, "Cobalt-Catalyzed Growth of Carbon Nanotubes with Single-Atomic-Layerwalls," *Nature,* vol. 363, pp. 605-607, Jun 17 1993.

[55] A. Oberlin, M. Endo, and T. Koyama, "Filamentous Growth of Carbon through Benzene Decomposition," *Journal of Crystal Growth,* vol. 32, pp. 335-349, 1976.

[56] R. H. Baughman, A. A. Zakhidov, and W. A. de Heer, "Carbon nanotubes--the route toward applications," *Science,* vol. 297, pp. 787-92, Aug 2 2002.

[57] C. N. R. Rao, R. Voggu, and A. Govindaraj, "Selective generation of single-walled carbon nanotubes with metallic, semiconducting and other unique electronic properties," *Nanoscale,* vol. 1, pp. 96-105, 2009.

[58] S. Park, J. An, I. Jung, R. D. Piner, S. J. An, X. Li, "Colloidal suspensions of highly reduced graphene oxide in a wide variety of organic solvents," *Nano Letters,* vol. 9, pp. 1593-7, Apr 2009.

[59] M. F. Yu, O. Lourie, M. J. Dyer, K. Moloni, T. F. Kelly, and R. S. Ruoff, "Strength and breaking mechanism of multiwalled carbon nanotubes under tensile load," *Science,* vol. 287, pp. 637-640, Jan 28 2000.

[60] B. G. Demczyk, Y. M. Wang, J. Cumings, M. Hetman, W. Han, A. Zettl,., "Direct mechanical measurement of the tensile strength and elastic modulus of multiwalled carbon nanotubes," *Materials Science and Engineering a-Structural Materials Properties Microstructure and Processing,* vol. 334, pp. 173-178, Sep 1 2002.

[61] X. Lu and Z. Chen, "Curved pi-conjugation, aromaticity, and the related chemistry of small fullerenes (< C60) and single-walled carbon nanotubes," *Chemical Reviews,* vol. 105, pp. 3643-96, Oct 2005.

[62] S. Hong and S. Myung, "Nanotube electronics: a flexible approach to mobility," *Nat Nanotechnology,* vol. 2, pp. 207-8, Apr 2007.

[63] E. Pop, D. Mann, Q. Wang, K. Goodson, and H. Dai, "Thermal conductance of an individual single-wall carbon nanotube above room temperature," *Nano Letters,* vol. 6, pp. 96-100, Jan 2006.

[64] S. Sinha, S. Barjami, G. Iannacchione, A. Schwab, and G. Muench, "Off-axis thermal properties of carbon nanotube films," *Journal of Nanoparticle Research,* vol. 7, pp. 651-657, Dec 2005.

[65] J. C. Charlier and J. P. Issi, "Electronic structure and quantum transport in carbon nanotubes," *Applied Physics a-Materials Science & Processing,* vol. 67, pp. 79-87, Jul 1998.

[66] M. Kiuchi, Y. Isono, S. Sugiyama, T. Morita, and S. Matsui, "Mechanical and electrical properties evaluation of carbon nanowire using electrostatic actuated nano tensile testing devices (EANAT)," in *Nanotechnology, 2005. 5th IEEE Conference on*, 2005, pp. 486-489 vol. 2.

[67] H. S. Park, W. Cai, H. D. Espinosa, and H. C. Huang, "Mechanics of Crystalline Nanowires (vol 34, pg 178, 2009)," *Mrs Bulletin,* vol. 34, pp. 232-232, Apr 2009.

[68] G. Jia, H. Wang, L. Yan, X. Wang, R. Pei, T. Yan, "Cytotoxicity of carbon nanomaterials: single-wall nanotube, multi-wall nanotube, and fullerene," *Environmental Sciience & Technology,* vol. 39, pp. 1378-83, Mar 1 2005.

[69] D. Pantarotto, J. P. Briand, M. Prato, and A. Bianco, "Translocation of bioactive peptides across cell membranes by carbon nanotubes," *Chemical Communications (Camb),* pp. 16-7, Jan 7 2004.

[70] A. Bianco, K. Kostarelos, and M. Prato, "Applications of carbon nanotubes in drug delivery," *Current Opinion in Chemical Biology,* vol. 9, pp. 674-9, Dec 2005.

[71] E. Katz and I. Willner, "Biomolecule-functionalized carbon nanotubes: applications in nanobioelectronics," *Chemphyschem,* vol. 5, pp. 1084-104, Aug 20 2004.

[72] H. J. Dai, "Carbon nanotubes: Synthesis, integration, and properties," *Accounts of Chemical Research,* vol. 35, pp. 1035-1044, Dec 2002.

[73] L. P. Zanello, B. Zhao, H. Hu, and R. C. Haddon, "Bone cell proliferation on carbon nanotubes," *Nano Letters,* vol. 6, pp. 562-567, Mar 2006.

[74] A. Abarrategi, M. C. Gutierrez, C. Moreno-Vicente, M. J. Hortiguela, V. Ramos, J. L. Lopez-Lacomba, "Multiwall carbon nanotube scaffolds for tissue engineering purposes," *Biomaterials,* vol. 29, pp. 94-102, Jan 2008.

[75] P. C. P. Watts, P. K. Fearon, W. K. Hsu, N. C. Billingham, H. W. Kroto, and D. R. M. Walton, "Carbon nanotubes as polymer antioxidants," *Journal of Materials Chemistry,* vol. 13, pp. 491-495, 2003.

[76] M. Pacurari, X. J. Yin, J. S. Zhao, M. Ding, S. S. Leonard, D. Schwegier-Berry, "Raw single-wall carbon nanotubes induce oxidative stress and activate MAPKs, AP-1, NF-kappa B, and Akt in normal and malignant human mesothelial cells," *Environmental Health Perspectives,* vol. 116, pp. 1211-1217, Sep 2008.

[77] I. Fenoglio, M. Tomatis, D. Lison, J. Muller, A. Fonseca, J. B. Nagy, "Reactivity of carbon nanotubes: Free radical generation or scavenging activity?," *Free Radical Biology and Medicine,* vol. 40, pp. 1227-1233, Apr 1 2006.

[78] V. Lovat, D. Pantarotto, L. Lagostena, B. Cacciari, M. Grandolfo, M. Righi, "Carbon nanotube substrates boost neuronal electrical signaling," *Nano Letters,* vol. 5, pp. 1107-1110, Jun 2005.

[79] A. Mazzatenta, M. Giugliano, S. Campidelli, L. Gambazzi, L. Businaro, H. Markram, "Interfacing neurons with carbon nanotubes: Electrical signal transfer and synaptic stimulation in cultured brain circuits," *Journal of Neuroscience,* vol. 27, pp. 6931-6936, Jun 27 2007.

[80] E.-S. Park, *Preparation, Characterization and Applicability of Covalently Functionalized MWNT*, 2013.

[81] Y. C. Ni, H. Hu, E. B. Malarkey, B. Zhao, V. Montana, R. C. Haddon, "Chemically functionalized water soluble single-walled carbon nanotubes modulate neurite outgrowth," *Journal of Nanoscience and Nanotechnology,* vol. 5, pp. 1707-1712, Oct 2005.

[82] A. L. Benabid, B. Wallace, J. Mitrofanis, C. Xia, B. Piallat, V. Fraix, "Therapeutic electrical stimulation of the central nervous system," *Comptes Rendus Biologies,* vol. 328, pp. 177-186, Feb 2005.

[83] B. J. Nuttin, L. Gabriels, K. van Kuyck, and P. Cosyns, "Electrical stimulation of the anterior limbs of the internal capsules in patients with severe obsessive-compulsive disorder: anecdotal reports," *Neurosurgery Clinics of North America,* vol. 14, pp. 267-+, Apr 2003.

[84] H. S. Mayberg, A. M. Lozano, V. Voon, H. E. McNeely, D. Seminowicz, C. Hamani, "Deep brain stimulation for treatment-resistant depression," *Neuron,* vol. 45, pp. 651-60, Mar 3 2005.

[85] F. A. Mussa-Ivaldi and L. E. Miller, "Brain-machine interfaces: computational demands and clinical needs meet basic neuroscience," *Trends Neurosci,* vol. 26, pp. 329-34, Jun 2003.

[86] M. A. Lebedev and M. A. Nicolelis, "Brain-machine interfaces: past, present and future," *Trends Neurosci,* vol. 29, pp. 536-46, Sep 2006.

[87] M. K. Gottipati, I. Kalinina, E. Bekyarova, R. C. Haddon, and V. Parpura, "Chemically functionalized water-soluble single-walled carbon nanotubes modulate morpho-functional characteristics of astrocytes," *Nano Lett,* vol. 12, pp. 4742-7, Sep 12 2012.

[88] M. P. Mattson, R. C. Haddon, and A. M. Rao, "Molecular functionalization of carbon nanotubes and use as substrates for neuronal growth," *Journal of Molecular Neuroscience,* vol. 14, pp. 175-182, Jun 2000.

[89] M. Meyyappan, "Carbon nanotubes in composites.," *Abstracts of Papers of the American Chemical Society,* vol. 229, pp. U1147-U1147, Mar 13 2005.

[90] M. A. Hussain, M. A. Kabir, and A. K. Sood, "On the cytotoxicity of carbon nanotubes," *Current Science,* vol. 96, pp. 664-673, Mar 10 2009.

[91] M. Davoren, E. Herzog, A. Casey, B. Cottineau, G. Chambers, H. J. Byrne, "In vitro toxicity evaluation of single walled carbon nanotubes on human A549 lung cells," *Toxicology in Vitro,* vol. 21, pp. 438-448, Apr 2007.

[92] F. R. Tian, D. X. Cui, H. Schwarz, G. G. Estrada, and H. Kobayashi, "Cytotoxicity of single-wall carbon nanotubes on human fibroblasts," *Toxicology in Vitro,* vol. 20, pp. 1202-1212, Oct 2006.

[93] P. Wick, P. Manser, L. K. Limbach, U. Dettlaff-Weglikowska, F. Krumeich, S. Roth, "The degree and kind of agglomeration affect carbon nanotube cytotoxicity," *Toxicology Letters,* vol. 168, pp. 121-131, Jan 30 2007.

[94] L. Zhu, D. W. Chang, L. M. Dai, and Y. L. Hong, "DNA damage induced by multiwalled carbon nanotubes in mouse embryonic stem cells," *Nano Letters,* vol. 7, pp. 3592-3597, Dec 2007.

[95] A. Magrez, S. Kasas, V. Salicio, N. Pasquier, J. W. Seo, M. Celio, "Cellular toxicity of carbon-based nanomaterials," *Nano Letters,* vol. 6, pp. 1121-1125, Jun 2006.

[96] M. Kalbacova, M. Kalbac, L. Dunsch, H. Kataura, and U. Hempel, "The study of the interaction of human mesenchymal stem cells and monocytes/macrophages with single-walled carbon nanotube films," *Physica Status Solidi B-Basic Solid State Physics,* vol. 243, pp. 3514-3518, Nov 2006.

[97] J. Meng, L. Song, J. Meng, H. Kong, G. J. Zhu, C. Y. Wang, "Using single-walled carbon nanotubes nonwoven films as scaffolds to enhance long-term cell proliferation in vitro," *Journal of Biomedical Materials Research Part A,* vol. 79A, pp. 298-306, Nov 2006.

[98] D. Khang, M. Sato, and T. J. Webster, "Directed osteoblast functions on micro-aligned patterns of carbon nanofibers on a polymer matrix," *Reviews on Advanced Materials Science,* vol. 10, pp. 205-208, Sep 2005.

99] K. Balani, R. Anderson, T. Laha, M. Andara, J. Tercero, E. Crumpler, "Plasma-sprayed carbon nanotube reinforced hydroxyapatite coatings and their interaction with human osteoblasts in vitro," *Biomaterials,* vol. 28, pp. 618-624, Feb 2007.

[100] A. M. Li, K. N. Sun, W. F. Dong, and D. M. Zhao, "Mechanical properties, microstructure and histocompatibility of MWCNTs/HAp biocomposites," *Materials Letters,* vol. 61, pp. 1839-1844, Apr 2007.

[101] X. F. Shi, B. Sitharaman, Q. P. Pham, F. Liang, K. Wu, W. E. Billups, "Fabrication of porous ultra-short single-walled carbon nanotube nanocomposite scaffolds for bone tissue engineering," *Biomaterials,* vol. 28, pp. 4078-4090, Oct 2007.

[102] P. R. Supronowicz, P. M. Ajayan, K. R. Ullmann, B. P. Arulanandam, D. W. Metzger, and R. Bizios, "Novel current-conducting composite substrates for exposing osteoblasts to alternating current stimulation," *Journal of Biomedical Materials Research,* vol. 59, pp. 499-506, Mar 5 2002.

[103] M. A. Correa-Duarte, N. Wagner, J. Rojas-Chapana, C. Morsczeck, M. Thie, and M. Giersig, "Fabrication and biocompatibility of carbon nanotube-based 3D networks as scaffolds for cell seeding and growth," *Nano Letters,* vol. 4, pp. 2233-2236, Nov 2004.

[104] A. A. Shvedova, E. R. Kisin, D. Porter, P. Schulte, V. E. Kagan, B. Fadeel, "Mechanisms of pulmonary toxicity and medical applications of carbon nanotubes: Two faces of Janus?," *Pharmacology & Therapeutics,* vol. 121, pp. 192-204, Feb 2009.

[105] L. Y. Wang, S. Luanpitpong, V. Castranova, W. Tse, Y. J. Lu, V. Pongrakhananon, "Carbon Nanotubes Induce Malignant Transformation and Tumorigenesis of Human Lung Epithelial Cells," *Nano Letters,* vol. 11, pp. 2796-2803, Jul 2011.

[106] T. Tsukahara and H. Haniu, "Cellular cytotoxic response induced by highly purified multi-wall carbon nanotube in human lung cells," *Molecular and Cellular Biochemistry,* vol. 352, pp. 57-63, Jun 2011.

[107] J. Kolosnjaj-Tabi, K. B. Hartman, S. Boudjemaa, J. S. Ananta, G. Morgant, H. Szwarc, "In vivo behavior of large doses of ultrashort and full-length single-walled carbon nanotubes after oral and intraperitoneal administration to Swiss mice," *Acs Nano,* vol. 4, pp. 1481-1492, 2010.

[108] C. A. Poland, R. Duffin, I. Kinloch, A. Maynard, W. A. Wallace, A. Seaton, "Carbon nanotubes introduced into the abdominal cavity of mice show asbestos-like pathogenicity in a pilot study," *Nature nanotechnology,* vol. 3, pp. 423-428, 2008.

[109] A. E. Porter, M. Gass, J. S. Bendall, K. Muller, A. Goode, J. N. Skepper, "Uptake of Noncytotoxic Acid-Treated Single-Walled Carbon Nanotubes into the Cytoplasm of Human Macrophage Cells," *Acs Nano,* vol. 3, pp. 1485-1492, Jun 2009.

[110] Y. Liu, Y. L. Zhao, B. Y. Sun, and C. Y. Chen, "Understanding the Toxicity of Carbon Nanotubes," *Accounts of Chemical Research,* vol. 46, pp. 702-713, Mar 19 2013.

[111] K. Wang, J. Ruan, H. Song, J. L. Zhang, Y. Wo, S. W. Guo, "Biocompatibility of Graphene Oxide," *Nanoscale Research Letters,* vol. 6, 2011.

[112] K. Koziol, J. Vilatela, A. Moisala, M. Motta, P. Cunniff, M. Sennett, "High-performance carbon nanotube fiber," *Science,* vol. 318, pp. 1892-5, Dec 21 2007.

[113] M. O'Connell, *Carbon nanotubes : properties and applications*. Boca Raton, FL: CRC/Taylor & Francis, 2006.

[114] K. S. Novoselov, A. K. Geim, S. V. Morozov, D. Jiang, M. I. Katsnelson, I. V. Grigorieva, "Two-dimensional gas of massless Dirac fermions in graphene," *Nature,* vol. 438, pp. 197-200, Nov 10 2005.

[115] Z. F. DONG JunTang, ZHANG WeiHu, ZHANG ZhiYong, "First-principles study on electronic structures and optical properties of the single-walled (n, 0) ZnO nanotubes," *SCIENCE CHINA Physics, Mechanics & Astronomy,* vol. 56, pp. 706-712, 2013-03-20 2013.

[116] J. C. Meyer, A. K. Geim, M. I. Katsnelson, K. S. Novoselov, T. J. Booth, and S. Roth, "The structure of suspended graphene sheets," *Nature,* vol. 446, pp. 60-3, Mar 1 2007.

[117] S. V. Morozov, K. S. Novoselov, M. I. Katsnelson, F. Schedin, D. C. Elias, J. A. Jaszczak, "Giant intrinsic carrier mobilities in graphene and its bilayer," *Phys Rev Lett,* vol. 100, p. 016602, Jan 11 2008.

[118] A. Akturk and N. Goldsman, "Electron transport and full-band electron-phonon interactions in graphene," *Journal of Applied Physics,* vol. 103, Mar 1 2008.

[119] C. Lee, X. D. Wei, J. W. Kysar, and J. Hone, "Measurement of the elastic properties and intrinsic strength of monolayer graphene," *Science,* vol. 321, pp. 385-388, Jul 18 2008.

[120] J. Nilsson, A. H. Neto, F. Guinea, and N. M. Peres, "Electronic properties of graphene multilayers," *Physical Review Letters,* vol. 97, p. 266801, Dec 31 2006.

[121] A. A. Balandin, "Thermal properties of graphene and nanostructured carbon materials," *Nature Materials,* vol. 10, pp. 569-581, Aug 2011.

[122] W. F. A. Den Dunnen, J. M. Schakenraad, G. J. Zondervan, A. J. Pennings, B. Van Der Lei, and P. H. Robinson, "A new PLLA/PCL copolymer for nerve regeneration," *Journal of Materials Science: Materials in Medicine,* vol. 4, pp. 521-525, 1993/09/01 1993.

[123] N. Mohanty and V. Berry, "Graphene-based single-bacterium resolution biodevice and DNA transistor: interfacing graphene derivatives with nanoscale and microscale biocomponents," *Nano Letters,* vol. 8, pp. 4469-76, Dec 2008.

[124] Y. Chen, H. Vedala, G. P. Kotchey, A. Audfray, S. Cecioni, A. Imberty, "Electronic detection of lectins using carbohydrate-functionalized nanostructures: graphene versus carbon nanotubes," *ACS Nano,* vol. 6, pp. 760-70, Jan 24 2012.

[125] Y. Ohno, K. Maehashi, and K. Matsumoto, "Label-free biosensors based on aptamer-modified graphene field-effect transistors," *Journal of American Chemical Society,* vol. 132, pp. 18012-3, Dec 29 2010.

[126] C. Chung, Y. K. Kim, D. Shin, S. R. Ryoo, B. H. Hong, and D. H. Min, "Biomedical applications of graphene and graphene oxide," *Accounts of Chemical Research,* vol. 46, pp. 2211-24, Oct 15 2013.

[127] K. Yang, S. A. Zhang, G. X. Zhang, X. M. Sun, S. T. Lee, and Z. A. Liu, "Graphene in Mice: Ultrahigh In Vivo Tumor Uptake and Efficient Photothermal Therapy," *Nano Letters,* vol. 10, pp. 3318-3323, Sep 2010.

[128] Z. Liu, W. B. Cai, L. N. He, N. Nakayama, K. Chen, X. M. Sun, "In vivo biodistribution and highly efficient tumour targeting of carbon nanotubes in mice," *Nature Nanotechnology,* vol. 2, pp. 47-52, Jan 2007.

[129] L. Z. Feng and Z. A. Liu, "Graphene in biomedicine: opportunities and challenges," *Nanomedicine,* vol. 6, pp. 317-324, Feb 2011.

[130] W. Hu, C. Peng, W. Luo, M. Lv, X. Li, D. Li, "Graphene-based antibacterial paper," *ACS Nano,* vol. 4, pp. 4317-23, Jul 27 2010.

[131] K. H. Liao, Y. S. Lin, C. W. Macosko, and C. L. Haynes, "Cytotoxicity of graphene oxide and graphene in human erythrocytes and skin fibroblasts," *ACS Appl Mater Interfaces,* vol. 3, pp. 2607-15, Jul 2011.

[132] H. Shen, L. Zhang, M. Liu, and Z. Zhang, "Biomedical applications of graphene," *Theranostics,* vol. 2, pp. 283-94, 2012.

[133] N. Li, X. M. Zhang, Q. Song, R. G. Su, Q. Zhang, T. Kong, "The promotion of neurite sprouting and outgrowth of mouse hippocampal cells in culture by graphene substrates," *Biomaterials,* vol. 32, pp. 9374-9382, Dec 2011.

[134] C. Heo, J. Yoo, S. Lee, A. Jo, S. Jung, H. Yoo, "The control of neural cell-to-cell interactions through non-contact electrical field stimulation using graphene electrodes," *Biomaterials,* vol. 32, pp. 19-27, Jan 2011.

[135] N. Li, Q. Zhang, S. Gao, Q. Song, R. Huang, L. Wang, "Three-dimensional graphene foam as a biocompatible and conductive scaffold for neural stem cells," *Scientific Reports,* vol. 3, Apr 3 2013.

[136] H. X. Chang, L. H. Tang, Y. Wang, J. H. Jiang, and J. H. Li, "Graphene Fluorescence Resonance Energy Transfer Aptasensor for the Thrombin Detection," *Analytical Chemistry,* vol. 82, pp. 2341-2346, Mar 15 2010.

[137] H. Jang, Y. K. Kim, H. M. Kwon, W. S. Yeo, D. E. Kim, and D. H. Min, "A graphene-based platform for the assay of duplex-DNA unwinding by helicase," *Angewandte Chemie Intternational Edition Engl,* vol. 49, pp. 5703-7, Aug 2 2010.

[138] C. H. Lu, J. Li, J. J. Liu, H. H. Yang, X. Chen, and G. N. Chen, "Increasing the Sensitivity and Single-Base Mismatch Selectivity of the Molecular Beacon Using Graphene Oxide as the "Nanoquencher"," *Chemistry-a European Journal,* vol. 16, pp. 4889-4894, 2010.

[139] Y. Zhang, S. F. Ali, E. Dervishi, Y. Xu, Z. Li, D. Casciano, "Cytotoxicity effects of graphene and single-wall carbon nanotubes in neural phaeochromocytoma-derived PC12 cells," *ACS Nano,* vol. 4, pp. 3181-6, Jun 22 2010.

[140] D. G. Dresselhaus M.S., Avouris P, "Carbon Nanotubes: Synthesis, Structure, Properties, and Applications," *Springer,* p. pp 12, 2001.

[141] J. O'Brien, I. Wilson, T. Orton, and F. Pognan, "Investigation of the Alamar Blue (resazurin) fluorescent dye for the assessment of mammalian cell cytotoxicity," *European Journal of Biochemistry,* vol. 267, pp. 5421-5426, 2000.

[142] S. Al-Nasiry, N. Geusens, M. Hanssens, C. Luyten, and R. Pijnenborg, "The use of Alamar Blue assay for quantitative analysis of viability, migration and invasion of choriocarcinoma cells," *Human reproduction,* vol. 22, pp. 1304-1309, 2007.

[143] H. L. L. Karakoti A.S., and Seal S, "The Potential Toxicity of Nanomaterials-The Role of Surfaces," *Journal of the Minerals,* pp. 77-82.

[144] R. Asmatulu and H. Misak, "Hands-On Nanotechnology Experience in the College of Engineering at WSU: A Curriculum Development," *Journal of Nano Education,* vol. 3, pp. 13-23, // 2011.

[145] L. Belyanskaya, S. Weigel, C. Hirsch, U. Tobler, H. F. Krug, and P. Wick, "Effects of carbon nanotubes on primary neurons and glial cells," *Neurotoxicology,* vol. 30, pp. 702-711, 2009.

[146] G. Oberdörster, Z. Sharp, V. Atudorei, A. Elder, R. Gelein, A. Lunts, "Extrapulmonary translocation of ultrafine carbon particles following whole-body inhalation exposure of rats," *Journal of Toxicology and Environmental Health Part A,* vol. 65, pp. 1531-1543, 2002.

[147] E. Oberdörster, "Manufactured nanomaterials (fullerenes, C60) induce oxidative stress in the brain of juvenile largemouth bass," *Environmental health perspectives,* vol. 112, p. 1058, 2004.

[148] V. L. Colvin, "The potential environmental impact of engineered nanomaterials," *Nature biotechnology,* vol. 21, pp. 1166-1170, 2003.

[149] Chronakis, "Novel nanocomposites and nanoceramics based on polymer nanofibers using electrospinning process - A review," *Journal of Materials Processing Technology,* vol. 167, pp. 283-293, august 2005 2005.

[150] V. Beachley and X. Wen, "Effect of electrospinning parameters on the nanofiber diameter and length," *Mater Sci Eng C Mater Biol Appl,* vol. 29, pp. 663-668, Apr 30 2009.

[151] T. N. Stanger J, Fullick S, Sellier M, Staiger M.P, "Insights into the power law relationships that describe mass deposition rates during electrospinning," *Journal of Materials Science: Materials in Medicine,* vol. 47, pp. 1113-1118, 2012.

[152] K. Cheng and W. S. Kisaalita, "Exploring cellular adhesion and differentiation in a micro-/nano-hybrid polymer scaffold," *Biotechnol Prog,* vol. 26, pp. 838-46, May-Jun 2010.

[153] H. Q. Liu and Y. L. Hsieh, "Ultrafine fibrous cellulose membranes from electrospinning of cellulose acetate," *Journal of Polymer Science Part B-Polymer Physics,* vol. 40, pp. 2119-2129, Sep 15 2002.

[154] X. Wang, H. Niu, T. Lin, and X. Wang, "Needleless electrospinning of nanofibers with a conical wire coil," *Polymer Engineering & Science,* vol. 49, pp. 1582-1586, 2009.

[155] H. Fong, I. Chun, and D. H. Reneker, "Beaded nanofibers formed during electrospinning," *Polymer,* vol. 40, pp. 4585-4592, 1999.

[156] R. Jaeger, H. Schonherr, and G. J. Vancso, "Chain packing in electro-spun poly(ethylene oxide) visualized by atomic force microscopy," *Macromolecules,* vol. 29, pp. 7634-7636, Nov 4 1996.

[157] Z. M. Huang, Y. Z. Zhang, M. Kotaki, and S. Ramakrishna, "A review on polymer nanofibers by electrospinning and their applications in nanocomposites," *Composites Science and Technology,* vol. 63, pp. 2223-2253, Nov 2003.

[158] Y. Liu, J. H. He, J. Y. Yu, and H. M. Zeng, "Controlling numbers and sizes of beads in electrospun nanofibers," *Polymer International,* vol. 57, pp. 632-636, Apr 2008.

[159] D. Lukas, A. Sarkar, and P. Pokorny, "Self-organization of jets in electrospinning from free liquid surface: a generalized approach," *Journal of Applied Physics,* vol. 103, p. 084309, 2008.

[160] M. M. Demir, I. Yilgor, E. Yilgor, and B. Erman, "Electrospinning of polyurethane fibers," *Polymer,* vol. 43, pp. 3303-3309, May 2002.

[161] J. Doshi and D. H. Reneker, "Electrospinning Process and Applications of Electrospun Fibers," *Ias 93, Pts 1-3,* pp. 1698-1703, 1993.

[162] C. Moura-Netto, C. D. A. Guglielmi, A. C. V. Mello-Moura, R.M. Palo, D. P. Raggio and C.L. Caldeira, "Nd:YAG laser irradiation effect on apical intracanal dentin - a microleakage and SEM evaluation," *Brazilian Dental Journal,* vol. 22, 2011.

[163] M. M. Hohman, M. Shin, G. Rutledge, and M. P. Brenner, "Electrospinning and electrically forced jets. II. Applications," *Physics of Fluids,* vol. 13, pp. 2221-2236, Aug 2001.

[164] C. J. Buchko, L. C. Chen, Y. Shen, and D. C. Martin, "Processing and microstructural characterization of porous biocompatible protein polymer thin films," *Polymer,* vol. 40, pp. 7397-7407, Dec 1999.

[165] C. J. Buchko, K. M. Kozloff, and D. C. Martin, "Surface characterization of porous, biocompatible protein polymer thin films," *Biomaterials,* vol. 22, pp. 1289-1300, Jun 2001.

[166] C. J. Buchko, M. J. Slattery, K. M. Kozloff, and D. C. Martin, "Mechanical properties of biocompatible protein polymer thin films," *Journal of Materials Research,* vol. 15, pp. 231-242, Jan 2000.

[167] S. A. Athreya and D. C. Martin, "Impedance spectroscopy of protein polymer modified silicon micromachined probes," *Sensors and Actuators A: Physical,* vol. 72, pp. 203-216, 2/16/ 1999.

[168] H. J. Jin, S. V. Fridrikh, G. C. Rutledge, and D. L. Kaplan, "Electrospinning Bombyx mori silk with poly(ethylene oxide)," *Biomacromolecules,* vol. 3, pp. 1233-9, Nov-Dec 2002.

[169] H. Schreuder-Gibson, P. Gibson, K. Senecal, M. Sennett, J. Walker, W. Yeomans, "Protective textile materials based on electrospun nanofibers," *Journal of Advanced Materials,* vol. 34, pp. 44-55, Jul 2002.

[170] E. Zussman, A. Yarin, and D. Weihs, "A micro-aerodynamic decelerator based on permeable surfaces of nanofiber mats," *Experiments in Fluids,* vol. 33, pp. 315-320, 2002/08/01 2002.

[171] A. Frenot and I. S. Chronakis, "Polymer nanofibers assembled by electrospinning," *Current opinion in colloid & interface science,* vol. 8, pp. 64-75, 2003.

[172] X. Y. Wang, S. H. Lee, C. Drew, K. J. Senecal, J. Kumar, and L. A. Samuelson, "Highly sensitive optical sensors using electrospun polymeric nanofibrous membranes," *Organic Optoelectronic Materials, Processing and Devices,* vol. 708, pp. 397-402, 2002.

[173] X. Y. Wang, C. Drew, S. H. Lee, K. J. Senecal, J. Kumar, and L. A. Sarnuelson, "Electrospun nanofibrous membranes for highly sensitive optical sensors," *Nano Letters,* vol. 2, pp. 1273-1275, Nov 2002.

[174] S. H. Lee, B. C. Ku, X. Wang, L. A. Samuelson, and J. Kumar, "Design, synthesis and electrospinning of a novel fluorescent polymer for optical sensor applications," *Organic Optoelectronic Materials, Processing and Devices,* vol. 708, pp. 403-408, 2002.

[175] H. Q. Hou, Z. Jun, A. Reuning, A. Schaper, J. H. Wendorff, and A. Greiner, "Poly(p-xylylene) nanotubes by coating and removal of ultrathin polymer template fibers," *Macromolecules,* vol. 35, pp. 2429-2431, Mar 26 2002.

[176] C. T. Laurencin, A. M. A. Ambrosio, M. D. Borden, and J. A. Cooper, "Tissue engineering: Orthopedic applications," *Annual Review of Biomedical Engineering,* vol. 1, pp. 19-46, 1999.

[177] J. D. Hartgerink, E. Beniash, and S. I. Stupp, "Self-assembly and mineralization of peptide-amphiphile nanofibers," *Science,* vol. 294, pp. 1684-8, Nov 23 2001.

[178] P. X. Ma and R. Zhang, "Microtubular architecture of biodegradable polymer scaffolds," *J Biomed Mater Res,* vol. 56, pp. 469-77, Sep 15 2001.

[179] S. J. Hollister, R. D. Maddox, and J. M. Taboas, "Optimal design and fabrication of scaffolds to mimic tissue properties and satisfy biological constraints," *Biomaterials,* vol. 23, pp. 4095-4103, 2002.

[180] K. Tuzlakoglu, N. Bolgen, A. J. Salgado, M. E. Gomes, E. Piskin, and R. L. Reis, "Nano- and micro-fiber combined scaffolds: a new architecture for bone tissue engineering," *J Mater Sci Mater Med,* vol. 16, pp. 1099-104, Dec 2005.

[181] A. Hokugo, T. Takamoto, and Y. Tabata, "Preparation of hybrid scaffold from fibrin and biodegradable polymer fiber," *Biomaterials,* vol. 27, pp. 61-7, Jan 2006.

[182] S. H. Park, T. G. Kim, H. C. Kim, D. Y. Yang, and T. G. Park, "Development of dual scale scaffolds via direct polymer melt deposition and electrospinning for applications in tissue regeneration," *Acta Biomater,* vol. 4, pp. 1198-207, Sep 2008.

[183] F. Yang, R. Murugan, S. Ramakrishna, X. Wang, Y. X. Ma, and S. Wang, "Fabrication of nano-structured porous PLLA scaffold intended for nerve tissue engineering," *Biomaterials,* vol. 25, pp. 1891-900, May 2004.

[184] Q. P. Pham, U. Sharma, and A. G. Mikos, "Electrospun poly(epsilon-caprolactone) microfiber and multilayer nanofiber/microfiber scaffolds: characterization of scaffolds and measurement of cellular infiltration," *Biomacromolecules,* vol. 7, pp. 2796-805, Oct 2006.

[185] Y. Lee, J. Jeong, I. J. Youn, and W. H. Lee, "Modified liquid displacement method for determination of pore size distribution in porous membranes," *Journal of Membrane Science,* vol. 130, pp. 149-156, Jul 23 1997.

[186] A. Schindler, R. Jeffcoat, G. L. Kimmel, C. G. Pitt, M. E. Wall, and R. Zweidinger, "Biodegradable Polymers for Sustained Drug Delivery," in *Contemporary Topics in Polymer Science*, E. Pearce and J. Schaefgen, Eds., ed: Springer US, 1977, pp. 251-289.

[187] C. S. Yoon and D. S. Ji, "Effects of in vitro degradation on the weight loss and tensile properties of PLA/LPCL/HPCL blend fibers," *Fibers and Polymers,* vol. 6, pp. 13-18, Mar 2005.

[188] Y. M. Wang, M. A. Rodriguez-Perez, R. L. Reis, and J. F. Mano, "Thermal and thermomechanical behaviour of polycaprolactone and starch/polycaprolactone blends for biomedical applications," *Macromolecular Materials and Engineering,* vol. 290, pp. 792-801, Aug 12 2005.

[189] D. S. Rosa, D. R. Lopes, and M. R. Calil, "Thermal properties and enzymatic degradation of blends of poly(epsilon-caprolactone) with starches," *Polymer Testing,* vol. 24, pp. 756-761, Sep 2005.

[190] R. Izquierdo, N. Garcia-Giralt, M. T. Rodriguez, E. Caceres, S. J. Garcia, J. L. G. Ribelles, "Biodegradable PCL scaffolds with an interconnected spherical pore network for tissue engineering," *Journal of Biomedical Materials Research Part A,* vol. 85A, pp. 25-35, Apr 2008.

[191] H. Yoshimoto, Y. M. Shin, H. Terai, and J. P. Vacanti, "A biodegradable nanofiber scaffold by electrospinning and its potential for bone tissue engineering," *Biomaterials,* vol. 24, pp. 2077-2082, May 2003.

[192] H. Kettenmann and A. Verkhratsky, "Neuroglia - Living Nerve Glue," *Fortschritte Der Neurologie Psychiatrie,* vol. 79, pp. 588-597, Oct 2011.

[193] N. J. Allen and B. A. Barres, "Neuroscience: Glia - more than just brain glue," *Nature,* vol. 457, pp. 675-7, Feb 5 2009.

[194] H. K. Kimelberg and M. Nedergaard, "Functions of Astrocytes and their Potential As Therapeutic Targets," *Neurotherapeutics,* vol. 7, pp. 338-353, Oct 2010.

[195] M. Nedergaard, B. Ransom, and S. A. Goldman, "New roles for astrocytes: redefining the functional architecture of the brain," *Trends Neurosci,* vol. 26, pp. 523-30, Oct 2003.

[196] N. A. Oberheim, X. Wang, S. Goldman, and M. Nedergaard, "Astrocytic complexity distinguishes the human brain," *Trends Neurosci,* vol. 29, pp. 547-53, Oct 2006.

[197] M. V. Sofroniew, "Reactive Astrocytes in Neural Repair and Protection," *The Neuroscientist,* vol. 11, pp. 400-407, October 1, 2005 2005.

[198] Y. Dong and E. N. Benveniste, "Immune function of astrocytes," *Glia,* vol. 36, pp. 180-90, Nov 2001.

[199] J. A. Nicoll and R. O. Weller, "A new role for astrocytes: beta-amyloid homeostasis and degradation," *Trends Molecular Medicine,* vol. 9, pp. 281-2, Jul 2003.

[200] M. Noble, J. Fok-Seang, and J. Cohen, "Glia are a unique substrate for the in vitro growth of central nervous system neurons," *Journal Neuroscience,* vol. 4, pp. 1892-903, Jul 1984.

[201] J. R. Fallon, "Preferential outgrowth of central nervous system neurites on astrocytes and Schwann cells as compared with nonglial cells in vitro," *J Cell Biol,* vol. 100, pp. 198-207, Jan 1985.

[202] M. Obara, M. Szeliga, and J. Albrecht, "Regulation of pH in the mammalian central nervous system under normal and pathological conditions: facts and hypotheses," *Neurochemistry International,* vol. 52, pp. 905-19, May 2008.

[203] R. Sattler and J. D. Rothstein, "Regulation and dysregulation of glutamate transporters," *Handbook Expperimental Pharmacol,* pp. 277-303, 2006.

[204] G. Seifert, K. Schilling, and C. Steinhauser, "Astrocyte dysfunction in neurological disorders: a molecular perspective," *Nature Review Neuroscience,* vol. 7, pp. 194-206, Mar 2006.

[205] P. Ballabh, A. Braun, and M. Nedergaard, "The blood-brain barrier: an overview: structure, regulation, and clinical implications," *Neurobiol Dis,* vol. 16, pp. 1-13, Jun 2004.

[206] G. R. Gordon, S. J. Mulligan, and B. A. MacVicar, "Astrocyte control of the cerebrovasculature," *Glia,* vol. 55, pp. 1214-21, Sep 2007.

[207] R. F. Haseloff, I. E. Blasig, H. C. Bauer, and H. Bauer, "In search of the astrocytic factor(s) modulating blood-brain barrier functions in brain capillary endothelial cells in vitro," *Cellular and Molecular Neurobiology,* vol. 25, pp. 25-39, Feb 2005.

[208] R. C. Koehler, D. Gebremedhin, and D. R. Harder, "Role of astrocytes in cerebrovascular regulation," *Journal of Applied Physiology,* vol. 100, pp. 307-317, Jan 2006.

[209] X. M. Qian, Q. Shen, S. K. Goderie, W. L. He, A. Capela, A. A. Davis, "Timing of CNS cell generation: A programmed sequence of neuron and glial cell production from isolated murine cortical stem cells," *Neuron,* vol. 28, pp. 69-80, Oct 2000.

[210] J. Schummers, H. B. Yu, and M. Sur, "Tuned responses of astrocytes and their influence on hemodynamic signals in the visual cortex," *Science,* vol. 320, pp. 1638-1643, Jun 20 2008.

[211] S. H. Oliet, R. Piet, and D. A. Poulain, "Control of glutamate clearance and synaptic efficacy by glial coverage of neurons," *Science,* vol. 292, pp. 923-6, May 4 2001.

[212] T. Fellin, "Communication between neurons and astrocytes: relevance to the modulation of synaptic and network activity," *Journal of Neurochemistry,* vol. 108, pp. 533-544, Feb 2009.

[213] M. M. Halassa, T. Fellin, H. Takano, J. H. Dong, and P. G. Haydon, "Synaptic islands defined by the territory of a single astrocyte," *Journal of Neuroscience,* vol. 27, pp. 6473-6477, Jun 13 2007.

[214] T. A. Fiacco and K. D. McCarthy, "Astrocyte calcium elevations: Properties, propagation, and effects on brain signaling," *Glia,* vol. 54, pp. 676-690, Nov 15 2006.

[215] P. G. Haydon and G. Carmignoto, "Astrocyte control of synaptic transmission and neurovascular coupling," *Physiological Reviews,* vol. 86, pp. 1009-1031, Jul 2006.

[216] G. Perea and A. Araque, "Synaptic information processing by astrocytes," *Journal of Physiology-Paris,* vol. 99, pp. 92-97, Mar-May 2006.

[217] E. Shigetomi, D. N. Bowser, M. V. Sofroniew, and B. S. Khakh, "Two forms of astrocyte calcium excitability have distinct effects on NMDA receptor-mediated slow inward currents in pyramidal neurons," *J Neurosci,* vol. 28, pp. 6659-63, Jun 25 2008.

[218] E. M. Ullian, S. K. Sapperstein, K. S. Christopherson, and B. A. Barres, "Control of synapse number by glia," *Science,* vol. 291, pp. 657-61, Jan 26 2001.

[219] B. A. Barres, "The Mystery and Magic of Glia: A Perspective on Their Roles in Health and Disease," *Neuron,* vol. 60, pp. 430-440, 11/6/ 2008.

[220] J. Silver and J. H. Miller, "Regeneration beyond the glial scar," *Nature Reviews Neuroscience,* vol. 5, pp. 146-156, Feb 2004.

[221] J. W. Fawcett and R. A. Asher, "The glial scar and central nervous system repair," *Brain Research Bulletin,* vol. 49, pp. 377-391, Aug 1999.

[222] A. Rolls, R. Shechter, and M. Schwartz, "NEURON - GLIA INTERACTIONS - OPINION The bright side of the glial scar in CNS repair," *Nature Reviews Neuroscience,* vol. 10, pp. 235-U91, Mar 2009.

[223] K. Yamanaka, S. J. Chun, S. Boillee, N. Fujimori-Tonou, H. Yamashita, D. H. Gutmann, "Astrocytes as determinants of disease progression in inherited amyotrophic lateral sclerosis," *Nature Neuroscience,* vol. 11, pp. 251-253, Mar 2008.

[224] G. E. Barreto and L. Morales, *Role of astrocytes in neurodegenerative diseases*.

[225] M. Eddleston and L. Mucke, "Molecular profile of reactive astrocytes—Implications for their role in neurologic disease," *Neuroscience,* vol. 54, pp. 15-36, 5// 1993.

[226] T. Chu, H. Zhou, F. Li, T. Wang, L. Lu, and S. Feng, "Astrocyte transplantation for spinal cord injury: current status and perspective," *Brain Res Bull,* vol. 107, pp. 18-30, Aug 2014.

[227] R. D. Fields and G. Burnstock, "Purinergic signalling in neuron-glia interactions," *Nat Rev Neuroscience,* vol. 7, pp. 423-36, Jun 2006.

[228] H. Zimmermann, "Signalling via ATP in the nervous system," *Trends Neurosci,* vol. 17, pp. 420-6, Oct 1994.

[229] S. M. Allan and N. J. Rothwell, "Cytokines and acute neurodegeneration," *Nat Rev Neuroscience,* vol. 2, pp. 734-44, Oct 2001.

[230] D. Davalos, J. Grutzendler, G. Yang, J. V. Kim, Y. Zuo, S. Jung, "ATP mediates rapid microglial response to local brain injury in vivo," *Nature Neuroscience,* vol. 8, pp. 752-8, Jun 2005.

[231] S. Hindley, M. A. Herman, and M. P. Rathbone, "Stimulation of reactive astrogliosis in vivo by extracellular adenosine diphosphate or an adenosine A2 receptor agonist," *Journal of Neuroscience Research,* vol. 38, pp. 399-406, Jul 1 1994.

[232] P. Illes, W. Norenberg, and P. J. Gebicke-Haerter, "Molecular mechanisms of microglial activation. B. Voltage- and purinoceptor-operated channels in microglia," *Neurochemistry International,* vol. 29, pp. 13-24, Jul 1996.

[233] M. P. Abbracchio, S. Ceruti, C. Bolego, L. Puglisi, G. Burnstock, and F. Cattabeni, "Trophic roles of P2 purinoceptors in central nervous system astroglial cells," *Ciba Found Symp,* vol. 198, pp. 142-7; discussion 147-8, 1996.

[234] B. M. Ajtai and M. Kalman, "Reactive glia support and guide axon growth in the rat thalamus during the first postnatal week. A sharply timed transition from permissive to non-permissive stage," *International Journal of Developmental Neuroscience,* vol. 19, pp. 589-97, Oct 2001.

[235] W. Kang and J. M. Hebert, "Signaling pathways in reactive astrocytes, a genetic perspective," *Molecular Neurobiology,* vol. 43, pp. 147-54, Jun 2011.

[236] J. L. Ridet, S. K. Malhotra, A. Privat, and F. H. Gage, "Reactive astrocytes: cellular and molecular cues to biological function," *Trends Neuroscience,* vol. 20, pp. 570-7, Dec 1997.

[237] J. R. Faulkner, J. E. Herrmann, M. J. Woo, K. E. Tansey, N. B. Doan, and M. V. Sofroniew, "Reactive astrocytes protect tissue and preserve function after spinal cord injury," *Journal of Neuroscience,* vol. 24, pp. 2143-55, Mar 3 2004.

[238] M. T. Fitch and J. Silver, "CNS injury, glial scars, and inflammation: Inhibitory extracellular matrices and regeneration failure," *Experimental Neurology,* vol. 209, pp. 294-301, Feb 2008.

[239] A. J. Mathewson and M. Berry, "Observations on the astrocyte response to a cerebral stab wound in adult rats," *Brain Research,* vol. 327, pp. 61-9, Feb 18 1985.

[240] M. Koistinaho, S. Lin, X. Wu, M. Esterman, D. Koger, J. Hanson, "Apolipoprotein E promotes astrocyte colocalization and degradation of deposited amyloid-beta peptides," *Nature Medicine,* vol. 10, pp. 719-26, Jul 2004.

[241] O. Ikeda, M. Murakami, H. Ino, M. Yamazaki, T. Nemoto, M. Koda,., "Acute up-regulation of brain-derived neurotrophic factor expression resulting from experimentally induced injury in the rat spinal cord," *Acta Neuropathol,* vol. 102, pp. 239-45, Sep 2001.

[242] S. Costa, T. Planchenault, C. Charriere-Bertrand, Y. Mouchel, C. Fages, S. Juliano, , "Astroglial permissivity for neuritic outgrowth in neuron-astrocyte cocultures depends on regulation of laminin bioavailability," *Glia,* vol. 37, pp. 105-13, Feb 2002.

[243] T. G. Bush, N. Puvanachandra, C. H. Horner, A. Polito, T. Ostenfeld, C. N. Svendsen, "Leukocyte infiltration, neuronal degeneration, and neurite outgrowth after ablation of scar-forming, reactive astrocytes in adult transgenic mice," *Neuron,* vol. 23, pp. 297-308, Jun 1999.

[244] J. D. Rothstein, M. Dykes-Hoberg, C. A. Pardo, L. A. Bristol, L. Jin, R. W. Kuncl, "Knockout of glutamate transporters reveals a major role for astroglial transport in excitotoxicity and clearance of glutamate," *Neuron,* vol. 16, pp. 675-86, Mar 1996.

[245] R. A. Swanson, W. Ying, and T. M. Kauppinen, "Astrocyte influences on ischemic neuronal death," *Curr Mol Med,* vol. 4, pp. 193-205, Mar 2004.

[246] Z. Zador, S. Stiver, V. Wang, and G. T. Manley, "Role of aquaporin-4 in cerebral edema and stroke," *Handbook Experimental Pharmacology,* pp. 159-70, 2009.

[247] A. R. Filous, J. H. Miller, Y. M. Coulson-Thomas, K. P. Horn, W. J. Alilain, and J. Silver, "Immature astrocytes promote CNS axonal regeneration when combined with chondroitinase ABC," *Developmental Neurobiology,* vol. 70, pp. 826-41, Oct 2010.

[248] S. R. Chen Y, "Astrocytes and brain injury," *Jornal of Cerebral Blood Flow and Metabolism,* vol. 23, pp. 137-412, 2003.

[249] A. Verkhratsky, M. Olabarria, H. N. Noristani, C. Y. Yeh, and J. J. Rodriguez, "Astrocytes in Alzheimer's Disease," *Neurotherapeutics,* vol. 7, pp. 399-412, Oct 2010.

[250] M. Kliot, G. M. Smith, J. D. Siegal, and J. Silver, "Astrocyte-polymer implants promote regeneration of dorsal root fibers into the adult mammalian spinal cord," *Experimantal Neurology,* vol. 109, pp. 57-69, Jul 1990.

[251] J. J. Wang, M. I. Chuah, D. T. Yew, P. C. Leung, and D. S. Tsang, "Effects of astrocyte implantation into the hemisected adult rat spinal cord," *Neuroscience,* vol. 65, pp. 973-81, Apr 1995.

[252] E. A. Joosten, W. B. Veldhuis, and F. P. Hamers, "Collagen containing neonatal astrocytes stimulates regrowth of injured fibers and promotes modest locomotor recovery after spinal cord injury," *Journal of Neuroscience Research,* vol. 77, pp. 127-42, Jul 1 2004.

[253] J. E. Davies, C. Huang, C. Proschel, M. Noble, M. Mayer-Proschel, and S. J. Davies, "Astrocytes derived from glial-restricted precursors promote spinal cord repair," *Journal of Biology,* vol. 5, p. 7, 2006.

[254] J. E. Davies, C. Proschel, N. Zhang, M. Noble, M. Mayer-Proschel, and S. J. Davies, "Transplanted astrocytes derived from BMP- or CNTF-treated glial-restricted precursors have opposite effects on recovery and allodynia after spinal cord injury," *Journal of Biology,* vol. 7, p. 24, 2008.

[255] M. Ni and M. Aschner, "NEONATAL RAT PRIMARY MICROGLIA: ISOLATION, CULTURING AND SELECTED APPLICATIONS," *Current protocols in toxicology / editorial board, Mahin D. Maines (editor-in-chief) ,* vol. CHAPTER, pp. Unit-12.17, 2010.

[256] Y. Zhang, H. Ouyang, C. T. Lim, S. Ramakrishna, and Z. M. Huang, "Electrospinning of gelatin fibers and gelatin/PCL composite fibrous scaffolds," *Journal of Biomedical Material Research B Application Biomater,* vol. 72, pp. 156-65, Jan 15 2005.

[257] K. S. Tiaw, S. W. Goh, M. Hong, Z. Wang, B. Lan, and S. H. Teoh, "Laser surface modification of poly(epsilon-caprolactone) (PCL) membrane for tissue engineering applications," *Biomaterials,* vol. 26, pp. 763-9, Mar 2005.

[258] P. S. Tan and S. H. Teoh, "Effect of stiffness of polycaprolactone (PCL) membrane on cell proliferation," *Materials Science & Engineering C-Biomimetic and Supramolecular Systems,* vol. 27, pp. 304-308, Mar 2007.

[259] W. Fu, Z. L. Liu, B. Feng, R. J. Hu, X. M. He, H. Wang, "Electrospun gelatin/PCL and collagen/PLCL scaffolds for vascular tissue engineering," *International Journal of Nanomedicine,* vol. 9, pp. 2335-2344, 2014.

[260] E. Azemi, G. T. Gobbel, and X. T. Cui, "Seeding neural progenitor cells on silicon-based neural probes Laboratory investigation," *Journal of Neurosurgery,* vol. 113, pp. 673-681, Sep 2010.

[261] Y. Tajima, T. Matsuura, Y. Numata, D. Yamazaki, H. Kawamura, and H. Osedo, "Surface free energy and wettability determination of various fullerene derivative films on amorphous carbon wafer," *Japanese Journal of Applied Physics,* vol. 47, p. 5730, 2008.

[262] C. Della Volpe, D. Maniglio, M. Brugnara, S. Siboni, and M. Morra, "The solid surface free energy calculation. I. In defense of the multicomponent approach," *journal of Colloid Interface SciENCE,* vol. 271, pp. 434-53, Mar 15 2004.

[263] T. Werder, J. H. Walther, R. L. Jaffe, T. Halicioglu, F. Noca, and P. Koumoutsakos, "Molecular dynamics simulation of contact angles of water droplets in carbon nanotubes," *Nano Letters,* vol. 1, pp. 697-702, Dec 2001.

[264] Y. J. Shin, Y. Y. Wang, H. Huang, G. Kalon, A. T. S. Wee, Z. X. Shen, "Surface-Energy Engineering of Graphene," *Langmuir,* vol. 26, pp. 3798-3802, Mar 16 2010.

[265] F. Taherian, V. Marcon, N. F. A. van der Vegt, and F. Leroy, "What Is the Contact Angle of Water on Graphene?," *Langmuir,* vol. 29, pp. 1457-1465, Feb 5 2013.

[266] E. Masaeli, M. Morshed, M. H. Nasr-Esfahani, S. Sadri, J. Hilderink, A. van Apeldoorn, "Fabrication, characterization and cellular compatibility of poly(hydroxy alkanoate) composite nanofibrous scaffolds for nerve tissue engineering," *PLoS One,* vol. 8, p. e57157, 2013.

[267] K. Saeedfar, L. Y. Heng, T. L. Ling, and M. Rezayi, "Potentiometric Urea Biosensor Based on an Immobilised Fullerene-Urease Bio-Conjugate," *Sensors,* vol. 13, pp. 16851-16866, Dec 2013.

[268] T. A. Saleh, *The Role of Carbon Nanotubes in Enhancement of Photocatalysis*, 2013.

[269] M. Naebe, J. Wang, A. Amini, H. Khayyam, N. Hameed, L. H. Li, "Mechanical property and structure of covalent functionalised graphene/epoxy nanocomposites," *Sci Rep,* vol. 4, p. 4375, 2014.

[270] H. Cui and P. J. Sinko, "The role of crystallinity on differential attachment/proliferation of osteoblasts and fibroblasts on poly (caprolactone-co-glycolide) polymeric surfaces," *Frontiers of Materials Science,* vol. 6, pp. 47-59, Mar 2012.

[271] L. Chou, B. Marek, and W. R. Wagner, "Effects of hydroxylapatite coating crystallinity on biosolubility, cell attachment efficiency and proliferation in vitro," *Biomaterials,* vol. 20, pp. 977-985, May 1999.

[272] R. Dell'Erba, G. Groeninckx, G. Maglio, M. Malinconico, and A. Migliozzi, "Immiscible polymer blends of semicrystalline biocompatible components: thermal properties and phase morphology analysis of PLLA/PCL blends," *Polymer,* vol. 42, pp. 7831-7840, 2001.

[273] M. B. Clark Jr, C. A. Burkhardt, and J. A. Gardella Jr, "Surface studies of polymer blends. 3. An ESCA, IR and DSC study of poly (. epsilon.-caprolactone)/poly (vinyl chloride) homopolymer blends," *Macromolecules,* vol. 22, pp. 4495-4501, 1989.

[274] A. Monshi, M. R. Foroughi, and M. R. Monshi, "Modified Scherrer equation to estimate more accurately nano-crystallite size using XRD," *World Journal of Nano Science and Engineering,* vol. 2, p. 154, 2012.

[275] Z. Jian and W. Hejing, "The physical meanings of 5 basic parameters for an X-ray diffraction peak and their application," *Chinese Journal of Geochemistry,* vol. 22, pp. 38-44, 2003.

[276] J. I. Langford and A. Wilson, "Scherrer after sixty years: a survey and some new results in the determination of crystallite size," *Journal of Applied Crystallography,* vol. 11, pp. 102-113, 1978.

[277] R. H. Bragg and J. B. Aladekomo, "Diffraction by diffusely scattering materials of high transparency," *Journal of applied crystallography,* vol. 28, pp. 14-19, 1995.

[278] M. X. Zhu and H. J. Wang, "Very low-grade metamorphism of the Lengjiaxi and Banxi Groups around the area of Changsha-Liling-Liuyang, Hunan province, China," *Acta Petrologica Sinica,* vol. 17, pp. 291-300, Apr 2001.

[279] O. Hartman, C. Zhang, E. L. Adams, M. C. Farach-Carson, N. J. Petrelli, B. D. Chase, "Biofunctionalization of electrospun PCL-based scaffolds with perlecan domain IV peptide to create a 3-D pharmacokinetic cancer model," *Biomaterials,* vol. 31, pp. 5700-18, Jul 2010.

[280] C. Mead, "Neuromorphic electronic systems," *Proceedings of the IEEE,* vol. 78, pp. 1629-1636, 1990.

[281] R. D. Knight, B. Jones, and S. Field, *college physics*: Pearson Education, 2009.

[282] J. Joe T. Evans, " The Importance of ε," *Radient Technologies Inc,* vol. , 2008.

[283] F. Martini, *Anatomy and Physiology'2007 Ed*: Rex Bookstore, Inc., 2005.

[284] M. M. Sternheim and J. W. Kane, "General Physics, Study Guide," *General Physics, Study Guide, 2nd Edition, by Morton M. Sternheim, Joseph W. Kane, pp. 360. ISBN 0-471-53485-4. Wiley-VCH, January 1991.,* vol. 1, 1991.

[285] S. M. Aguilar, J. D. Shea, M. A. Al-Joumayly, B. D. Van Veen, N. Behdad, and S. C. Hagness, "Dielectric Characterization of PCL-Based Thermoplastic Materials for Microwave Diagnostic and Therapeutic Applications," *Ieee Transactions on Bio-Medical Engineering,* vol. 59, pp. 627-633, 05/27 2012.

[286] D. S. Kalenov, V. V. Meriakri, M. P. Parkhomenko, and S. Zhou, "Dielectric Properties of Biocompatible and Biodegradable Polycaprolone and Polylactide and Their Nanocomposites in the Millimeter Wave Band," *6th International Conference on Times of Polymers (Top) and Composites,* vol. 1459, pp. 77-79, 2012.

[287] C. Antczak, D. Shum, S. Escobar, B. Bassit, E. Kim, V. E. Seshan, "High-throughput identification of inhibitors of human mitochondrial peptide deformylase," *J Biomol Screen,* vol. 12, pp. 521-35, Jun 2007.

[288] J. Gartlon, A. Kinsner, A. Bal-Price, S. Coecke, and R. H. Clothier, "Evaluation of a proposed in vitro test strategy using neuronal and non-neuronal cell systems for detecting neurotoxicity," *Toxicology in Vitro,* vol. 20, pp. 1569-1581, Dec 2006.

[289] G. J. Doherty and H. T. McMahon, "Mediation, modulation, and consequences of membrane-cytoskeleton interactions," *Annual Review of Biophysics,* vol. 37, pp. 65-95, 2008.

[290] D. M. Baorto, W. Mellado, and M. L. Shelanski, "Astrocyte Process Growth Induction by Actin Breakdown," *Journal of Cell Biology,* vol. 117, pp. 357-367, Apr 1992.

[291] L. F. Eng, R. S. Ghirnikar, and Y. L. Lee, "Glial fibrillary acidic protein: GFAP-thirty-one years (1969-2000)," *Neurochem Res,* vol. 25, pp. 1439-51, Oct 2000.

[292] A. D. Garcia, N. B. Doan, T. Imura, T. G. Bush, and M. V. Sofroniew, "GFAP-expressing progenitors are the principal source of constitutive neurogenesis in adult mouse forebrain," *Nature Neuroscience,* vol. 7, pp. 1233-41, Nov 2004.

[293] M. Brenner, A. B. Johnson, O. Boespflug-Tanguy, D. Rodriguez, J. E. Goldman, and A. Messing, "Mutations in GFAP, encoding glial fibrillary acidic protein, are associated with Alexander disease," *Nature Genetics,* vol. 27, pp. 117-20, Jan 2001.

[294] R. E. M cLendon and D. D. Bigner, "Immunohistochemistry of the Glial Fibrill Protein: Basic and Applied Consideration," *Brain Pathology,* vol. 4, pp. 221-228, 1994.

[295] Y. Yagita, K. Kitagawa, T. Ohtsuki, K. Takasawa, T. Miyata, H. Okano, "Neurogenesis by progenitor cells in the ischemic adult rat hippocampus," *Stroke,* vol. 32, pp. 1890-6, Aug 2001.

[296] M. V. Sofroniew, "Molecular dissection of reactive astrogliosis and glial scar formation," *Trends Neuroscience,* vol. 32, pp. 638-47, Dec 2009.

[297] K. Cluff, A. M. Kelly, P. Koutakis, X. N. He, X. Huang, Y. F. Lu, "Surface-enhanced Raman spectral biomarkers correlate with Ankle Brachial Index and characterize leg muscle biochemical composition of patients with peripheral arterial disease," *Physiol Rep,* vol. 2, Sep 1 2014.

[298] Z. Movasaghi, S. Rehman, and I. U. Rehman, "Raman Spectroscopy of Biological Tissues," *Applied Spectroscopy Reviews,* vol. 42, pp. 493-541, 2007/09/01 2007.

[299] G. Kister, G. Cassanas, M. Bergounhon, D. Hoarau, and M. Vert, "Structural characterization and hydrolytic degradation of solid copolymers of D,L-lactide-co-epsilon-caprolactone by Raman spectroscopy," *Polymer,* vol. 41, pp. 925-932, Feb 2000.

[300] M. Di Foggia, U. Corda, E. Plescia, P. Taddei, and A. Torreggiani, "Effects of sterilisation by high-energy radiation on biomedical poly-(epsilon-caprolactone)/hydroxyapatite composites," *Journal of Materials Science-Materials in Medicine,* vol. 21, pp. 1789-1797, Jun 2010.

[301] M. Kohler, S. Machill, R. Salzer, and C. Krafft, "Characterization of lipid extracts from brain tissue and tumors using Raman spectroscopy and mass spectrometry," *Analytical and Bioanalytical Chemistry,* vol. 393, pp. 1513-1520, Mar 2009.